

Molecular physiology of signal transmission along the auditory pathway

Dissertation

for the award of the degree
“Doctor rerum naturalium”
of the Georg-August-Universität Göttingen

within the IMPRS Neuroscience program
of the Georg-August University School of Science (GAUSS)

Submitted by
Tanvi Butola

born in
Bangalore, India

2017

Members of the thesis committee

Reviewer: Prof. Dr. T. Moser

Institute for Auditory Neuroscience and InnerEarLab, University Medical Center, Göttingen

Reviewer: Prof. Dr. Erwin Neher

Department of Membrane Biophysics, Max Planck Institute for Biophysical Chemistry, Göttingen

Prof. Dr. Thomas Dresbach

Department of Anatomy and Embryology, University of Göttingen, Göttingen

Further members of the examination board

Prof. Dr. S. Rizzoli

Department of Neuro- and Sensory Physiology, University Medical Center, Göttingen

Prof. Dr. N. Brose

Department of Molecular Neurobiology, Max Planck Institute for Experimental Medicine, Göttingen

Dr. M. Silies

European Neuroscience Institute, Göttingen

Date of oral examination: 16th of May, 2017

“If our brains were simple enough for us to understand them, we'd be so simple that we couldn't”

- *Ian Stewart*

Table of Contents

1 Abstract	1
2. Introduction.....	3
2.1 Electrical synapses.....	3
2.2 Chemical synapses.....	3
2.3 Synaptic vesicle cycle.....	4
2.3.1 Synaptic vesicle pools	6
2.3.2 Synaptic vesicle exocytosis	7
2.3.3 Synaptic vesicle endocytosis.....	10
2.4 Cytomatrix of the active zone.....	11
2.4.1 CAZ as organizers of the synapse: formation, scaffolding and maintenance	11
2.4.2 CAZ: Orchestration of Neurotransmitter release	13
2.4.3 CAZ: setup for synaptic vesicle endocytosis.....	15
2.5 Synaptic plasticity	16
2.6 Auditory system: Model system to study synaptic transmission.....	17
2.7 Aim of the study	21
3 Materials and methods	22
3.1 Animals	22
3.2 <i>in vitro</i> electrophysiology	23
3.3 Immunohistochemistry and confocal imaging.....	26
3.4 <i>in vivo</i> recordings.....	28

3.5 Data analysis	30
Chapter 1: Role of Piccolo in high frequency signal transmission at a central auditory synapse – the endbulb of Held	
1b Results	36
1b.1 Perturbation of Piccolo expression in central but not peripheral auditory synapses .	36
1b.2 Changes in molecular composition of the active zone upon Piccolo disruption	39
1b.3 Piccolo disruption reduces the amplitude of evoked EPSCs at the endbulb of Held while leaving the eEPSC kinetics and miniature EPSCs unaltered.....	43
1b.4 Reduced RRP size and a slower recovery from short-term depression in Piccolo mutants.....	49
1b.5 In the absence of Piccolo, partial loss of Bassoon has no effect on spontaneous release, but influences evoked transmission, short-term depression and recovery from depression at the endbulb of Held	54
1c Discussion	63
1c.1 Changes in molecular composition of endbulb AZs upon Piccolo disruption	64
1c.2 Piccolo disruption mildly affects synaptic transmission at the endbulb of Held.....	65
1c.3 Segregation of the roles of Piccolo and Bassoon at the active zone	67
Chapter 2: RIM-BP2 as a regulator of neurotransmitter release at a central auditory synapse – the endbulb of Held	
2a Introduction.....	72
Neurotransmitter release: Need for Speed.....	72
Cytomatrix of the Active Zone: Coupling synaptic vesicles to VGCC.....	72
2b Results	75

2b.1 Knocking-out RIM-BP2 reduces the amplitude and alters the kinetics of evoked EPSCs at the endbulb of Held but leaves miniature EPSCs unaltered	75
2b.2 Absence of RIM-BP2 the changes the characteristic short-term depression observed at the endbulb of Held to facilitation	78
2b.3 RIM-BP2 deficiency slows down the speed of recovery from short-term depression and leads to increased asynchronous release after stimulation at the endbulb of Held	80
2c Discussion	82
2c.1 Loss of RIM-BP2 changes short-term plasticity at the endbulb of Held and impairs evoked release.....	82
2c.2 Loss of RIM-BP2 increases asynchronous release which may slow down recovery from short-term depression.....	85
Chapter 3: Role of LRBA2 in cochlear hair cell function and hearing	
3a Introduction.....	88
BEACH proteins and LRBA	88
Sound encoding: Hair cells and Spiral ganglion neurons	89
3b Results	92
3b.1 Progressive hearing loss and compromised cochlear amplification in LRBA2 KO mice	92
3b.2 Hearing deficit in LRBA2 KO – <i>in vivo</i> analysis.....	94
3c Discussion	97
4 Outlook.....	100
4.1 CAZ: from individual proteins to the network.....	100
4.2 LRBA2: from systems function to molecular mechanism.....	102

5 References.....	103
Acknowledgements.....	122
List of abbreviations.....	124
List of figures.....	126
List of tables.....	130
Declaration.....	131
Curriculum Vitae.....	132

1 Abstract

Signal transmission lies at the core of brain function. Understanding how information is transferred from one neuron to the other is the first step toward deciphering not just normal brain processing but the pathology of a diseased brain. This thesis investigates the role of three proteins (Piccolo, Bassoon and RIM-BP2) that are crucial for the neurotransmitter release machinery and of the BEACH protein, LRBA2 that drew attention as a candidate to study sensory signal processing because of the hearing deficit reported in LRBA2 KO mice. Through a combination of *in vitro* and *in vivo* electrophysiology, and fluorescence imaging, this thesis studies the molecular physiology of signal transmission at the synapses in the central and peripheral auditory system. Piccolo and Bassoon were found to maintain vesicle replenishment, with Bassoon possibly having an additional role in regulating release probability at the central auditory synapse, the endbulb of Held. RIM-BP2 was indicated to be a key player in coupling presynaptic Ca^{2+} influx to the release of neurotransmitters, hence orchestrating ultrafast signal transmission at the endbulb of Held synapse. LRBA2 was found to be essential for proper hair bundle morphology of the sensory hair cells of the cochlea, and hence maintaining functional cochlear amplification and reliable transduction of the acoustic signal.

2. Introduction

Brain function relies on information transfer from one neuron to the other, which occurs at specialized sites of contact called synapse. Although the information travels along a neuron in electrical form as action potentials, the transmission of signal at the synapse can be either electrical or chemical, giving rise to two forms of synapses.

2.1 Electrical synapses

Electrical synapses serve as conduits, termed 'gap-junctions' for bi-directional transfer of ions or small organic molecules between two cells (neuron-neuron, neuron-glia cell or glial cell-glia cell). Gap junctions comprise of special proteins called connexins, six of which combine to form a hemi-channel called connexon. Two connexons then interact to form a gap junction channel, electrically coupling two neurons. In an electrical synapse two neurons are separated by only 3-4 nm, with barely any synaptic delay between the signal transfer from one neuron to the other. They serve as fast, fail-proof transmission systems that help shape the activity of neuronal networks, transfer metabolites between cells and play a crucial role in the early stages of neuronal development (Connors and Long, 2004; Hormuzdi et al., 2004; Pereda, 2014). In the auditory system, gap junctions, formed mostly between glia-like supporting cells and fibrocytes of the cochlea, are essential to develop and maintain proper cochlear function, as is evident by syndromic or non-syndromic deafness due to mutations in connexin genes (Jagger and Forge, 2015; Wang et al., 2015).

2.2 Chemical synapses

Most neuronal communication occurs at chemical synapses, where the presynaptic and the postsynaptic membranes are separated by a 20-50nm wide synaptic cleft. At a chemical synapse the incoming electrical signal in the form of action potential is converted into a chemical signal by the release of neurotransmitters into the synaptic cleft. These neurotransmitters are intercepted by the postsynaptic receptors that conduct ionic current that can eventually lead to the generation of a postsynaptic action potential, i.e. electrical signals. Both the pre- and postsynapse are equipped with sophisticated molecular

architecture to maintain synaptic transmission. In addition, existence of trans-synaptic nanocolumns has been proposed to co-ordinate the alignment of the pre- and postsynaptic compartments to maintain efficient and reliable transmission (Figure I. 1; Tang et al., 2016).

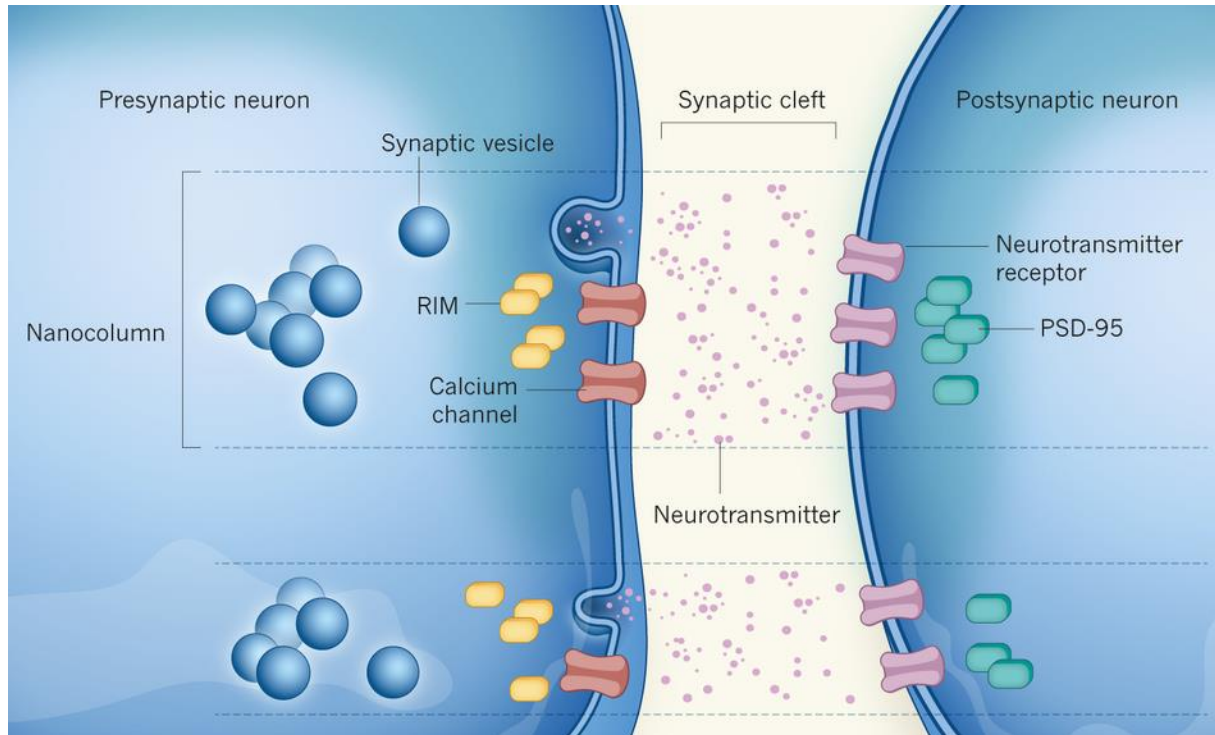


Figure I. 1: Structure of a chemical synapse

Illustration of the architecture a chemical synapse with pre- and postsynaptic compartments separated by a synaptic cleft where synaptic vesicles in the presynapse release neurotransmitters to be received by postsynaptic receptors. Image taken from (Sigrist and Petzoldt, 2016).

2.3 Synaptic vesicle cycle

The currency of communication at a chemical synapse is the neurotransmitters and the basic unit of neurotransmitter release is the 'quantum' (del Castillo and Katz, 1954) or 'mini'. Each of the stochastic, spontaneous fusion events with a narrow amplitude distribution, corresponds to a quantum of neurotransmitter released (Fatt and Katz, 1950). The synaptic vesicle (SV) is the morphological equivalent of a quantum of neurotransmitters. SVs are spherical membrane-bound secretory organelles, about 50nm in diameter, densely packed with a plethora of transmembrane and membrane-associated proteins (Takamori et al.,

2006). An evoked event with larger amplitude than the 'mini' represents multiple quanta released synchronously.

For synaptic transmission, vesicles undergo rounds of release and recycling (Figure I. 2), elaborated in the following sections. The release by vesicle fusion occurs at specialized regions in the presynapse called active zones (AZ). For release, SVs are docked at the AZ membrane, primed, and fusion machinery (*trans*-SNARE complex; explained in section 1.3.2) is assembled to finally fuse the SVs with the presynaptic membrane releasing neurotransmitters. Docking, priming and *trans*-SNARE complex assembly represent the morphological, functional and molecular manifestations of the same process to make the SVs release ready (Imig et al., 2014). The recycling step begins with endocytosis of fused membrane at regions surrounding the AZ, called peri-active zones (Haucke et al., 2011). Several mechanisms have been described for SV endocytosis: Ultrafast endocytosis (Watanabe et al., 2013), Kiss and run (Alabi and Tsien, 2013), Clathrin mediated endocytosis (McMahon and Boucrot, 2011), Bulk endocytosis (Clayton and Cousin, 2009) and Clathrin independent endocytosis followed by clathrin mediated SV reformation (Soykan et al., 2017).

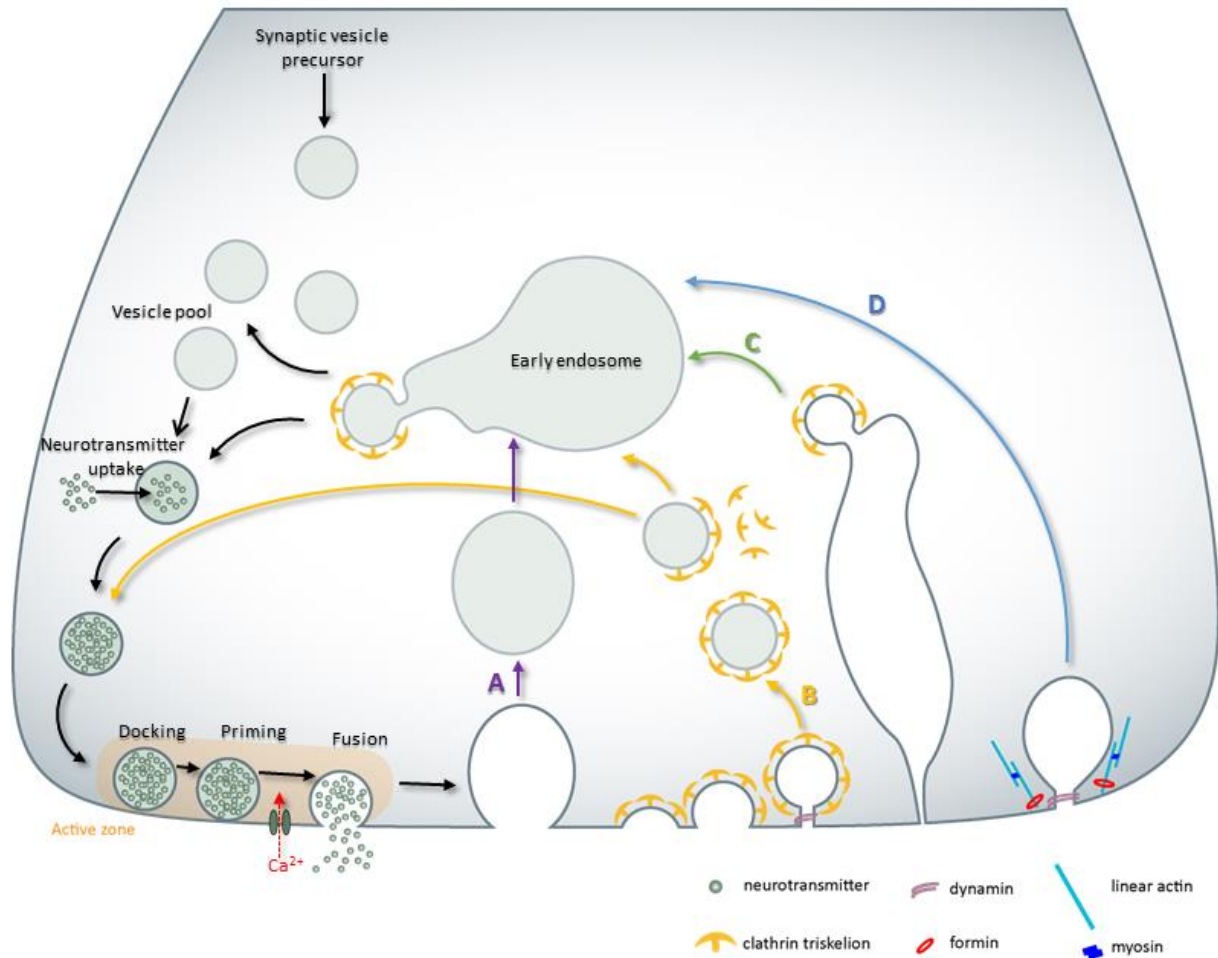


Figure I. 2: Synaptic vesicle cycle

Synaptic vesicles undergo a cycle of release and recycling to maintain neurotransmitter release at the presynapse. The vesicles from the pool are tethered to the AZ membrane, which are then docked and primed, and finally fuse with the presynaptic membrane to release neurotransmitter. Different mechanisms described for endocytosis are represented as: (A) Ultrafast endocytosis (B) Clathrin mediated endocytosis, (C) Bulk endocytosis and (D) Clathrin independent endocytosis followed by clathrin mediated SV reformation.

2.3.1 Synaptic vesicle pools

Synaptic vesicles are formed as precursor vesicles at the trans-Golgi network and then transported by kinesin motor proteins along microtubules traversing the length of the neuronal axon to reach the presynapse (Okada et al., 1995), where they are filled with neurotransmitter molecules (Farsi et al., 2016; Nelson and Lill, 1994). Overtime, the population of synaptic vesicles at the presynapse has come to be viewed as being organized into distinct vesicle pools. The three pool model (Alabi and Tsien, 2012; Harata et al., 2001;

Rizzoli and Betz, 2005; Schikorski and Stevens, 2001), that has stood the test of time, defines: (1) the readily releasable pool (RRP) which makes up 1-2% of all vesicles, (2) recycling pool, making up 10-20% of the vesicle store and (3) reserve pool accounting for the remaining 80-90% of the vesicles.

Membrane-attached (docked) vesicles are considered as the morphological correlate of the fusion competent vesicles composing the RRP (Imig et al., 2014). Electrophysiologically, the RRP represents the first line of response when the synapse is stimulated. The RRP is depleted rapidly, within a few milliseconds of electrical stimulation (Elmqvist and Quastel, 1965; Schneggenburger et al., 1999). RRP can be further distinguished into two sub-categories (Sakaba and Neher, 2001a): (1) a fast pool (~ 0.9ms time constant of release), (2) a slow pool (~4ms time constant of release) where the time constants are derived from mature, p16-p19 calyx of Held synapse (Chen et al., 2015). Recently, a third superprimed synaptic pool has been proposed, where SVs are in a state of elevated release probability and are released even before the fast pool (Taschenberger et al., 2016).

Upon RRP depletion, the recycling pool maintains release under moderate physiological stimulation and is continuously recycled (Rizzoli and Betz, 2005). Recycling pool is maintained by vesicle endocytosis, and the vesicles therein undergo cycles of release till they mature into the release-reluctant immobile reserve pool (Denker and Rizzoli, 2010). The reserve pool is only released under intense stimulation and may act as a buffer for synaptic proteins involved in vesicle recycling, preventing their escape into the axon (Denker et al., 2011).

2.3.2 Synaptic vesicle exocytosis

The primary step in the synaptic vesicle cycle is the exocytosis of fusion-ready releasable vesicles. At most synapses fusion of vesicular membrane with presynaptic plasma membrane is driven by a cycle of association and dissociation of SNAREs (soluble NSF attachment receptor proteins). The V-SNARE (vesicular SNAREs on the vesicular membrane; Synaptobrevin) and T-SNAREs (target SNAREs on presynaptic membrane; SNAP-25 and Syntaxin1) assemble in a α -helical *trans*-SNARE complex that forces the two membranes

Introduction

together. SM proteins (Sec1/Munc18) wrap around this SNARE complex via interaction with Syntaxin1, and are essential partners for SNARE proteins in vesicle fusion. Initially, Munc18 is bound to closed conformation of Syntaxin1 that occludes the SNARE motif. Priming of SVs involves change of Syntaxin1 to open conformation to initiate *trans*-SNARE complex assembly (Gerber et al., 2008).

This primed pre-fusion assembly of SNARE/SM proteins complex acts as a substrate for Ca^{2+} triggered fusion. Upon the arrival of action potential at the presynaptic terminal, VGCCs open and cause influx of Ca^{2+} . This Ca^{2+} influx is detected by the Ca^{2+} sensor Synaptotagmin that then binds to the core fusion assembly and is thought to bring about the full zippering of the SNARE complex, leading to fusion-pore opening. Upon fusion completion, the two membranes completely merge, converting the *trans*-SNARE complex to *cis*-SNARE complex, which is then dissociated by ATPase, NSF (N-ethylmaleimide sensitive factor) into reactive monomeric SNARE proteins ready to undergo another cycle.

The molecules and steps involved in synaptic vesicle fusion are illustrated in (Figure I. 3) and the summary was derived from recent studies presented and reviewed in the field (Kaesler and Regehr, 2014; Südhof, 2013; Südhof and Rizo, 2011).

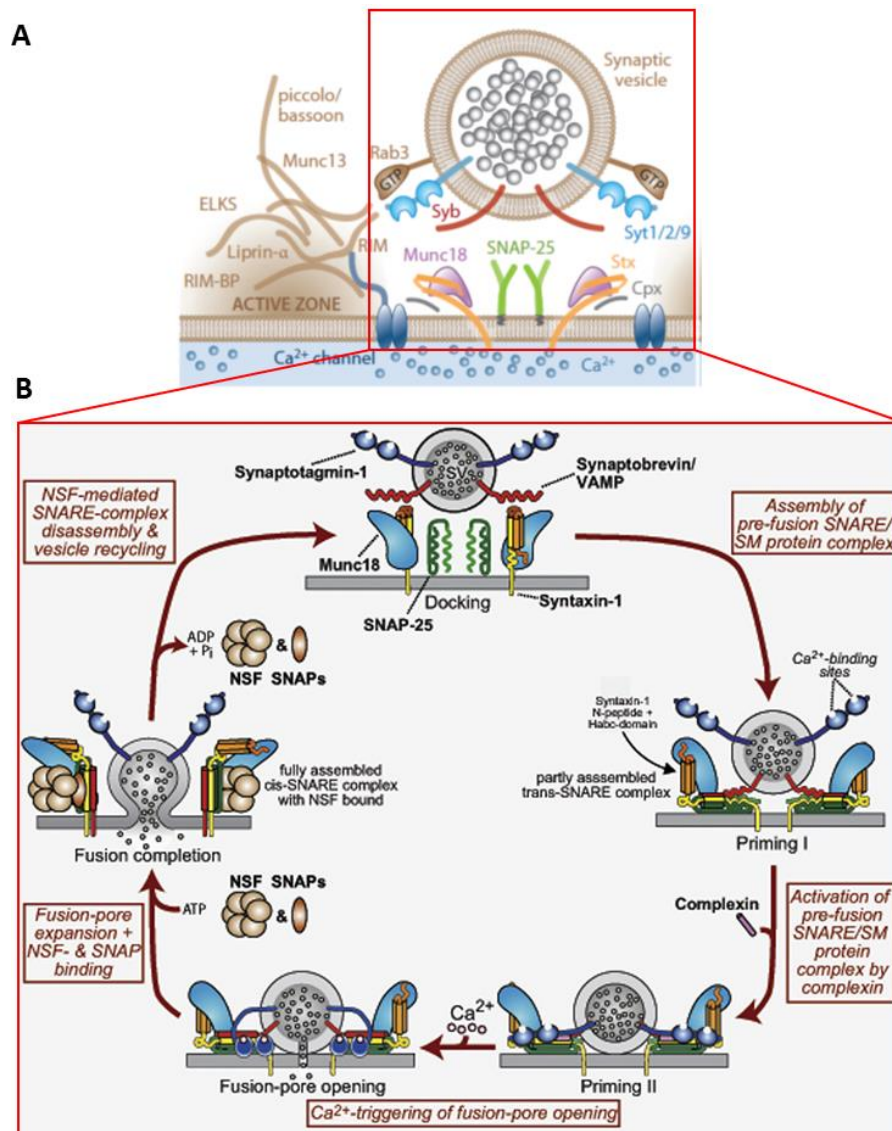


Figure I. 3: Schematic of SNARE/SM protein cycle illustrating the vesicle fusion machinery

(A) Representation of the presynapse highlighting a synaptic vesicle, the presynaptic membrane, and the repertoire of proteins involved in vesicle fusion. Syb: Synaptobrevin, Stx: Syntaxin1, Syt: Synaptotagmin, Cpx: Complexin. Image adapted from (Kaeser and Regehr, 2014) (B) Cycle of SNARE/SM protein association and dissociation in the vesicle fusion scheme. Image taken from (Südhof, 2013).

Apart from Ca^{2+} triggered synchronous release, there are two other modes of neurotransmitter release (Kaeser and Regehr, 2014): asynchronous release and spontaneous release. While synchronous release is tightly coupled to the action potential, asynchronous release occurs with a longer, variable delay after the stimulus. Spontaneous release occurs as random events in the absence of any action potential. Although, all three modes of

release share the same core fusion machinery, the Ca^{2+} regulation of asynchronous and synchronous release is less clear. It is also suggested that the pool of vesicles contributing to these modes might be distinct from that contributing to synchronous release (Fredj and Burrone, 2009; Raingo et al., 2012; Sara et al., 2005). However, there is another school of thought that rejects this hypothesis and maintains that the vesicles released through the three modes of release come from the same pool (Groemer and Klingauf, 2007; Hua et al., 2010; Wilhelm et al., 2010).

2.3.3 Synaptic vesicle endocytosis

Since, the release sites are located away from the protein synthesis machinery, local recycling of vesicles becomes necessary to replenish the depleted pool of vesicles, during prolonged activity. Additionally, to maintain sustained exocytosis in response to repetitive stimuli, fused vesicle membrane needs to be endocytosed to clear release sites, as the availability of release sites rather than vesicle supply might prove to be the bottle-neck for sustained exocytosis (Neher, 2010).

Synaptic vesicle recycling essentially involves two steps: (1) membrane retrieval after SV fusion and (2) SV reformation from the retrieved membrane which includes correct sorting of SV proteins to achieve a functional composition of SV. Mechanisms proposed for endocytic membrane retrieval include (Figure I. 2): (1) Kiss-and-run, where the fusion pore transiently opens and closes rapidly without full vesicle collapse, hence preserving the molecular composition of vesicles (Alabi and Tsien, 2013) and supporting fast kinetics of SV recycling (He et al., 2006), remains controversial. (2) Clathrin mediated endocytosis (CME; Figure I. 2B), where the SV components are retrieved directly from the plasma membrane as clathrin-coated vesicles which are subsequently uncoated and enter the recycling vesicle pool. CME however, operates on a time scale of tens of seconds and hence, is not very compatible with maintaining vesicle recycling under high frequency stimulation. (3) Ultrafast endocytosis (Figure I. 2A), is postulated to be the mode of SV retrieval under physiological temperatures within 50-100ms after stimulation (Watanabe et al., 2013). Membrane invagination corresponding to as many as 4 SVs may be endocytosed. (4) Bulk endocytosis (Figure I. 2C), is proposed to occur following strong stimulation with membrane being

retrieved as large endocytic structures (Clayton and Cousin, 2009). Following both ultrafast and bulk endocytosis, the endosome-like vacuoles are resolved into individual SVs in a clathrin dependent manner (Jung et al., 2015a; Kononenko et al., 2014; Watanabe et al., 2014), that rejoin the synaptic vesicle cycle.

A recent study (Soykan et al., 2017) states that at physiological temperature SV endocytosis occurs over several time scales ranging from less than a second to several seconds depending on the number of SVs fused. The endocytic membrane is retrieved in a clathrin independent manner mediated by Formin-dependent actin assembly, in the form of endosome like vacuoles (ELVs) (Figure I. 2D). These ELVs are subsequently, reformed into SVs either in a clathrin-dependent manner or via other SV budding events (Wu et al., 2014).

2.4 Cytomatrix of the active zone

Synaptic vesicle release occurs at specialized regions in the presynapse, called active zones (AZ). At the AZ, there exists an electron-dense network of proteins called the cytomatrix of the active zone (CAZ) proteins. CAZ proteins comprise of multi-domain protein families: Munc13s, Rab3-interacting molecules (RIMs), RIM-binding proteins (RIM-BPs), CAST/ELKS proteins, Piccolo/Aczonin and Bassoon, and Liprins- α . Domain structures and interactions between these proteins are illustrated in Figure I. 4. These proteins are thought to regulate key aspects of the neurotransmitter release machinery: such as maintaining releasable SV pools by docking, tethering and priming of SVs, localizing VGCC (Voltage gated Ca^{2+} channels) to release sites for efficient stimulus-exocytosis coupling and modulating synaptic strength by regulating short-term plasticity. The different roles of CAZ proteins in synaptic function are introduced in the light of the research performed for the thesis.

2.4.1 CAZ as organizers of the synapse: formation, scaffolding and maintenance

The assembly of the presynaptic active zone begins at the trans-Golgi network, where components of the AZ such as Piccolo, Bassoon, Syntaxin, SNAP-25 and N-cadherin are loaded on $\sim 80\text{nm}$ dense core transport vesicles called Piccolo-Bassoon transport vesicles (PTVs) (Zhai et al., 2001). These transport vesicles then travel to the nascent synapses where AZ network is assembled through interactions with trans-synaptic adhesion molecules like

Introduction

neurexins and neuroligins (Siddiqui and Craig, 2011; Waites et al., 2005). It was shown in cultured hippocampal neurons that two to three PTVs integrate to build an active zone (Shapira et al., 2003). A recent study indicates that CAST/ELKS also exit the Golgi network with Piccolo and Bassoon, while Munc13 and synaptic vesicle proteins employ a distinct set of transport vesicles and RIM1 α joins Golgi-derived transport vesicles in a post-Golgi compartment (Maas et al., 2012).

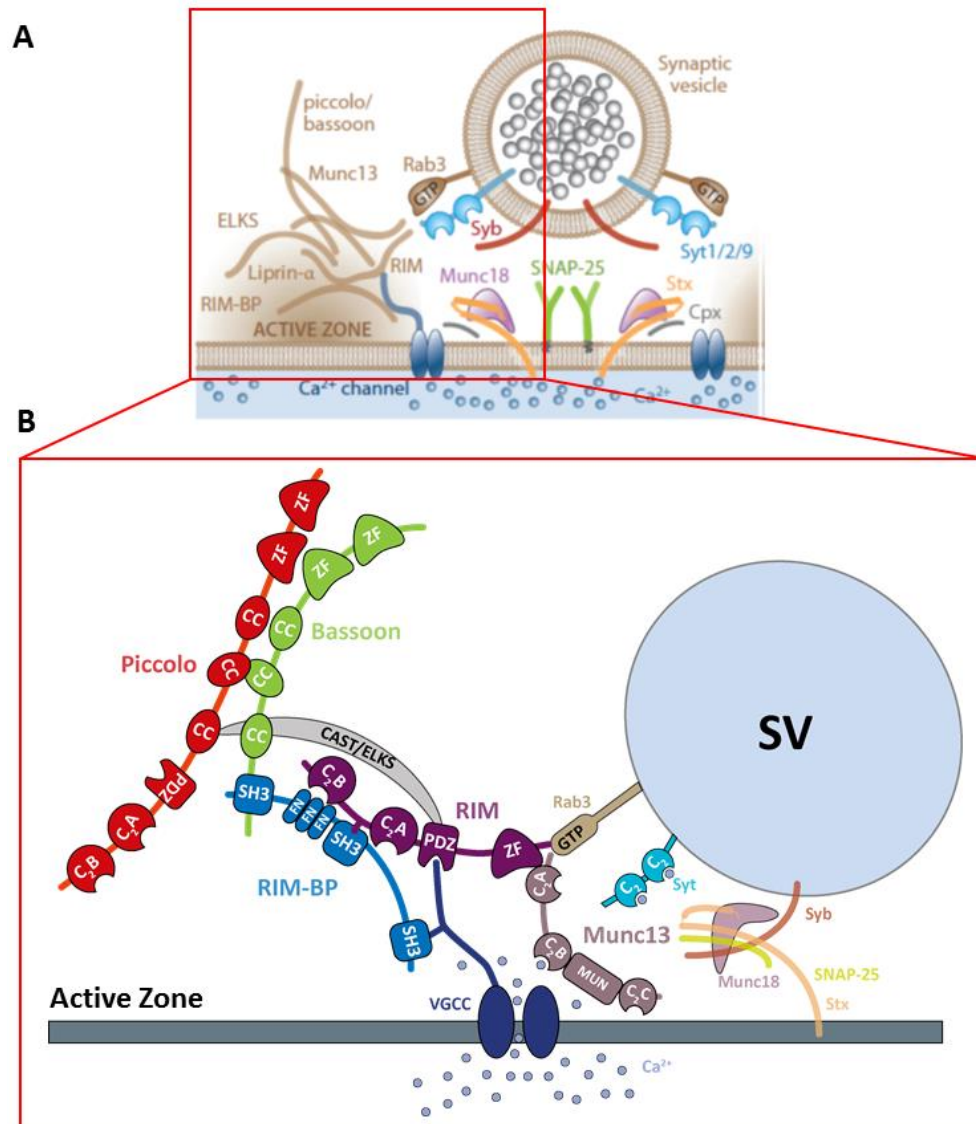


Figure I. 4: Cytomatrix of the active zone

(A) Representation of the presynapse highlighting CAZ proteins in relation to the SV fusion machinery. Image adapted from (Kaeser and Regehr, 2014). (B) Domains structures and interactions of the CAZ proteins. ZF: Zinc finger domain, CC: Coiled-Coiled domain, SH3: SRC homology domain,

FN: Fibronectin domain, VGCC: Voltage gated Ca^{2+} channel, SV: Synaptic vesicle, Syb: Synaptobrevin, Syt: Synaptotagmin, Stx: Syntaxin. Image not to scale.

CAZ proteins interact with each other to form the scaffold for maintaining the structural functional organization of the active zone (Figure 1. 4; Gundelfinger and Fejtova, 2012; Schoch and Gundelfinger, 2006). Through their CC domains Piccolo and Bassoon bind to the CC domain of CAST/ELKS (Takao-Rikitsu et al., 2004). CAST/ELKS in turn bind to RIM1 and through it to Munc13-1 forming a ternary complex (Ohtsuka et al., 2002). 5 CAZ proteins: Munc13-1, RIM1, Bassoon, Piccolo and CAST/ELKS all converge on an interaction node centered on N-terminal domain of Munc13-1 (Wang et al., 2009). Other major interactions include Bassoon binding to RIM-BP which in turn binds to VGCC (Davydova et al., 2014), and RIM interacting with RIM-BP and VGCC (Han et al., 2011; Hibino et al., 2002; Kaeser et al., 2011). Together these protein-protein interactions form a network regulating the functioning of the presynaptic active zone.

The sensory system provides examples of the importance of CAZ proteins for structural and functional integrity of the active zone. In the absence of Bassoon, the presynaptic ribbon is not attached properly to the presynaptic density in inner hair cells (Khimich et al., 2005) and retinal photoreceptors (Dick et al., 2003; tom Dieck et al., 2005). While the loss of Piccolino (shorter isoform of Piccolo, predominant at ribbon synapses) alters the maturation and ultrastructure of the ribbon at the retinal photoreceptor cells (Regus-Leidig et al., 2014).

Another major function for regulating synaptic function and stability is to ensure synaptic protein turnover and hence, their timely degradation. Piccolo and Bassoon maintain synaptic integrity by regulating presynaptic ubiquitination and proteostasis (Waites et al., 2013). Recently, it has been shown that Bassoon specifically controls presynaptic autophagy (Okerlund et al., 2017).

2.4.2 CAZ: Orchestration of Neurotransmitter release

As introduced in section 2.3.2 synaptic vesicle exocytosis at most synapses involves an intricate fusion machinery employing SNARE proteins. However, the SNARE complex requires the CAZ proteins to tether, dock and prime the SVs to be released. Munc13s are

Introduction

crucial for docking and priming of SVs and rendering them release ready (Imig et al., 2014). Munc13s mediate priming of SVs through their MUN domain (Basu et al., 2005; Stevens et al., 2005), which likely activates priming of SVs by opening Syntaxin1 for SNARE complex assembly (Ma et al., 2011; Richmond et al., 2001). Munc13s however, cannot regulate SV priming on their own. Munc13s form homodimers via their N-terminal C₂A domains, which inactivates their priming function. RIMs activate their priming function by reversing this autoinhibition by forming a RIM-Munc13 heterodimer via their N-terminal Zn finger domain (Deng et al., 2011; Dulubova et al., 2005; Lu et al., 2006). The priming action mediated by Munc13s and RIMs might be more complicated than this, given that the N-terminal of Munc13 acts as an interaction node for 3 other CAZ proteins (Bassoon, Piccolo and CAST/ELKS) apart from RIM (Wang et al., 2009). RIMs in addition, are important for dock SVs via its interaction with Rab3 (Gracheva et al., 2008) and have been implicated in vesicle tethering (Fernández-Busnadiego et al., 2013a; Jung et al., 2015b).

CAZ proteins also orchestrate neurotransmitter release by positioning VGCC to the active zone and hence, bring the source of Ca²⁺ close to the SVs to be released. RIMs tether the VGCC to the active zone (Grabner et al., 2015; Han et al., 2011; Jung et al., 2015b; Kaeser et al., 2011; Kintscher et al., 2013) via its PDZ domain (Kaeser et al., 2011) and through its C-terminus interaction with Ca_vβ subunits (Gebhart et al., 2010; Kiyonaka et al., 2007). RIMs in addition interact with RIM-BP, which in turn bind to the Ca²⁺ channels themselves (Hibino et al., 2002). RIMs also directly modulate Ca²⁺ channel inactivation (Gebhart et al., 2010; Kaeser et al., 2012). Aside from RIMs and RIM-BPs, Bassoon has been recently found to specifically position P/Q type Ca²⁺ channels in the vicinity of SV release sites through its interaction with RIM-BP (Davydova et al., 2014). Bassoon's role in Ca²⁺ channel clustering was also reported for ribbon-type synapses in inner hair cells (Frank et al., 2010) and in retinal photoreceptor cells (tom Dieck et al., 2005).

Mover, a small SV associated protein, identified based on its interaction with Bassoon (Kremer et al., 2007) has been shown to negatively regulate SV exocytosis (Körber et al., 2015a). It is still unclear how Bassoon might exert its role in SV exocytosis through its interaction with Mover.

Piccolo has also been implicated as a negative regulator of SV exocytosis (Leal-Ortiz et al., 2008). Additionally, Piccolo has two C₂ domains: C₂A and C₂B, both of which were reported to bind to Ca_v1.2 L-type voltage-dependent Ca²⁺ channels (Shibasaki et al., 2004). C₂A additionally, acts as a low-affinity Ca²⁺ sensor for exocytosis (Garcia et al., 2004; Gerber et al., 2001). Hence, Piccolo can also be a candidate in moderating release by influencing Ca²⁺ dynamics.

2.4.3 CAZ: Setup for synaptic vesicle endocytosis

Electrophysiological recordings have demonstrated that exocytosis is followed by endocytosis, at sensory synapses like the ribbon synapse (von Gersdorff and Matthews, 1994; Moser and Beutner, 2000) and at central synapses like the Calyx of Held (Wu et al., 2007). Recent studies (Hosoi et al., 2009; Hua et al., 2011; Wahl et al., 2013; Watanabe et al., 2013, 2014) postulated that endocytosis occurs right at the edge of the active zone and hence, it is conceivable that the endocytic machinery is functionally and physically linked to the AZ.

One candidate for this exo-endocytosis coupling is Ca²⁺. A Ca²⁺ dependence of recovery after stimulation has been shown at the ribbon synapses of the cochlear hair cells (Moser and Beutner, 2000; Spassova et al., 2004), endbulb of Held (Wang and Manis, 2008; Yang and Xu-Friedman, 2008) and the calyx of Held (Hosoi et al., 2009; Sakaba and Neher, 2001a; Wang and Kaczmarek, 1998). Although, the sensor for Ca²⁺ modulating endocytosis has been much debated, the Ca²⁺ channels that mediate exocytosis are common to endocytosis as well (Midorikawa et al., 2014; Xue et al., 2012; Yamashita et al., 2010). As introduced earlier, the CAZ proteins are intricately involved in tethering VGCC at the presynaptic plasma membrane and hence, regulate Ca²⁺ signaling at the AZ.

Yet another candidate for the exo-endocytosis coupling is actin. Actin is a prime suspect in endocytic membrane retrieval (Sakaba and Neher, 2003; Soykan et al., 2017; Watanabe et al., 2013). Actin can be conceived to provide structural basis for guiding SVs back to the recycling pool. The CAZ protein Piccolo interacts with actin binding proteins like Profilin and Daam1 and has been shown to regulate F-actin assembly in an activity-dependent manner

(Wagh et al., 2015; Waites et al., 2011). Piccolo also interacts with actin-binding protein Abp1 (Fenster et al., 2003), which in turn interacts with endocytic GTPase Dynamin (Kessels et al., 2001). Dynamin catalyzes membrane scission of Ω -shaped clathrin coated pits to form SVs (Figure I. 2). Another interaction partner for Piccolo is the protein GIT (Kim et al., 2003), which directly binds to endocytic adaptor protein Stonin2 (Podufall et al., 2014). GIT protein has also been shown to regulate release probability at the presynapse (Montesinos et al., 2015). Hence, Piccolo could potentially contribute to the exo-endocytosis coupling.

2.5 Synaptic plasticity

When stimulated repeatedly, a synapse typically does not respond with uniform strength overtime. It alters its postsynaptic response in an activity and time dependent manner, leading to either depression or facilitation of synaptic strength. This dynamic change in the strength of synaptic response is termed plasticity. For the scope of this thesis, only short-term plasticity, functioning over tens of milliseconds to seconds, and the presynaptic factors contributing to it, will be introduced.

Presynaptic factors contributing to short-term synaptic plasticity include: changes in presynaptic residual Ca^{2+} levels, changes in the vesicle pools available for release or changes in the release machinery itself. As introduced earlier, the CAZ proteins regulate all these aspects and hence, contribute to the modulation of synaptic strength. This is corroborated by the changes in short-term plasticity observed in mutations of CAZ proteins. This is exemplified by the enhancement of short-term depression at endbulb of Held (Schulz et al., 2014) and at cerebellar mossy fiber to granule cell synapse (Hallermann et al., 2010a) in the absence of Bassoon or the impaired short-term plasticity at hippocampal CA1 synapses in the absence of RIM1 α (Schoch et al., 2002). While glutamatergic RIM1 α deficient synapses showed an increase in facilitation, GABAergic synapses showed reduced facilitation in the absence of RIM1 α . The absence of RIM1 α enhances short-term facilitation at cerebellar parallel fiber synapses as well (Kintscher et al., 2013). Munc13 is also report to alter short-term depression when mutated to be insensitive to Ca^{2+} -Calmodulin interaction (Lipstein et al., 2013).

Short-term plasticity plays a crucial role in information processing (Abbott and Regehr, 2004; Deng and Klyachko, 2011). To mention a few, it can mediate sensory adaptation (Chung et al., 2002; Furukawa and Matsuura, 1978; Goutman and Glowatzki, 2007; Moser and Beutner, 2000) and contrast adaptation (Chance et al., 1998; Oesch and Diamond, 2011), and act as a dynamic filter optimized for specific transmission patterns or frequencies (Fortune and Rose, 2001; Klyachko and Stevens, 2006). Specifically in the auditory system short-term plasticity at central auditory synapses seems important for sound localization (Cook et al., 2003; Kuba et al., 2002) and intensity coding (MacLeod, 2011), while others have questioned its relevance in auditory processing (Kuenzel et al., 2011).

The quantification of the strength of synaptic response is derived from the quantal theory (del Castillo and Katz, 1954; Fatt and Katz, 1952), which postulated that in response to stimulation multiple units or ‘quanta’ of neurotransmitters are released. Quantum or quantal size (q) is posited to be the content of one synaptic vesicle derived from the amplitude of miniature excitatory post synaptic current (mEPSC; Fatt and Katz, 1950). Simplifying the model of neurotransmitter release, where N is the number of vesicular release sites at a presynaptic terminal, and P_r is the release probability, which is the product of probability of occupancy of a vesicle at a release site and probability of successful fusion of a vesicle at the release site (Neher, 2017); strength of a synapse can be determined in terms of the postsynaptic current (PSC) through:

$$PSC = N \times P_r \times q$$

This relationship can be used as a framework to determine changes in P_r , and N by measuring PSC and q experimentally (Neher, 2017; Schneggenburger et al., 1999, 2002).

2.6 Auditory system: Model system to study synaptic transmission

The lower auditory pathway is specialized for fast signal transmission with high temporal fidelity (Kopp-Scheinflug and Tempel, 2015; Moser et al., 2006; Trussell, 1999; Wichmann, 2015) and harbors synapses that are structurally and functionally adapted to cope with this challenge. The need for fast and efficient vesicle cycling makes these synapses ideal models

Introduction

for the study of CAZ proteins. Figure I. 5 shows a schematic of the first few synapses in the auditory system.

The mechanical signal of the sound waves is transduced into electrical signal by the hair cells in the organ of Corti in the cochlea. The organ of Corti has two types of hair cells: one row of inner hair cells (IHCs) and 3-4 rows of outer hair cells (OHCs). Both types of hair cells are characterized by highly organized arrays of actin-rich microvilli (stereocilia), at their apical pole. This 'hair bundle' is equipped with mechano-electrical transduction (MET) channels that are gated by the movement of the stereocilia. Upon physical hair bundle deflection by the sound-driven travelling wave, the coordinated opening of mechanically-gated ion channels in the stereociliary tips mediate hair cell depolarization. This depolarization leads to synchronized electromotile contraction of OHCs, which enables them to mechanically amplify the sound-induced vibrations (Brownell, 1990; Liberman et al., 2002; Zheng et al., 2000). In the IHCs, on the other hand, the depolarization, causes Ca^{2+} influx through voltage-dependent Ca^{2+} channels at the basal pole, which triggers vesicle fusion at ribbon-type active zones to release glutamate into the synaptic cleft (Nouvian et al., 2006). There are about 5-20 ribbons in the IHCs, each apposed by a single postsynaptic bouton of the spiral ganglion neurons (SGNs), which relay the signal from the ribbon synapse as action potentials to the cochlear nucleus in the brain stem (Meyer et al., 2009; Rutherford et al., 2012).

Entering the cochlear nucleus, the central axons of the SGNs bifurcate into ascending and descending branches (Fekete et al., 1984). The ascending fibers converge on to two major cell types in the anterior ventral cochlear nucleus (aVCN): stellate cells (SC) and bushy cells (BC) (Wu and Oertel, 1984). While SCs receive bouton-like glutamatergic inputs (Cant, 1981), bushy cells primarily receive large calyceal synapses called endbulbs of Held (Cant and Morest, 1979; Held, 1893). Bushy cells are further subdivided into two groups: spherical bushy cells (SBC) and globular bushy cells (GBC). In mice, GBC typically receive 4-6 smaller modified endbulbs of Held (Rouiller et al., 1986), while SBC receive 2-3 larger endbulbs (Cao and Oertel, 2010; Nicol and Walmsley, 2002). This convergence of multiple inputs to one postsynaptic cell in the aVCN results in an enhanced phase-locking to sound frequency as

compared to the SGNs (Howard and Rubel, 2010; Joris et al., 1994; Trussell, 1999), which have one to one, ribbon to postsynapse connectivity (Liberman, 1982).

The BCs of aVCN provide input to the next nuclei of the auditory pathway some of which are involved in processing sound localization in the horizontal plane. Binaural cues of interaural time differences (ITDs) and interaural level differences (ILDs) are processed in parallel in many mammals. While ILDs are mostly important for high frequency sounds due to poor attenuation of low frequencies, ITDs become relevant for low frequencies (Grothe et al., 2010). ITDs are processed in the medial superior olive (MSO), which receives excitatory inputs from both ipsi- and contralateral SBCs. Thus, MSO can identify the direction of the source of the sound by determining the ITD between the acoustic inputs from each ear (Fitzpatrick et al., 1997; Yin and Chan, 1990). The lateral superior olive (LSO) on the other hand, detects ILDs for sound localization. GBCs send their projections across the brainstem midline to the principle cells of the contralateral medial nucleus of the trapezoid body (MNTB) forming large glutamatergic calyx of Held synapses. The principle cells of MNTB then send inhibitory glycinergic projections to the LSO. LSO also receives excitatory input from ipsilateral SBCs. Thus, the monosynaptic ipsilateral excitation and disynaptic contralateral inhibition converges on the LSO. LSO acts as a coincidence detector of binaural signals where the ILDs are represented as differences in the timing of excitatory and inhibitory inputs (von Gersdorff and Borst, 2002).

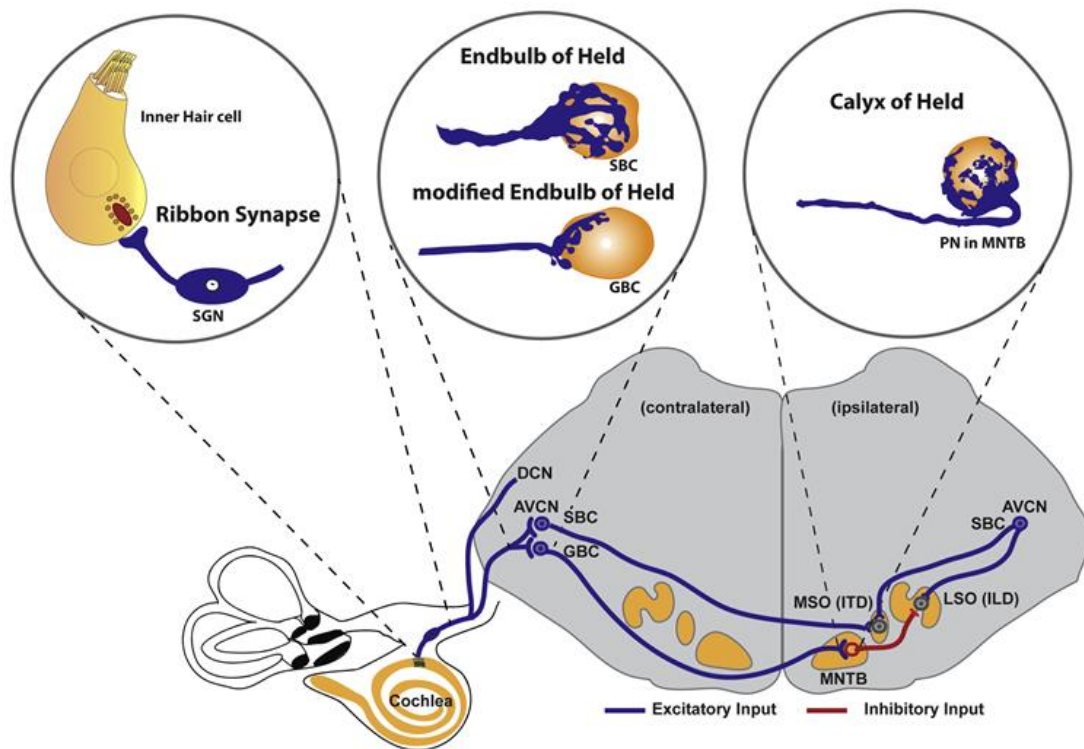


Figure I. 5: The auditory pathway

Image taken from Yu and Goodrich, 2014.

Thus, there is a high functional demand on the auditory system to maintain fast and temporally precise synaptic transmission (Wichmann, 2015). The first three synapses of the auditory pathway: IHC ribbon synapse, endbulb of Held and the calyx of Held, act as relay centers fulfilling these demands and are hence, ideal to reveal any defect in the neurotransmitter release machinery arising from molecular perturbations. Another advantage is that every compartment of the three synapses is accessible for physiological recording for assessing synaptic transmission: inner hair cells (Moser and Beutner, 2000), postsynaptic bouton of the SGNs (Glowatzki and Fuchs, 2002), endbulb of Held (Lin et al., 2011), postsynaptic BCs (Cao and Oertel, 2010), and calyx of Held together with its postsynaptic cell (Chen et al., 2015).

The auditory pathway as a model also allows correlating the synaptic data to the systems physiology and processing of acoustic information, to assess synaptic transmission in the context of its sensory function. The auditory brainstem response (ABR) is a recording of the auditory evoked potentials in response to sound stimulus, recorded from the scalp in a

stimulus-locked manner. ABR waves reflect the electrical activity at different stations along the auditory pathway (Melcher and Kiang, 1996; Melcher et al., 1996a, 1996b), hence providing a measure of signal processing in the whole system.

2.7 Aim of the study

This study aims to elucidate the molecular machinery driving neurotransmission at auditory synapses specialized for ultrafast and high-fidelity signal transmission. Towards this goal, the function of three CAZ proteins: Piccolo, Bassoon and RIM-BP2 is investigated at the central auditory synapse of endbulb of Held. In addition, a BEACH protein LRBA2, whose deficiency leads to hearing impairment, is studied to unveil its role in sensory information processing at the ribbon synapses of the cochlear hair cells.

3 Materials and methods

3.1 Animals

Piccolo and Bassoon study: Mice with cre-mediated excision (Lakso et al., 1996) of exon 14 of the *Pclo* gene and insertion of a neomycin resistance cassette in the adjacent 3' intron (PicMut; Mukherjee et al., 2010), and their wildtype littermates (PicWT) were studied. The mouse line was derived by heterozygous breeding with C57Bl/6J genetic background. For a subset of experiments (recovery, Figure 1b. 13) PicBsn animals, with only one intact allele of the *Bsn* gene in addition to Piccolo mutation, were used. These were derived by heterozygous breeding of PicMut with *Bsn*^{ΔEx4/5} mice (exons 4 and 5 of Bassoon gene deleted; (Altrock et al., 2003a)).

RIM-BP2 study: Mice with cre-mediated excision of exon 17 of the *Rimbp2* gene (RIM-BP2 KO; Grauel et al., 2016) and their wildtype littermates were studied. In a subset of experiments, data from C57Bl/6 wildtype mice were pooled with littermate controls. The homologous recombination for KO mouse generation was carried out by genOway. The mouse line was derived by heterozygous breeding with C57Bl/6N genetic background.

LRBA2 study: LRBA2 KO mice (laboratory code for the line, Lrba2-A-C9) were constructed by constitutive deletion of coding exon 3 of *Lrba2* gene, generating a frameshift mutation (Figure M. 1). The mutation was generated in C57BL/6N ES cells, and subsequently propagated in the same background (five or more backcrosses at the time of analysis).

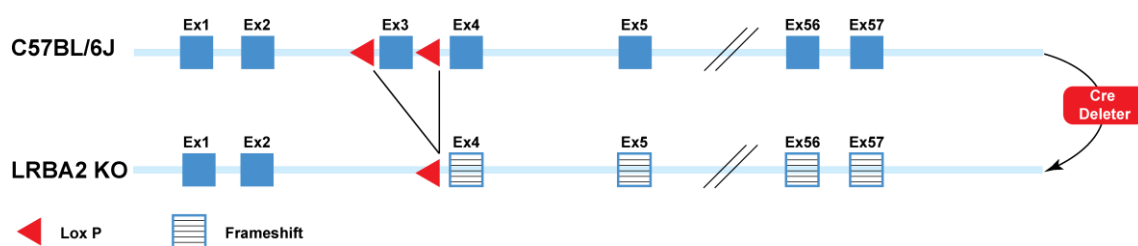


Figure M. 1: LRBA2 KO generation

Cre-mediated excision of exon 3 of *Lrba2* gene leads to a frameshift mutation and deletion of LRBA2 expression.

Mice of either sex, were studied from postnatal day 15 to 21 for the first two studies and for the LRBA2 study the age is mentioned in the figure legends. Animals were genotyped, and re-genotyped post experiments, using PCR. All experiments were performed in compliance with the guidelines dictated by the German animal welfare act and were approved by the board for animal welfare of the University Medical Center Göttingen and the animal welfare office of the state of Lower Saxony.

To facilitate easy visualization the following colour code is used in the thesis to present data from different genotypes. Wildtype data are presented in black, PicMut in red, PicBsn in green, RIM-BP2 KO in blue and LRBA2 KO in magenta (Figure M. 2).

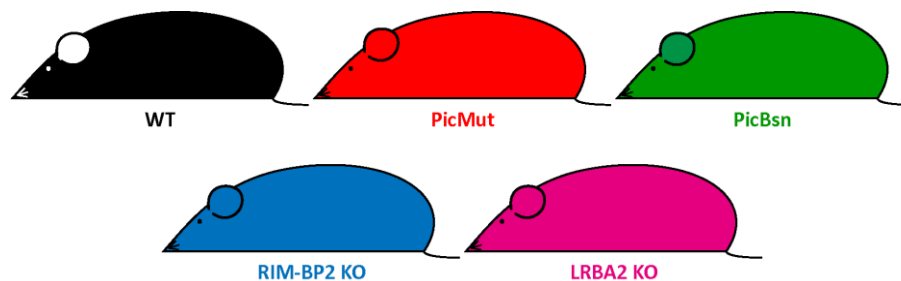


Figure M. 2: Colour code used in the thesis for different genotypes

Wildtype data are presented in black, PicMut in red, PicBsn in green, RIM-BP2 KO in blue and LRBA2 KO in magenta.

3.2 *in vitro* electrophysiology

Slice preparation: Acute parasagittal slices (150 μ m) from the cochlear nucleus were obtained (Figure M. 3) as described previously (Schulz et al., 2014). Briefly, after sacrifice by decapitation, brains were dissected out and quickly immersed in ice-cold low Na⁺ and low Ca²⁺ cutting solution containing (in mM): 50 NaCl, 26 NaHCO₃, 120 sucrose, 1.25 NaH₂PO₄.H₂O, 2.5 KCl, 20 glucose, 0.2 CaCl₂, 6 MgCl₂, 0.7 Na L-ascorbate, 2 Na pyruvate, 3 myo-inositol, 3 Na L-lactate with pH adjusted to 7.4 and osmolarity of around 310mOsm/l. After removal of the meninges from the ventral face of the brainstem, the two hemispheres were separated by a midsagittal cut and the forebrain was removed at the pons-midbrain junction. The brain blocks containing brain stem and cerebellum were then glued (cyanoacrylate glue; Loctite 401, Henkel) to the stage of a Leica (Wetzlar, Germany) VT

Materials and methods

1200S vibratome such that the medial side was glued on, the ventral side was facing the blade and the lateral side was facing upwards, submerged in ice-cold cutting solution. For sectioning, the blade was positioned at the height of cerebellar flocculus and sections were cut at a blade feed rate of 0.02mm/s with an amplitude of 1.50mm. Slices were incubated for 30min in artificial cerebrospinal fluid (aCSF) maintained at 35°C, and then kept in aCSF at room temperature (22-24°C) until recording. The composition of aCSF was identical to the cutting solution except for (in mM): 125 NaCl, 13 glucose, 1.5 (2 for RIM-BP2) CaCl₂ and 1 MgCl₂ and contained no sucrose. The pH of the solution was adjusted to 7.4 and osmolarity was around 310mOsm/l. All solutions were continuously aerated with carbogen (95% O₂, 5% CO₂).

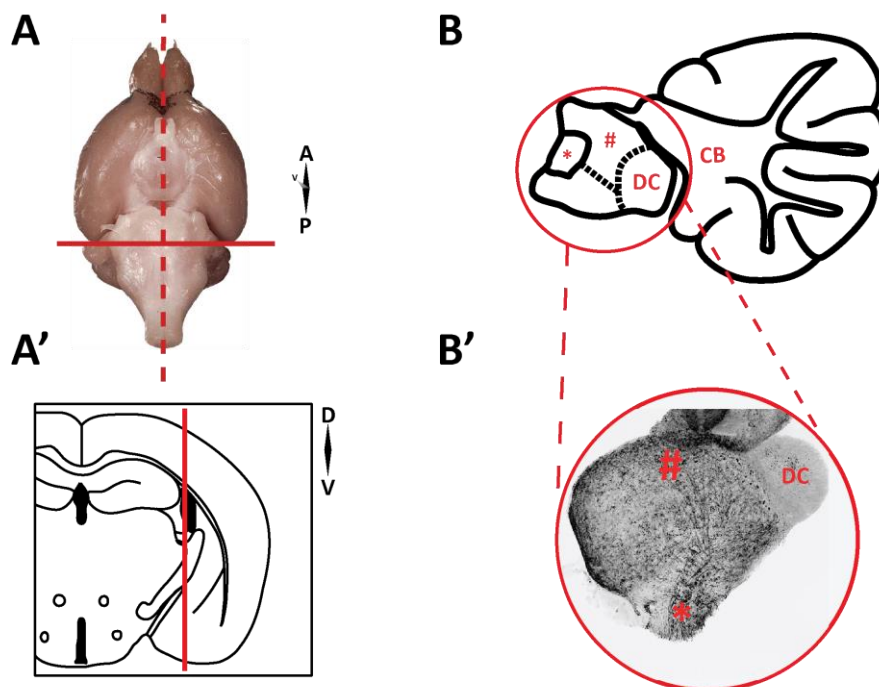


Figure M. 3: Illustration of the sagittal slice preparation of the aVCN

(A) Ventral aspect of a mouse brain. Dotted line indicates the midsagittal cut and the solid line demarcates the level at which aVCN is present. (A') Coronal section of the mouse brain with the solid line showing the target region for slicing. (B) Sagittal section of the mouse brain highlighting the cochlear nucleus, attached to the cerebellum. (B') Example of a cochlear nucleus slice as seen under the microscope (10x magnification) while recording. A' and B adapted from Paxinos and Franklin, 2001. #: aVCN (anterior ventral cochlear nucleus), DC: dorsal cochlear nucleus, CB: cerebellum, *: 8th cranial nerve (auditory vestibular nerve). Arrows indicate orientation - A: anterior, D: dorsal V: ventral.

Electrophysiology: Patch-clamp recordings were made from BCs of aVCN using EPC10 USB patch-clamp amplifier controlled by the Patchmaster software (HEKA Elektronik, Lambrecht/Pfalz, Germany). Sampling interval and filter settings were 25 μ s and 7.3kHz respectively. Cells were visualized by differential interference contrast (DIC) microscopy through a 40x water-immersion objective (NA 0.8; Zeiss, Oberkochen, Germany) using an Axioscope 2 FS plus microscope (Zeiss, Oberkochen, Germany). All experiments were conducted at a temperature of 33-35°C, maintained by constant superfusion (flow rate 3-4ml/min) of aCSF, heated by an inline solution heater (SH-27B with TC-324B controller; Warner Instruments, Hamden, CT, USA) and monitored by a thermistor placed between the inflow site and the slice, in the recording chamber.

Patch pipettes were pulled with P-87 micropipette puller (Sutter Instruments Co., Novato, CA, USA) from borosilicate glass capillaries with filament (GB150F, 0.86x1.50x80mm; Science Products, Hofheim, Germany). Open tip pipette resistance was 1.5-3 M Ω when filled with intracellular solution containing (in mM): 115 K-gluconate, 10 HEPES, 8 EGTA, 10 Na₂Phosphocreatine, 4 ATP-Mg, 0.3 GTP-Na, 4.5 MgCl₂, 10 NaCl and 1 N-(2,6-dimethylphenyl carbamoylmethyl)triethylammonium chloride (QX-314; Alomone Labs, Jerusalem, Israel) to block sodium channels, with a pH of 7.35 and an osmolarity of 300mOsm/l. Additionally, 1mM of fluorescent dye Alexa-488 (Invitrogen) was added to the recording pipette and cell structure was examined during experiments using a HXP 120 mercury lamp, with an FITC filter set (Semrock). Cells were voltage-clamped at a holding potential of -70mV, corrected for a liquid junction potential of 12mV. Mean series resistance was around 5M Ω and was compensated up to 70% with a 10 μ s lag. Presynaptic auditory nerve fibers were minimally stimulated with a monopolar electrode in a patch pipette filled with aCSF, placed at a distance of at least one cell diameter from the cell being recorded. Stimulating currents of 10-20 μ A were delivered through a stimulus isolator (A360 World Precision Instruments, Sarasota, FL, USA). During recordings, for the Piccolo and Bassoon study, bath solution (aCSF) was supplemented with: 1mM Kynurenic acid sodium salt (Abcam Biochemicals, Cambridge, UK), a low-affinity AMPAR antagonist, to prevent receptor saturation/desensitization, 100 μ M Cyclothiazide (CTZ; BioTrends, Wangen, Zurich), a positive allosteric AMPAR modulator, to prevent receptor desensitization, 10 μ M Bicuculline

Materials and methods

methchloride, a GABA_A receptor antagonist and 2 μ M Strychnine hydrochloride, a glycine receptor antagonist. For RIM-BP2 study, aCSF was supplemented with 10 μ M Strychnine hydrochloride only. Unless stated otherwise, chemicals were purchased from Sigma-Aldrich (St. Louis, USA).

3.3 Immunohistochemistry and confocal imaging

Brainstem immunohistochemistry: Animals were transcardially perfused with 2% freshly prepared ice-cold paraformaldehyde (2% PFA, 2N NaOH, 15% picric acid, 0.1M phosphate buffer). The fixed brain was then removed and brainstem was dissected with a coronal cut few millimetres nasal to the junction between occipital cortex and cerebellum. The brain block was washed overnight in 30% sucrose solution in PBS. For sectioning, the brain block was embedded in Tissue Tek Cryomatrix (Thermo Fisher Scientific, Waltham, MA, USA) and then fixed on the stage of the cryostat (Figocut E cryotome, Reichert-Jung, Depew, NY, USA) such that the caudal aspect was facing upwards and the dorsal side was towards the blade. Advancing from caudal to nasal, 30 μ m coronal sections (Figure M. 4) were cut (chamber temperature: -20°C, object temperature: -22°C) and discarded until the appearance of the 7th cranial nerve. Subsequent sections, containing aVCN were collected onto electrostatically charged microscope slides (SuperFrost Plus, ThermoFisher Scientific, MA, USA). For parallel processing, one slice of each genotype was collected per slide. Thereafter, the slices were washed for 10min in PBS and incubated in Goat Serum Dilution Buffer (GSDB; 16% normal goat serum, 450mM NaCl, 0.3% Triton X-100, 20mM phosphate buffer, pH 7.4) for 1h, followed by incubation in primary antibodies (see below) diluted in GSDB, for 3h, in a wet chamber at room temperature. After washing 2 x 10min with wash buffer (450mM NaCl, 0.3% Triton X-100, 2mM phosphate buffer) and 2 x 10min with PBS, the slices were incubated with secondary antibodies (see below) diluted in GSDB, for 1h, in a light-protected wet chamber at room temperature. The slices were then washed 2 x 10min with wash buffer, 2 x 10min with PBS and 1 x 10 min in 5mM phosphate buffer, and finally mounted with a drop of fluorescence mounting medium based on Mowiol 4-88 (Carl Roth, Karlsruhe, Germany) and covered with a thin glass coverslip.

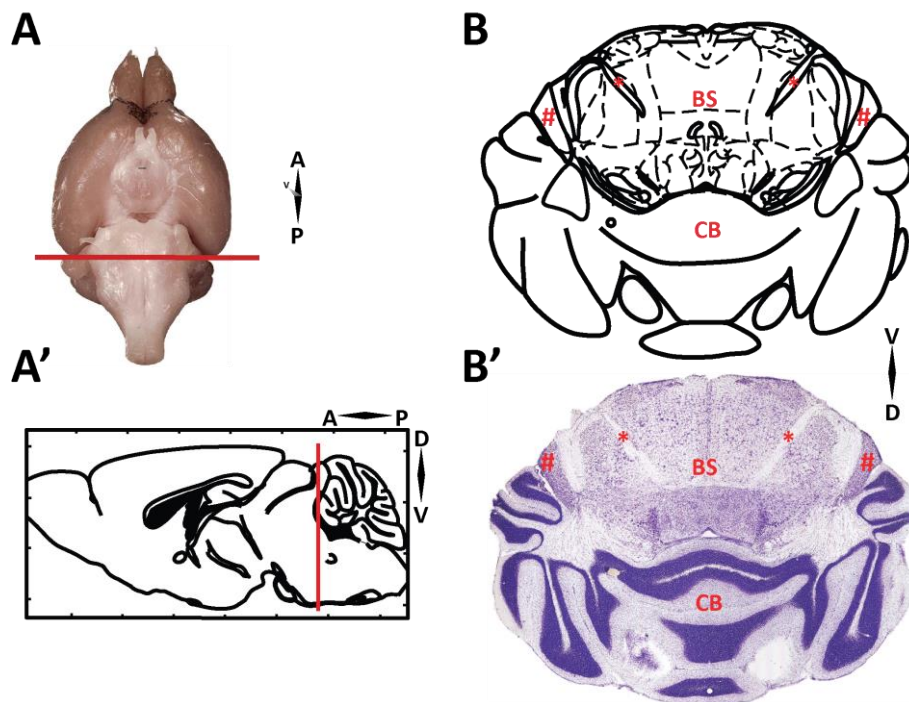


Figure M. 4: Illustration of the sagittal slice preparation of the aVCN

(A) Ventral aspect of a mouse brain with the solid line indicating the point at which the coronal sections were cut in the mouse brain. (A') Sagittal section of the mouse brain with the solid line showing the target region for slicing. (B-B') Coronal section of the mouse brain showing the aVCN and the 7th cranial nerve used as a landmark. A'-B' adapted from Paxinos and Franklin, 2001. #: aVCN (anterior ventral cochlear nucleus), BS: brainstem, CB: cerebellum, *: 7th cranial nerve (facial nerve). Arrows indicate orientation - A: anterior, D: dorsal V: ventral.

Inner hair cell immunohistochemistry: Apical turns of freshly dissected organ of Corti were fixed in 4% formaldehyde for 10 min and processed as described for fixed brain slices.

Primary antibodies: rabbit anti-Piccolo (Antibody #1; 1:200), guinea pig anti-Piccolo (Antibody #2; 1:200), mouse anti-Otoferlin (1:1000; Abcam Biochemicals, Cambridge, UK), guinea pig anti-VGLUT1 (1:500), rabbit anti-VGLUT1 (1:1000), mouse anti-Gephyrin (1:500), mouse anti-Sap7f407 to Bassoon (1:500; Abcam, Cambridge, UK), guinea pig anti-Bassoon (1:500), mouse anti-calretinin (1:300; Swant, Marly, Switzerland), guinea pig anti-VGAT (1:600), rabbit anti-Munc13-1 (1:200), rabbit anti-RIM1 (1:200), rabbit anti-RIM2 (1:200), rabbit anti-CAST (1:200). Unless stated otherwise, primary antibodies were purchased from Synaptic Systems, Göttingen, Germany.

Secondary antibodies: AlexaFluor488-, AlexaFluor568- and AlexaFluor647-labeled antibodies (1:200; Invitrogen).

Materials and methods

Confocal images were acquired using a laser-scanning confocal microscope (Leica TCS SP5; Leica Microsystems) equipped with 488 nm (Ar) and 561/633 nm (He-Ne) lasers and 63x/1.4 NA oil-immersion objective. Samples of genotypes: PicWT and PicMut were processed and imaged in parallel with the same settings.

3.4 *in vivo* recordings

Auditory brainstem response (ABR): Animals were anesthetized intraperitoneally with a combination of ketamine (125mg/kg) and xylazine (2.5mg/kg) and their core temperature was maintained at 37°C using a rectal temperature-controlled heating blanket (Hugo Sachs Elektronik; Harvard Apparatus). Additionally, their heart rate was constantly tracked to monitor the anesthesia. The electrode configuration of three subcutaneous needles was the following: the active electrode was positioned underneath the pinna, the reference electrode on the vertex and the ground electrode near the tail. For stimulus generation, presentation, and data acquisition TDT System II (Tucker-Davis Technologies) run by BioSig32 software (TDT) was used. Sound pressure levels were provided as dB SPL RMS (tonal stimuli) or dB SPL peak equivalent (PE, clicks) and were calibrated using a ¼ inch microphone (D 4039, Brüel and Kjaer GmbH). ABRs were obtained as an average of 2 repetitions of 2000 responses to tone bursts (10ms plateau, 1ms \cos^2 rise/fall) of increasing frequencies: 4, 6, 8, 12, 16, 24 and 32kHz presented at 40Hz or clicks of 0.03ms presented at 20Hz or 100Hz in the free field ipsilaterally using a JBL 2402 speaker (JBL GmbH & Co.). The potential difference between vertex and mastoid subdermal needles was amplified (50,000 times), filtered (low pass: 4kHz, high pass: 400Hz) and sampled at a rate of 50kHz for 20ms. ABR threshold was determined with 10dB precision, as the lowest stimulus intensity that evoked a reproducible response waveform in both traces by visual inspection.

Distortion product otoacoustic emissions (DPOAE): The ED1/EC1 speaker system (Tucker-Davis) was used to generate two continuous primary tones at frequency1 (f_1 : 10, 13.3, 18.9kHz) frequency2 (f_2) in the relation: $f_2=1.2 \times f_1$ and the respective sound intensities followed the rule: $\text{Intensity}_2=\text{Intensity}_1+10\text{dB}$. The two primary tones were coupled into the ear canal by a custom-made probe containing an MKE-2 microphone (Sennheiser) and adjusted to the desired sound intensities at the position of the ear drum as mimicked in a

mouse ear coupler. The microphone signal was amplified and digitalized (DMX 6 Fire; Terratec), and analyzed by fast Fourier transformation (MATLAB; MathWorks).

Recordings from single spiral ganglion neurons (SGNs): Mice were anesthetized (urethane 1.32 mg/kg, xylazine 5mg/kg, and buprenorphine 0.1mg/kg injected intraperitoneally), tracheotomized and placed in a custom-made head-holder. Their body temperature was maintained by heating the soundproof chamber to 26°C and by a custom-designed heat plate controlled by a rectal temperature probe. An opening was made in the left occipital bone and the cerebellum was partially removed. Subsequently, SGNs were stereotactically approached through the cochlear nucleus with a high-impedance glass electrode filled with 3M NaCl and 2% methylene blue. 50ms noise burst search stimuli of 80dB for wild-type and 90-100dB for LRBA2 KO were presented at 5Hz through a loudspeaker (JBL2402) to elicit spiking of auditory neurons. Upon detection of a sound-responsive unit, spontaneous firing rates were determined in silence for 10 – 30s. Tuning curves were obtained by varying stimulus intensities and frequencies of 15ms tone bursts, to estimate the best threshold of hearing and the characteristic frequency with a 1/32 octave and 2dB precision (Jing et al., 2013). In LRBA2 mutants, the automatic algorithm often failed because thresholds were too close to the maximum speaker output. In these cases, the best frequency was determined manually and the threshold was defined as the lowest intensity to which rates clearly increased over spontaneous rate in the rate-intensity function which employed 25 repetitions of 50ms tone bursts at 5Hz for each 5dB step. Post-stimulus time histograms to 50ms tone burst stimulation or paired stimuli (forward masking) were obtained at the characteristic/best frequency at sound intensities at which spike rates were mostly saturated: 30dB above threshold in WT and at least 10dB above threshold in KO.

SGNs were differentiated from cochlear nucleus neurons by (i) the electrode position (>1200µm below the surface of cochlear nucleus), (ii) their primary-like PSTHs to suprathreshold 50ms tone bursts presented at the characteristic/best frequency and (iii) their irregular firing pattern, as confirmed by a coefficient of variance of inter-spike interval of steady state firing response, >0.5.

Materials and methods

Electrocochleography: was performed by Dr. N. Strenzke. Mice were prepared for recording as stated for the SGN recordings. The Tucker Davis System III hardware was used, operated by custom-written Matlab software and a JBL2402 loudspeaker. For electrocochleography, the left bulla was opened to place a silver ball electrode on the round window membrane and responses to 100 clicks or 12ms tone bursts were amplified (50 times, custom-built amplifier) and sampled at a rate of 50kHz for 20ms. The summing potential (notch filtered for stimulus frequency) and cochlear microphonic amplitudes (low-pass filter: stimulus frequency/4) were determined as the mean or peak to peak amplitude in a window 7-11ms following stimulus onset, respectively.

3.5 Data analysis

Electrophysiology data were analyzed using Igor Pro (Wavemetrics, Lake Oswego, OR, USA), Mini Analysis (Synaptosoft Inc., Fort Lee, NJ, USA) and GraphPad Prism software (La Jolla, CA, USA). Confocal images were analyzed using NIH ImageJ software (Schneider et al., 2012), Imaris (Bitplane AG, Zurich, Switzerland) and custom Matlab (Mathworks) programs. Endbulb terminals were tracked and counted visually using ImageJ from calretinin-stained confocal image stacks. Figures were assembled for display using Adobe Illustrator (Adobe Systems, Munich, Germany). Means are presented \pm S.E.M. Statistical significance between groups was determined by either unpaired Student's t-test (in case of normally distributed data with comparable variances between the groups) or Wilcoxon rank sum test (when data distribution did not satisfy the criteria). Normality of distribution was tested with Jarque-Bera test and variances were compared with F-test. For multiple comparison, parametric data were tested for significance by 1-way ANOVA with post-hoc correction with Tukey's multiple comparison test. Non-parametric data were tested for significance by Kruskal-Wallis test with post-hoc correction with Dunn's multiple comparison test. *, **, ***, **** indicate $p < 0.05$, 0.01 , 0.001 and 0.0001 respectively.

Chapter 1

Role of Piccolo in high frequency transmission at a central
auditory synapse – the endbulb of Held

1a Introduction

Active zones (AZs) are specialized regions at the presynaptic terminals where neurotransmitter release occurs. AZs feature an electron-dense meshwork of proteins called the Cytomatrix of the AZ (CAZ). CAZ comprises of multi-domain protein families like: Munc13s, Rab3-interacting molecules (RIMs), RIM-binding proteins (RIM-BPs), CAST/ELKS proteins, Piccolo/Aczonin and Bassoon, and Liprins- α (Gundelfinger and Fejtova, 2012). The two largest members (>400kDa) of the CAZ, Piccolo (Fenster et al., 2000) and Bassoon (tom Dieck et al., 1998), are vertebrate-specific and structurally similar. They play an integral role in AZ assembly and scaffolding (Gundelfinger et al., 2016; Südhof, 2012), synaptic vesicle (SV) clustering (Mukherjee et al., 2010), presynaptic protein ubiquitination and degradation (Waites et al., 2013), and CtBP1-mediated activity-regulated gene expression via synapse-to-nucleus signaling (Ivanova et al., 2015, 2016). Piccolo (Figure 1b. 1A) and Bassoon, share 10 highly conserved regions, Piccolo Bassoon Homology domains (PBH) (tom Dieck et al., 1998; Fenster et al., 2000; Wang et al., 1999) containing Zn finger and coiled-coiled (CC) domains, which might explain partial overlap in function. However, despite their close homology, Piccolo has additional features that may ascribe unique functions to it, divergent from Bassoon.

As introduced earlier in section 2.3.3. Piccolo uniquely interacts with actin-binding proteins like Profilin2 (Waites et al., 2011; Wang et al., 1999) and Daam1 (Wagh et al., 2015), and hence regulates dynamic assembly of F-actin within the presynaptic terminal (Wagh et al., 2015; Waites et al., 2011). Actin has been a longstanding candidate for regulation of SV dynamics involved in exocytosis and endocytosis (Lee et al., 2012; Nguyen et al., 2012; Sakaba and Neher, 2003; Soykan et al., 2017; Watanabe et al., 2013). Hence, interactions with actin might indicate a role of Piccolo in translocating SV within the nerve terminal thereby regulating SV dynamics and synaptic transmission. Piccolo also interacts with its N-terminal glutamine-rich (Poly Q) motif to Abp1 (Fenster et al., 2003), which binds to endocytic GTPase Dynamin (Kessels et al., 2001). And through a region between its first and second CC domains, Piccolo interacts with GIT1 (Kim et al., 2003), which is associated with endocytic adaptor protein Stonin2 (Podufall et al., 2014). In addition, to its potential role

through actin-assembly, Piccolo's interactions with Abp1 and GIT1 also link it to the regulation of vesicle endocytosis. Unlike Bassoon, Piccolo additionally has a C-terminal PDZ domain and two C-terminal C₂ domains (C₂A and C₂B). The PDZ domain has been linked to exocytosis in pancreatic β -cells (Fujimoto et al., 2002; Shibasaki et al., 2004). Both C₂ domains were reported to bind to Ca_v1.2 L-type voltage-dependent Ca²⁺ channels (Shibasaki et al., 2004). Moreover, the C₂A domain was indicated to act as a low-affinity Ca²⁺ sensor for exocytosis, making Piccolo a candidate for detecting Ca²⁺ build-up during high frequency stimulation (Garcia et al., 2004; Gerber et al., 2001; Schoch and Gundelfinger, 2006). While several hypotheses have been put forward for the function of Piccolo, it remains challenging to unravel its physiological role(s). One study based on RNAi implicated Piccolo as an inhibitor of exocytosis (Leal-Ortiz et al., 2008), while the other, that generated the mouse mutant (Mukherjee et al., 2010) employed in this study revealed a role in SV clustering in conjunction with Bassoon, but failed to unmask any major exocytosis phenotype.

Here, the consequences of genetic Piccolo disruption were studied at the first central auditory synapse - the endbulb of Held synapse (von Gersdorff and Borst, 2002; Yu and Goodrich, 2014), formed by the spiral ganglion neurons (SGNs) synapsing onto the bushy cells (BCs) of the anterior ventral cochlear nucleus (aVCN) (Figure 1b. 1B). These large calyceal synapses typically employ more than 100 AZs for reliable and temporally precise signal transmission at frequencies of hundreds of Hertz (Trussell, 1999; Wang et al., 2011). Given the high functional demand, these synapses seem ideally poised for unveiling any discrepancies in synaptic transmission due to molecular perturbation. Here a combination of electrophysiological analysis and studies of the molecular composition of the AZ in endbulbs of Piccolo-deficient mice, indicates a role of Piccolo in promoting SV replenishment to the RRP and a, likely compensatory, up-regulation of Bassoon at Piccolo-deficient synapses.

Apart from deciphering unique function(s) of Piccolo independent of Bassoon at the active zone, this study briefly looks at the changes in synaptic transmission, with an additional Bassoon manipulation (Altrock et al., 2003b). Unlike Piccolo, Bassoon has been the focus of extensive investigation focused solely on its function and not just its role in conjunction with Piccolo (Ivanova et al., 2016; Mukherjee et al., 2010; Waites et al., 2013).

In sensory synapses, Bassoon is essential for tethering the synaptic ribbon at the active zones both at retinal photoreceptors (Dick et al., 2003; tom Dieck et al., 2005) and cochlear inner hair cells (Khimich et al., 2005). Bassoon was also found to maintain the Ca²⁺ channel clustering and synaptic vesicle pool at the presynapse (Frank et al., 2010), and hence establish reliable signal transmission to the auditory nerve fibers (Buran et al., 2010; Jing et al., 2013). In central synapses, Bassoon has been shown to localize P/Q type Ca²⁺ channels at the active zone (Davydova et al., 2014), and its absence was associated with increase in the number of silent synapse in hippocampal cultures (Altrock et al., 2003b), and impaired vesicle replenishment (Hallermann et al., 2010b; Schulz et al., 2014). Most recently, Bassoon has been proposed to be a regulator of presynaptic autophagy (Okerlund et al., 2017).

In context of the extensive research on the function of Bassoon, and its role together with Piccolo this study focuses on bringing forth the function of Piccolo in synaptic transmission. Since, the two proteins compensate for each other's absence (Schulz et al., 2014 and this study), studying Piccolo deficiency at the synapse, followed by a partial Bassoon loss in addition; the aim is to identify the non-overlapping functions of the proteins.

1b Results

1b.1 Perturbation of Piccolo expression in central but not peripheral auditory synapses

This study employed constitutive Piccolo mutants with a targeted deletion of exon 14 of Pclo gene and insertion of neomycin resistance cassette in the adjacent 3' intron, described previously (hereafter dubbed "PicMut"), which lowers the protein levels of Piccolo to approximately 5% in the brain (Mukherjee et al., 2010). A shorter, ~330kDa, C-terminal truncated Pclo splice variant, Piccolino (Figure 1b. 1A), is the predominant Pclo isoform at the ribbon synapse of inner hair cells (IHC) (Regus-Leidig et al., 2013), directly preceding the endbulb of Held (Figure 1b. 1B). Labeling with antibody #2 (directed against a central epitope, Figure 1b. 1A), showed that IHC ribbon synapses in PicMut still express Piccolino (Figure 1b. 1C), while the full-length variant, Piccolo, was absent (identified by antibody #1 directed against a C-terminal epitope, Figure 1b. 1A, C').

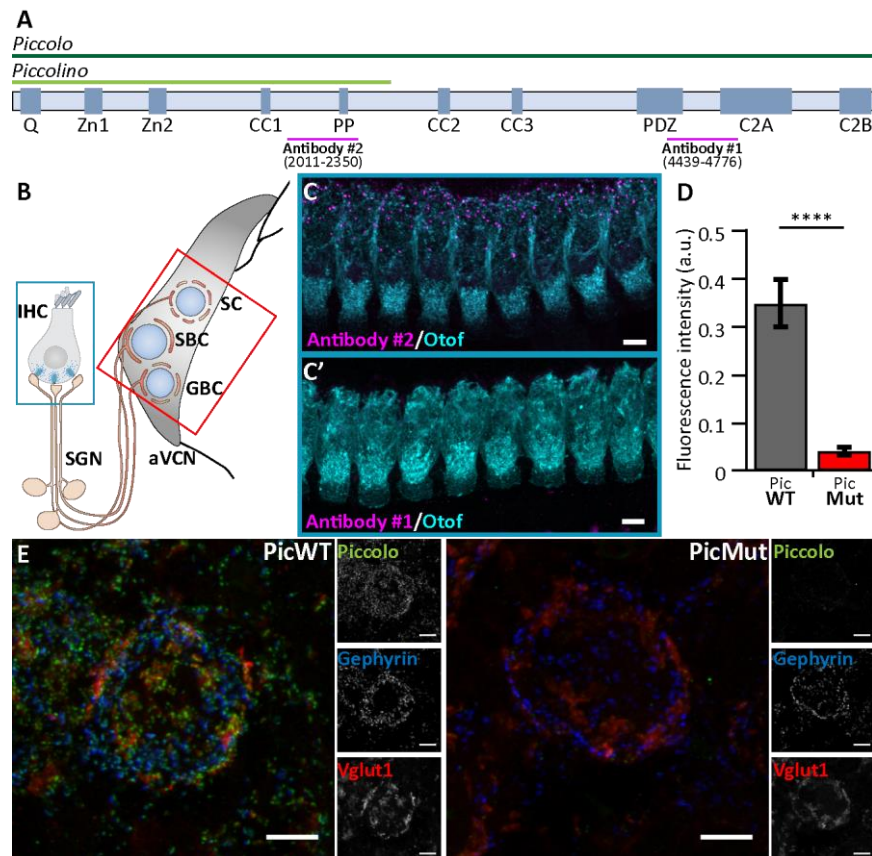


Figure 1b. 1: Selective expression of Piccolo (Aczonin) in central synapses

(A) Domain structure of Piccolo (dark green line) and its shorter isoform Piccolino (light green line). Magenta lines illustrate the position of antigenic peptides used to raise Piccolo antibodies employed in this study. Antibody #1 binding to the C-terminus, selectively identifies Piccolo, while antibody #2 binding to the central region recognizes both Piccolo and Piccolino. (B) Scheme of the site of investigation (not drawn to scale): the endbulbs of Held are formed by the auditory nerve fibers (central neurites of SGN) on bushy cells of the aVCN. SGNs receive their input from ribbon-type AZs of inner hair cells (IHC, blue box) of the organ of Corti. Spherical bushy cells (SBC) and Globular bushy cells (GBC) receive different numbers of endbulbs. SGNs form bouton-like synapses on stellate cells (SC). (C) Preservation of Piccolino in the organ of Corti of PicMut mice: Maximal projection of confocal images show immunofluorescent puncta of Piccolino (C, antibody #2) in otoferlin (Otof)-labeled IHCs of the organ of Corti, while no Piccolo signal (C', antibody #1) is found. Scale bar – 5 μ m. (D) Reduced fluorescence intensity of Piccolo (antibody #1) puncta at the BCs of aVCN in PicMut (N=3; n=8) mice compared to PicWT (N=3; n=14) mice as obtained in maximum projections of confocal images. Our estimates for endbulb AZs built on identification of excitatory AZs by co-localization of Piccolo puncta with Vglut1 (maximal center of mass distance 0.4 μ m in xy and 1.2 μ m in z) and distinction of inhibitory AZs by their co-localization with Gephyrin (center of mass distance 0.3 μ m in xy and 0.9 μ m in z). N, number of animals; n, number of BCs. Error bars represent S.E.M. (**** - p-value < 0.0001, Wilcoxon rank sum test). (E) Reduced expression of Piccolo in PicMut: Maximum projection of confocal image stack of a bushy cell in PicWT (left) and PicMut (right) labeled for Piccolo (antibody #1), Vglut1 (excitatory synapses) and Gephyrin (inhibitory synapses). Scale bar – 5 μ m.

Recordings of (ABR) showed normal thresholds and unaltered amplitudes of the spiral ganglion compound action potential, reflected in wave I of the ABRs, indicating normal cochlear sound encoding (Figure 1b. 2).

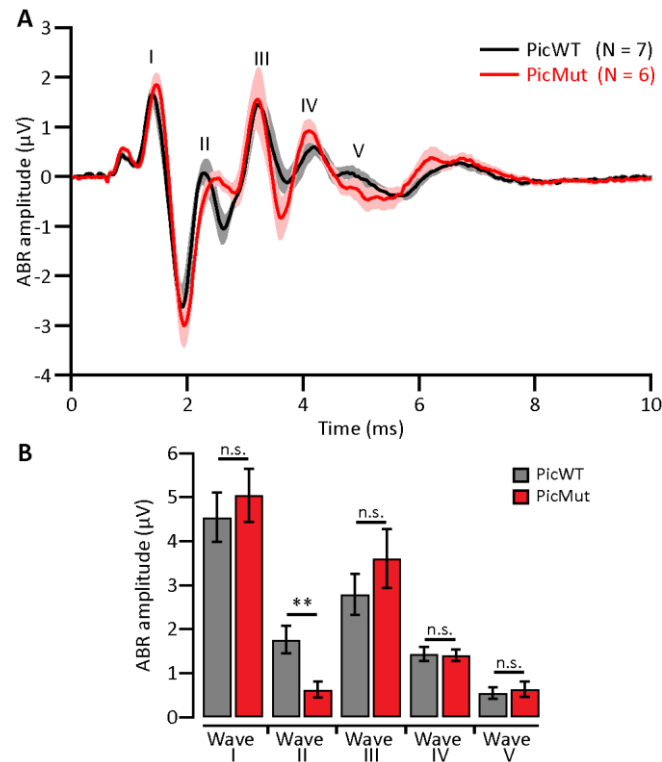


Figure 1b. 2: Auditory brainstem response (ABR) indicates preserved cochlear function but alteration in signal propagation at the cochlear nucleus in PicMut

(A) Grand averages (line) \pm S.E.M. (shaded area) of ABR waveform responses to 80dB click stimuli at a stimulus rate of 20Hz of PicWT (N=7) and PicMut (N=6) mice at P21-23. N is the number of animals. (B) Comparison of ABR wave amplitudes. In PicMut, wave I (compound action potential of spiral ganglion) has unaltered amplitude, but wave II thought to arise from activity in the cochlear nucleus demonstrates reduced amplitude. Interestingly, the later waves arising from downstream stations in the auditory pathway seem unaltered.

In contrast to IHCs, the excitatory AZs of the endbulb of Held synapse in the aVCN showed a near complete loss of Piccolo staining (10 % of control levels) indicating a major reduction of Piccolo expression at these central auditory synapses (D-E). The excitatory AZs at the aVCN were identified by co-localization of Piccolo with Vglut1, vesicular glutamate transporter1, (maximal center of mass distance 0.4µm in xy and 1.2µm in z), while inhibitory AZs were distinguished by co-localization with Gephyrin (maximal center of mass distance 0.3µm in xy and 0.9µm in z). This did not strictly differentiate AZs of endbulbs from those of

glutamatergic bouton endings, which, however, are much fewer in number (Gómez-Nieto and Rubio, 2009; Nicol and Walmsley, 2002). Therefore, and since Vglut1 is primarily associated with terminals of SGNs (Heeringa et al., 2016), estimates here were strongly dominated by endbulb AZs. Functionally, wave II of the ABRs, thought to arise from activity in the cochlear nucleus (Melcher and Kiang, 1996; Melcher et al., 1996a, 1996b) demonstrated reduced amplitude, suggesting a functional impairment of synaptic transmission from SGNs to the aVCN neurons (Figure 1b. 2). Interestingly, later ABR waves seemed unaltered suggesting potential compensation of Piccolo deficiency.

1b.2 Changes in molecular composition of the active zone upon Piccolo disruption

Further semi-quantitative immunohistochemistry was performed to analyze the effect of Piccolo disruption on the number of the endbulb of Held synapses and their AZs, as well as on the molecular composition of the AZs. For this analysis, PicWT and PicMut samples were strictly processed and imaged in parallel with the same settings. The number of endbulbs converging on to BCs was quantified by visually tracing and counting calretinin-stained endbulbs (Figure 1b. 3A) (Lohmann and Friauf, 1996), not differentiating between globular and spherical BCs. BCs of both genotypes received 3-4 endbulbs on average (3.67 ± 0.26 for PicWT and 3.56 ± 0.24 for PicMut, Figure 1b. 3B), which agrees with the number reported in the literature (Cao and Oertel, 2010; Schulz et al., 2014) for mice after onset of hearing (p15-p21).

Next, the number of excitatory AZs per endbulb was quantified. In stacks of confocal sections of BCs, the number of puncta immunofluorescent for the AZ markers (such as Bassoon, RIM1, RIM2 or Munc13-1), gave the total AZ count. Subtracting the number of immunofluorescent puncta juxtaposed with Gephyrin immunofluorescence (inhibitory AZ number, see above) from the total count of AZs yielded the number of excitatory AZs, which was unaltered in the PicMut synapses (455.16 ± 18.66 for PicWT and 426.40 ± 17.93 for PicMut, Figure 1b. 3D). Dividing this number by the average count of endbulbs gave the number of AZs per endbulb which was also comparable between the genotypes (124.14 for PicWT and 120.34 for PicMut) and agreed with previous reports (Nicol and Walmsley, 2002;

Schulz et al., 2014). Hence, there was no discernible change in the convergence of endbulbs to BCs or the number of AZs therein.

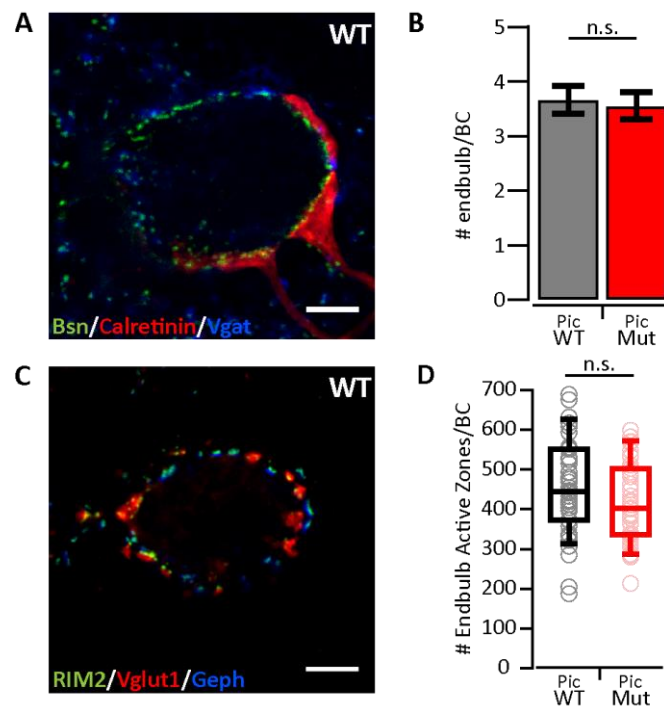


Figure 1b. 3: Number of endbulbs and endbulb AZ per bushy cell in aVCN

(A) Confocal section of a bushy cell in PicWT labeled with Bassoon (Bsn; AZ marker), Calretinin (endbulbs of Held) and Vgat (inhibitory presynaptic terminals). (B) Number of endbulbs converging onto a bushy cell was quantified by visually tracing and counting calretinin-stained endbulbs. PicWT (N=2; n=12) and PicMut (N=2; n=9) receive comparable number of endbulbs (n.s. – p-value > 0.05, Student’s t-test). (C) Confocal section of a bushy cell in PicWT labeled with RIM2 (AZ marker), Vglut1 (excitatory synapses) and Gephyrin (Geph, inhibitory synapses). (D) Number of endbulb AZ (approximated from the # of excitatory AZs) per bushy cell quantified by subtracting the number of inhibitory AZs (AZ marker puncta juxtaposed with Gephyrin) from the total number of AZ marker puncta. Endbulb AZ number in PicWT (N=9; n=43) and PicMut (N=9; n=47) was comparable (n.s. – p-value > 0.05, Wilcoxon rank sum test). Data information: N, number of animals; n, number of BCs.

To study the changes in molecular composition the immunofluorescence intensities of the CAZ proteins Bassoon, RIM1, RIM2 and Munc13-1 were quantified. All CAZ proteins exhibited a spot-like fluorescence pattern around the BCs depicting AZs. Immunofluorescence intensities of Vglut1 and Gephyrin, used for identifying excitatory AZs, remained unchanged (Figure 1b. 4).

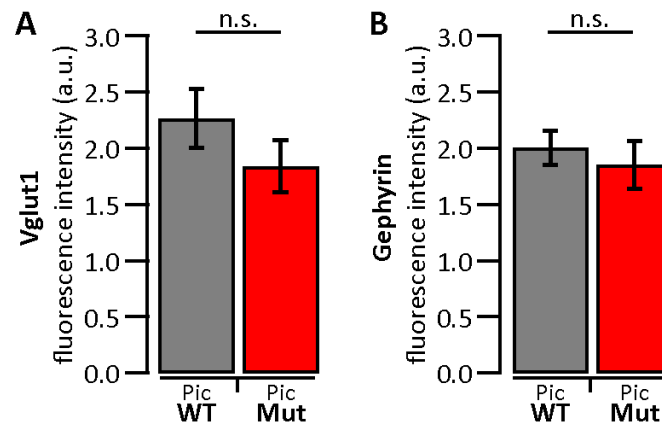


Figure 1b. 4: Unchanged immunofluorescence intensity of Vglut1 and Gephyrin in PicMut aVCN

(A) Quantification of fluorescence intensity of Vglut1 (staining excitatory synapses) in the confocal images used to analyze molecular composition of CAZ proteins in BCs of the aVCN (n.s. – p-value > 0.05, Wilcoxon signed rank test). (B) Quantification of fluorescence intensity of Gephyrin (staining inhibitory synapses) in the confocal images used to analyze molecular composition of CAZ proteins in BCs of the aVCN (n.s. – p-value > 0.05, paired Student's t-test). Data information: For paired samples of both Vglut1 and Gephyrin N=9; n = 17. N, number of animals; n, number of BCs.

Bassoon, a close homologue of Piccolo (Fenster et al., 2000), demonstrated significantly increased immunofluorescence intensity at both excitatory and inhibitory synapses (Figure 1b. 5A, B) in PicMut mice. Immunofluorescence intensities of RIM1 and RIM2 seemed overall weaker in PicMut mice, whereby RIM1 fluorescent intensity was significantly reduced at putative endbulb AZs and RIM2 at AZs of inhibitory synapses (Figure 1b. 5C-F). Munc13-1 immunofluorescence was slightly higher at AZs of inhibitory synapses in PicMut mice, while the intensity was not altered at endbulb AZs. It can be concluded that Piccolo disruption leads to a reduction in the abundance of RIM1 at AZs of endbulb synapses while Bassoon is upregulated, potentially as a compensatory mechanism.

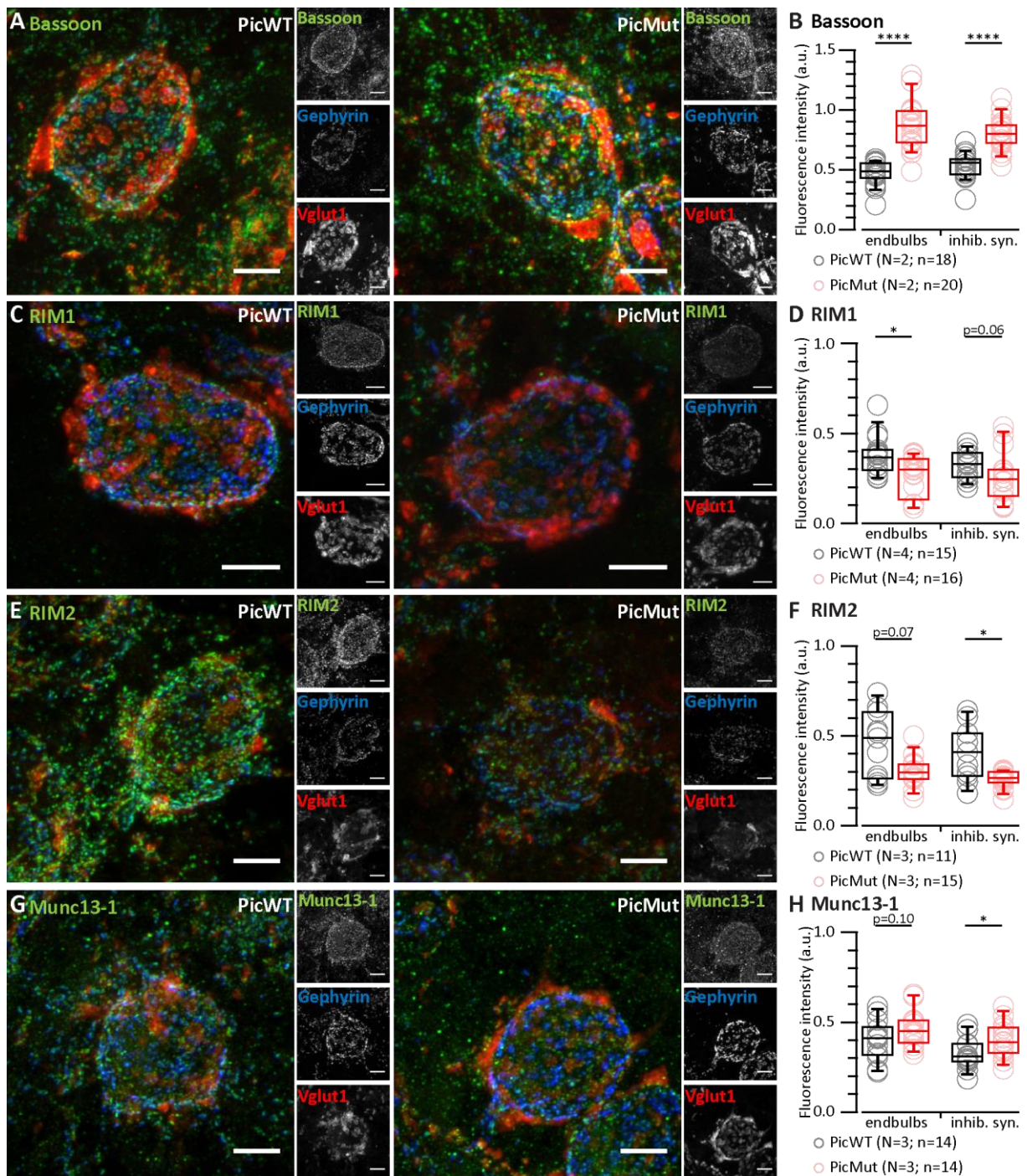


Figure 1b. 5: Molecular composition altered at aVCN synapses in PicMut

(A, C, E, G) Maximal projection of confocal image stacks of BCs in PicWT (left) and PicMut (right). Slices were labelled for different CAZ proteins: Bassoon (A), RIM1 (C), RIM2 (E) and Munc13-1 (G) and co-stained for Vglut1 (excitatory synapses) and Gephyrin (inhibitory synapses). (B, D, F, H) Quantification of fluorescence intensity of CAZ proteins at endbulbs and inhibitory synapses of BCs: Bassoon fluorescence intensity (B) was significantly increased at AZs of both endbulbs and inhibitory synapses in the mutant, RIM1 (D) fluorescence intensity was significantly lower at the endbulb AZs in mutant but tended to be lower at inhibitory AZs as well. RIM2 (F) fluorescence intensity tended to be

reduced at all AZs, but this reached significance only at inhibitory AZs. Munc13-1 (H) fluorescence intensity tended to be slightly increased, which reached significance only at inhibitory AZs. Data information: N, number of animals; n, number of BCs. All scale bars – 5 μ m. All data presented as box and whisker plots (median, lower/upper quartiles, 10-90 percentiles). Statistical significance between groups was determined by either unpaired Student's t-test (in case of normally distributed data with comparable variances between the groups) or Wilcoxon rank sum test (when data distribution did not satisfy the criteria). Normality of distribution was tested with Jarque-Bera test and variances were compared with F-test. * - p-value < 0.05, **** - p-value < 0.0001. PicWT and PicMut samples were strictly processed and imaged in parallel with the same settings.

1b.3 Piccolo disruption reduces the amplitude of evoked EPSCs at the endbulb of Held while leaving the eEPSC kinetics and miniature EPSCs unaltered

To determine the functional consequences of Piccolo disruption at the endbulb of Held synapse, synaptic transmission was studied in acute sagittal slices of the brainstem of PicMut and PicWT mice by recording EPSCs from BCs at postnatal days 15-21. BCs were distinguished from stellate cells (another major cell type in the aVCN) by the faster kinetics of their postsynaptic currents (Isaacson and Walmsley, 1995) and their characteristic short-term plasticity (Figure 1b. 10) (Chanda and Xu-Friedman, 2010). In addition to such functional identification, each recorded cell was filled with fluorescent dye Alexa 488 via the patch pipette for morphological distinction. BCs are spherical in appearance with one primary dendrite terminating in a dense bush-like dendritic tree (Figure 1b. 6) (Wu and Oertel, 1984), distinct from stellate cells, which are asymmetrical in shape and have multiple dendrites branching off in various directions giving them a star-like appearance.

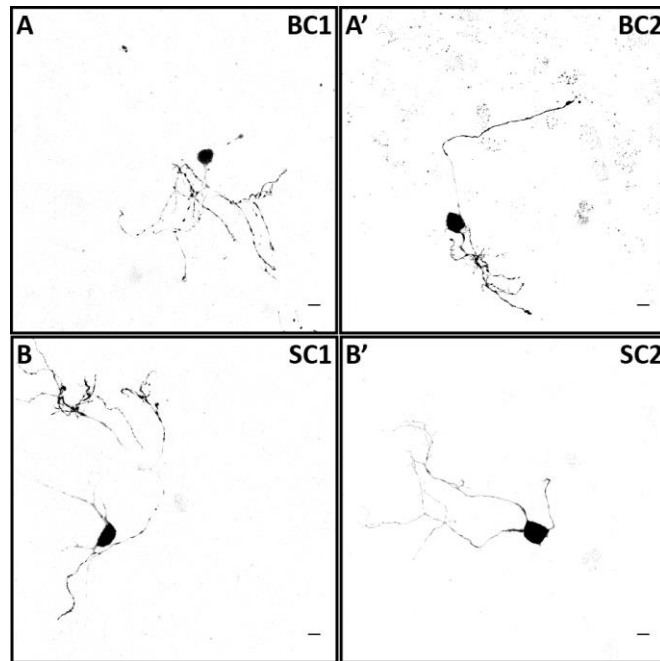


Figure 1b. 6: Morphological distinction between bushy cells and stellate cells of the aVCN

(A) Images of bushy cells (BC) filled with fluorescent dye Alexa 488 and fixed after the recording illustrating typical BC morphology, spherical with one primary dendrite ending in a dense bush-like dendritic tree. (B) Images of stellate cells (SC) filled with fluorescent dye Alexa 488 and fixed after the recording illustrating typical SC morphology, asymmetrical with multiple far-ranging dendrites branching off in different directions.

First the miniature EPSCs (mEPSC) were studied, in the presence of 1mM kynurenic acid (Kyn; Elmslie and Yoshikami, 1985) and 100 μ M cyclothiazide (CTZ; Yamada and Tang, 1993), to check if quantal size or kinetics of single vesicle release were altered at Piccolo-deficient endbulbs. mEPSCs were recorded as spontaneous events (Lu et al., 2007) in whole-cell recordings of BC that were voltage-clamped at -70mV (Figure 1b. 7, Table 1b. 1). We did not observe differences in the mEPSC amplitude (Figure 1b. 7B), kinetics (Figure 1b. 7B'-B''') and frequency (Figure 1b. 7B''''; $p > 0.05$ for all 3 quantities, Figure 1b. 7B-B'' Student's t-test, Figure 1b. 7B''''- B'''' Wilcoxon rank sum test).

Table 1b. 1: Miniature EPSC (mEPSC) amplitude and kinetics unchanged in PicMut

Parameter	PicWT	PicMut	p-value
Amplitude (pA)	60.82 ± 2.29	59.17 ± 2.10	0.60
10-90 Rise time (ms)	0.119 ± 0.003	0.116 ± 0.003	0.62
FWHM (ms)	0.24 ± 0.01	0.26 ± 0.01	0.27
Decay time (ms)	0.24 ± 0.01	0.28 ± 0.01	0.14
Frequency (Hz)	4.04 ± 0.41	4.11 ± 0.48	0.63

Data presented as mean (grand average of the means of all BCs) ± S.E.M. Statistical significance between groups was determined by either unpaired Student's t-test (in case of normally distributed data with comparable variances between the groups) or Wilcoxon rank sum test (when data distribution did not satisfy the criteria). Normality of distribution was tested with Jarque-Bera test and variances were compared with F-test. PicWT N = 23; n = 23, PicMut N = 17; n = 25 (N, number of animals; n, number of BCs).

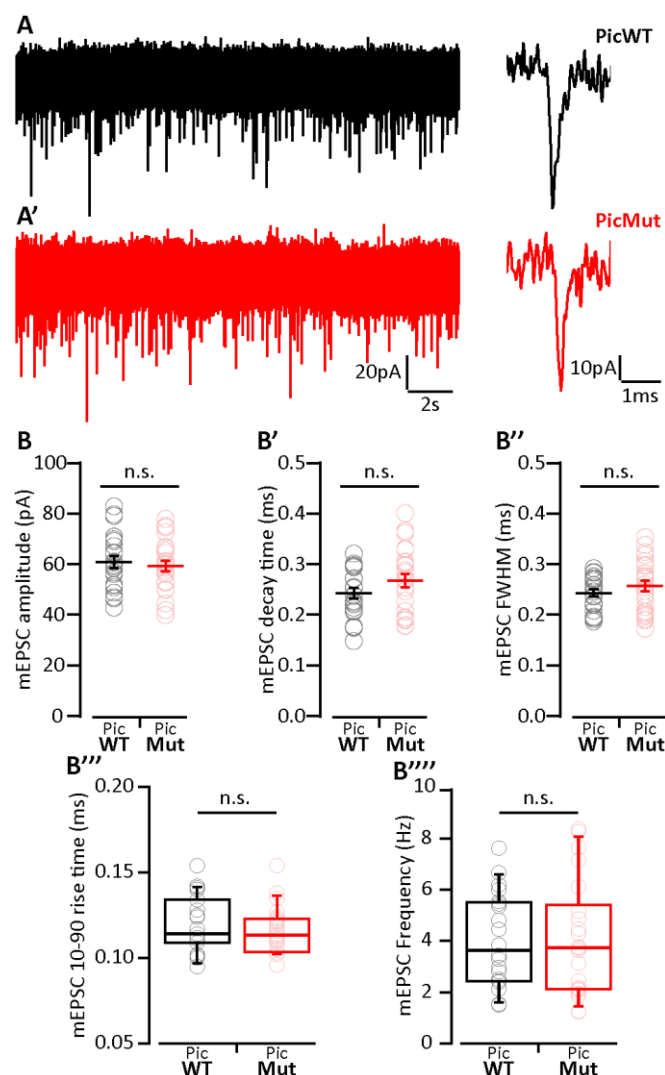


Figure 1b. 7: Miniature EPSC amplitude and kinetics preserved in PicMut synapses

(A) Representative traces of mEPSC: Continuous recording (left) and exemplary individual mEPSCs (right) for PicWT (A) and PicMut (A'). (B) Analysis of mEPSC: mEPSC amplitude (B), decay time (B'), full-width at half-maximum (FWHM; B''), rise time (B'''), and frequency (B''''') remain unaltered. Each data point represents the mean estimate of a given BC. Normally distributed data presented as mean (grand average of the means of all BCs) \pm S.E.M. (B, B', B''; n.s. – p-value > 0.05, Student's t-test). Non-normally distributed data presented as box and whisker plots (grand median (of the means of all BCs), lower/upper quartiles, 10-90 percentiles; B''', B'''''); n.s. – p-value > 0.05, Wilcoxon rank sum test). PicWT N = 23; n = 23, PicMut N = 17; n = 25 (N, number of animals; n, number of BCs).

Next, evoked synaptic transmission was investigated in the presence of 1mM Kyn and 100 μ M CTZ to avoid saturation and desensitization of AMPA receptors (Chanda and Xu-Friedman, 2010), respectively. Evoked EPSCs (eEPSC) were elicited by minimal electrical stimulation of the auditory nerve fibers by a monopolar electrode placed in the proximity of the recorded BC, whereby each stimulus is aimed to elicit one action potential in one endbulb (Yang and Xu-Friedman, 2008). To evaluate the importance of using Kyn and CTZ, paired pulse ratio (PPR) at the endbulb of PicWT and PicMut, in the presence and absence of the two drugs was compared. In this protocol, the recorded BC was presented with paired stimuli of two pulses separated by varying inter stimulus intervals of 3, 5 and 10ms. PPR is the ratio of the amplitude of EPSC elicited by the second pulse to the amplitude in response to the first pulse ($EPSC_2/EPSC_1$). Endbulbs of PicWT showed increased PPR in the presence of Kyn and CTZ only at an inter stimulus interval of 3ms, while at longer intervals of 5 and 10ms, the PPR was unchanged. Increased PPR implies a relief from receptor desensitization/saturation upon the application of the two drugs. This is in agreement with the previous studies (Chanda and Xu-Friedman, 2010; Yang and Xu-Friedman, 2008) reporting receptor desensitization at the endbulb for intervals <10ms. In contrast to the wildtype, endbulbs of PicMut mice showed an increased PPR at all three inter stimulus intervals in the presence of Kyn and CTZ. Since, the mutant demonstrated possible receptor desensitization, it was imperative to eliminate potential postsynaptic factors to focus on the presynaptic component of the study.

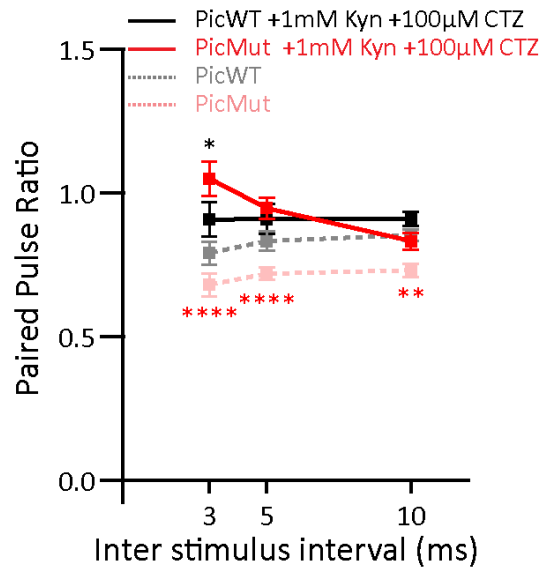


Figure 1b. 8: Paired pulse ratio (PPR) recorded with and without 1mM Kynurenic acid (Kyn) and 100µM Cyclothiazide (CTZ) demonstrating receptor desensitization and (or) saturation in PicMut

Data presented as mean (grand average of the means of all BCs) \pm S.E.M. Statistical significance between groups was determined by either unpaired Student's t-test (in case of normally distributed data with comparable variances between the groups) or Wilcoxon rank sum test (when data distribution did not satisfy the criteria). **** p-value < 0.0001, ** p-value < 0.01, * p-value < 0.05. **** - Significance between PicMut with and without Kyn and CTZ; *- Significance between PicWT with and without Kyn and CTZ. For sample size refer to Table 1b. 2

Table 1b. 2: Quantification of PPR recorded with and without 1mM Kynurenic acid (Kyn) and 100µM Cyclothiazide (CTZ)

Inter stimulus interval	PicWT +1mM Kyn +100µM CTZ	PicWT	p-value	PicMut +1mM Kyn +100µM CTZ	PicMut	p-value
3ms	0.91 \pm 0.06 (15)	0.79 \pm 0.04 (11)	0.02	1.05 \pm 0.06 (12)	0.68 \pm 0.04 (14)	1.30 x 10⁻⁵
5ms	0.91 \pm 0.05 (23)	0.83 \pm 0.03 (14)	0.13	0.95 \pm 0.04 (19)	0.72 \pm 0.02 (28)	9.19 x 10⁻⁶
10ms	0.91 \pm 0.02 (30)	0.85 \pm 0.02 (15)	0.08	0.83 \pm 0.03 (31)	0.73 \pm 0.02 (28)	0.008

Data presented as mean (grand average of the means of all BCs) \pm S.E.M. Statistical significance between groups was determined by either unpaired Student's t-test (in case of normally distributed data with comparable variances between the groups) or Wilcoxon rank sum test (when data distribution did not satisfy the criteria). Normality of distribution was tested with Jarque-Bera test and variances were compared with F-test. Sample size (number of BCs recorded) given in parentheses.

Importantly, the analysis eEPSC evoked by single stimulations (Figure 1b. 9, Table 1b. 2) revealed reduced eEPSC amplitude in BCs of PicMut mice (Figure 1b. 9B; $p < 0.01$, Wilcoxon rank sum test). The synaptic delay of eEPSCs and their kinetics of rise and decay remained unaltered (Figure 1b. 9C-F; $p > 0.05$, Student's t-test).

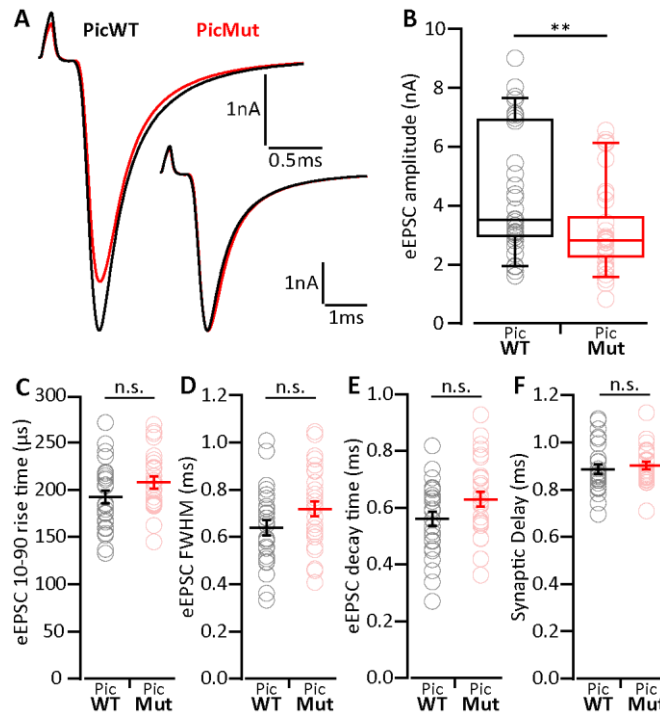


Figure 1b. 9: Reduced evoked EPSC amplitude in PicMut

(A) Average traces of evoked EPSC (eEPSC) in PicWT (black) and PicMut (red) showing a reduced eEPSC amplitude in the mutant. Inset: Average PicMut eEPSC trace scaled to the peak of the average wildtype trace demonstrating unaltered eEPSC kinetics in the mutant. Positive peak at onset of trace reflects the stimulation artifact. (B) Reduced eEPSC amplitude in PicMut ($N = 19$; $n = 36$) as compared to PicWT ($N = 21$; $n = 35$). Each data point represents the mean estimate of a given BC, box and whisker plots present grand median (of the means of all BCs), lower/upper quartiles, 10-90 percentiles). ** p -value < 0.01 , Wilcoxon rank sum test. (C-F) eEPSC kinetics: rise time (C), full-width at half-maximum (FWHM; D) and decay time (E), and synaptic delay (F) were not significantly altered in PicMut ($N = 19$; $n = 29$) as compared to PicWT ($N = 19$; $n = 28$). Data presented as grand average (of the means of all BCs) \pm S.E.M. (n.s. – p -value > 0.05 , Student's t-test). Data information: N , number of animals; n , number of BCs.

Table 1b. 3: Reduced evoked EPSC amplitude in PicMut

Parameter	PicWT	PicMut	p-value
Amplitude (nA)	4.43 ± 0.37	3.15 ± 0.25	0.002**
10-90 Rise time (ms)	0.19 ± 0.01	0.21 ± 0.01	0.10
FWHM (ms)	0.64 ± 0.03	0.72 ± 0.03	0.07
Decay time (ms)	0.56 ± 0.02	0.63 ± 0.03	0.06
Synaptic delay (ms)	0.89 ± 0.02	0.90 ± 0.02	0.63

Data presented as mean (grand average of the means of all BCs) ± S.E.M. Statistical significance between groups was determined by either unpaired Student's t-test (in case of normally distributed data with comparable variances between the groups) or Wilcoxon rank sum test (when data distribution did not satisfy the criteria). PicWT N = 19; n = 29, PicMut N = 19; n = 28 (N, number of animals; n, number of BCs).

1b.4 Reduced RRP size and a slower recovery from short-term depression in Piccolo mutants

Quantal size (mEPSC amplitude) being unaltered, the RRP size, release probability and pool dynamics were studied next to investigate the cause of the reduced eEPSC amplitude. For this, responses to high frequency train stimulation: 50 consecutive stimuli delivered at 100, 200 and 333Hz (in the presence of 1mM Kyn and 100µM CTZ) were employed. At all three frequencies, both PicMut and PicWT mice exhibited comparable short-term depression (Figure 1b. 10A-A'). Both genotypes, demonstrated similar kinetics of short term depression during train stimulation (Tau (τ), Table 1b. 4, Figure 1b. 10B-D). The paired pulse ratio (PPR) was not significantly altered at inter-stimulus intervals of 5ms and 2ms, but was lower at 10ms in PicMut (0.83 ± 0.03 PicMut vs. 0.91 ± 0.02 for PicWT, $p < 0.05$, Student's t-test, Table 1b. 4). The extent of depression assessed as the amplitude in the steady state reached after 30 train pulses was comparable ($EPSC_{30-50}/EPSC_1$, Table 1b. 4, Figure 1b. 10B-D).

Table 1b. 4: Comparison of pool size, vesicle replenishment, release probability and short-term depression at the endbulb of Held synapse in PicWT and PicMut

Frequency	Parameter	PicWT	PicMut	p-value
	q	60.82 pA	59.17 pA	0.59
100Hz	RRP (# vesicles)	300.76 ± 31.28	245.01 ± 24.22	0.22
	Repl.(#vesicles/ms)	1.79 ± 0.14	1.31 ± 0.11	0.007**
	P_r	0.26 ± 0.07	0.25 ± 0.02	0.59
	PPR	0.91 ± 0.02	0.83 ± 0.03	0.048*
	EPSC₃₀₋₅₀/EPSC₁	0.32 ± 0.03	0.28 ± 0.02	0.29
	τ (ms)	42.79 ± 3.31	48.72 ± 5.18	0.70
200Hz	RRP (# vesicles)	393.05 ± 46.09	265.40 ± 32.16	0.03*
	Repl.(#vesicles/ms)	2.11 ± 0.26	1.63 ± 0.15	0.21
	P_r	0.21 ± 0.02	0.20 ± 0.02	0.71
	PPR	0.91 ± 0.05	0.95 ± 0.04	0.56
	EPSC₃₀₋₅₀/EPSC₁	0.20 ± 0.03	0.21 ± 0.02	0.74
	τ (ms)	25.32 ± 2.76	29.11 ± 3.17	0.37
333Hz	RRP (# vesicles)	322.47 ± 37.88	267.59 ± 24.83	0.24
	Repl.(#vesicles/ms)	2.15 ± 0.22	2.08 ± 0.21	0.80
	P_r	0.24 ± 0.04	0.21 ± 0.03	0.44
	PPR	0.91 ± 0.06	1.05 ± 0.06	0.29
	EPSC₃₀₋₅₀/EPSC₁	0.13 ± 0.02	0.13 ± 0.02	0.78
	τ (ms)	14.43 ± 1.95	15.73 ± 1.81	0.63

q: quantal size, taken from mEPSC amplitude; RRP: readily releasable pool; Repl.: replenishment rate of vesicles; P_r: release probability; EPSC₃₀₋₅₀/EPSC₁: average amplitude of EPSC 30 to 50 normalized to the amplitude of EPSC₁; τ: time constant of a single exponential fit to the decay of evoked EPSC amplitudes during train stimulation. Data presented as mean (grand average of the means of all BCs) ± S.E.M. Statistical significance between groups was determined by either unpaired Student's t-test (in case of normally distributed data with comparable variances between the groups) or Wilcoxon rank sum test (when data distribution did not satisfy the criteria). Normality of distribution was tested with Jarque-Bera test and variances were compared with F-test. Sample size for RRP, Repl., P_r, EPSC₃₀₋₅₀/EPSC₁ and τ: 100 Hz- PicWT N = 19; n = 28, PicMut N = 19; n = 29, 200Hz- PicWT N = 13; n = 21, PicMut N = 13; n = 19, and 333Hz- PicWT N = 9; n = 13, PicMut N = 9; n = 11. N, number of animals; n, number of BCs. is the same as for Figure 1b. 10. Sample size for PPR same as for Table 1b.

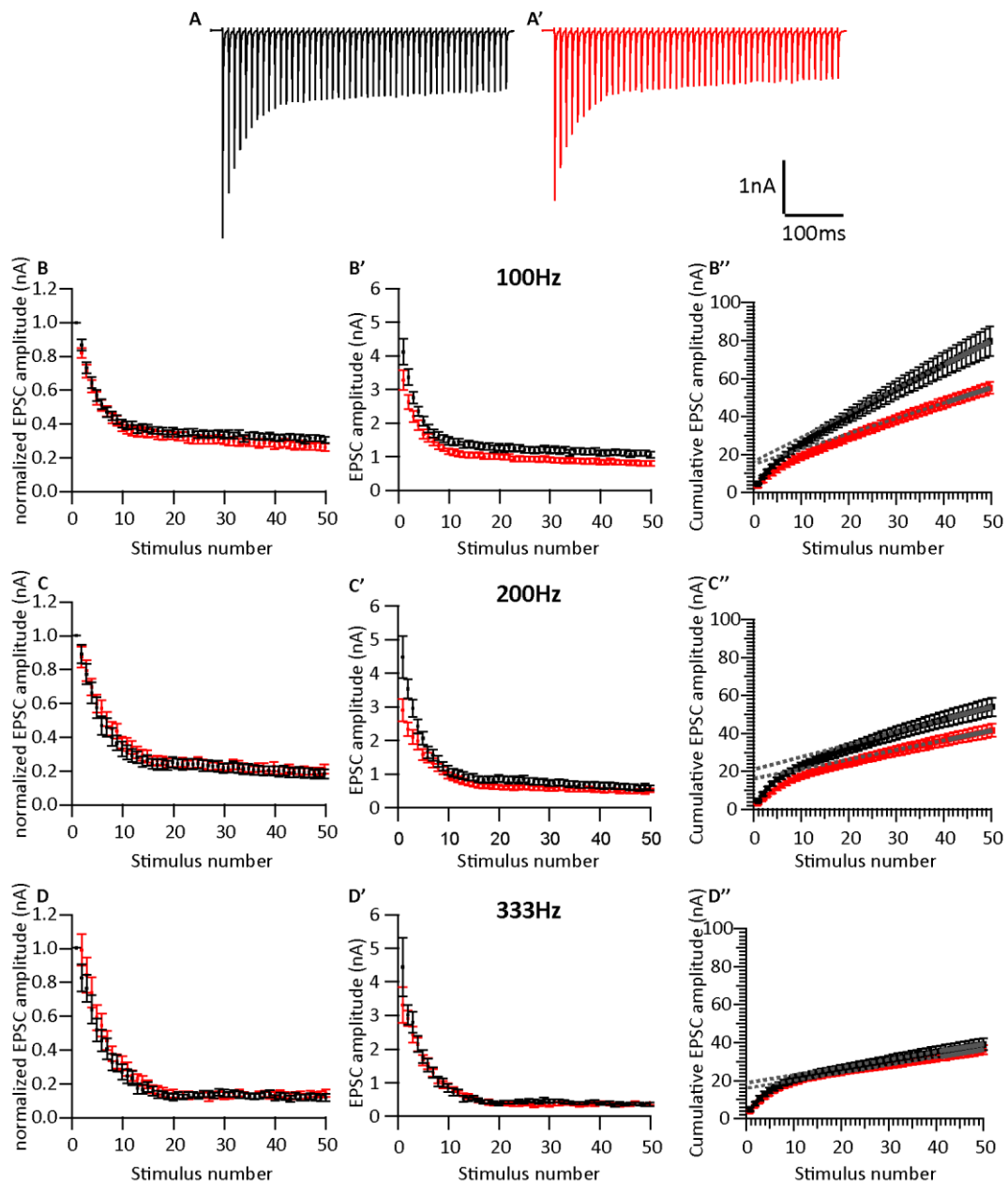


Figure 1b. 10: Analyzing vesicle pool dynamics during high-frequency stimulation at Piccolo-deficient endbulb of Held synapses

(A) Average traces of EPSCs evoked in response to 100Hz train stimulation, recorded from PicWT (A) and PicMut (A') synapses, illustrating fast kinetics and short-term depression characteristic for bushy cell EPSCs, which remain preserved in the mutant. (B-D) Comparable short-term depression (normalized eEPSC amplitude vs stimulus number) in PicWT (black) and PicMut (red) in response to high-frequency train stimulation at 100Hz (B), 200Hz (C) and 333Hz (D). (B'-D') Absolute eEPSC amplitude vs stimulus number in PicWT (black) and PicMut (red) in response to high-frequency train stimulation at 100Hz (B'), 200Hz (C') and 333Hz (D'). (B''-D'') To estimate the readily releasable pool size, replenishment rate and release probability, EPSCs from trains were plotted cumulatively against stimulus number and the linear fit to the last ten steady-state amplitudes was back-extrapolated to the y-axis, for 100Hz (B''), 200Hz (C'') and 333Hz (D''). Data information: (B-D'') Data presented as

mean trace (grand average of the means of all BCs) \pm S.E.M. Sample size for 100Hz:- PicWT N = 19; n = 28, PicMut N = 19; n = 29, 200Hz:- PicWT N = 13; n = 21, PicMut N = 13; n = 19, and 333Hz:- PicWT N = 9; n = 13, PicMut N = 9; n = 11. N, number of animals; n, number of BCs.

The size of the RRP, the release probability (P_r) and the SV replenishment rate were estimated by applying cumulative analysis (Schneppenburger et al., 1999) to the EPSC trains. In this method, EPSC amplitudes from trains are plotted cumulatively against the stimulus number. A line fit to the steady-state points (last 10 of the 50 points) is back-extrapolated to the y-axis, and the y-intercept divided by the mEPSC amplitude estimates the RRP size, while P_r is estimated by the ratio of vesicle content of EPSC1 to that of the RRP. The slope of the linear fit itself, approximates the rate of vesicle replenishment during the train. The analysis (Table 1b. 4), revealed a significantly reduced RRP size in the mutant at 200Hz stimulation, whereas at 100Hz and 333Hz only a non-significant trend towards RRP size reduction was found. Another finding was the reduced rate of vesicle replenishment in the mutant that reached significance at 100Hz stimulation. The estimate of P_r was not significantly changed upon Piccolo disruption at any stimulation frequency. Asynchronous release following the train stimulation was unchanged: the rate of mEPSCs was not different in first 100ms after the end of 100Hz trains between BCs of both genotypes.

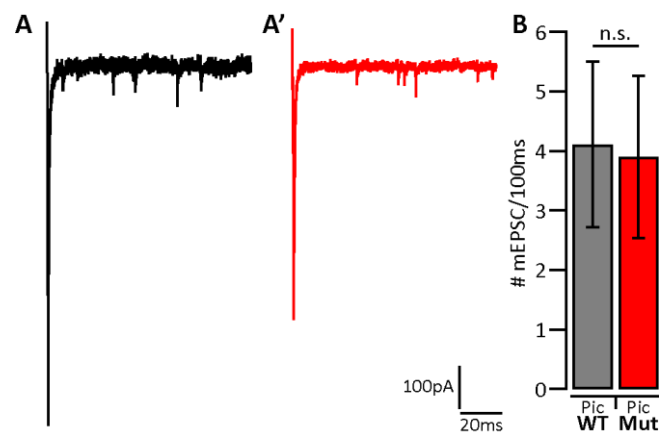


Figure 1b. 11: Unchanged asynchronous release at endbulb synapse in PicMut aVCN

(A) Representative traces of asynchronous release events after 100Hz train stimulation in PicWT (A) and PicMut (A'). Positive peaks at the beginning of each trace are the stimulus artifacts before the last EPSC of the train, which is followed by mEPSC corresponding to asynchronous release. (B) Asynchronous activity at the endbulb of Held synapse is quantified as number of mEPSC events per 100ms after the cessation of 100Hz train stimulation. Asynchronous activity remains unchanged at

the PicMut endbulbs (n.s. – p-value > 0.05, Student's t-test). Data information: PicWT (N=7; n=9) and PicMut (N=6; n=10). N, number of animals; n, number of BCs. EPSC bars represent S.E.M.

To further verify the finding of slower vesicle replenishment in PicMut endbulbs, recovery from short-term depression was studied, by measuring eEPSC amplitudes elicited by single stimuli presented at varying time intervals after a conditioning 100Hz train of 50 pulses (Figure 1b. 12A). Recovery is displayed as the eEPSC amplitudes normalized to the amplitude of the first eEPSC of the conditioning train (Figure 1b. 12B). A double exponential function was used to fit the time course of recovery. PicMut endbulbs showed a significantly slower recovery during the initial phase (longer time constants for the fast component of the double exponential fits: 101.9 ± 35.4 ms for PicMut vs. 30.2 ± 14.8 ms for PicWT). The kinetics of the slow components were comparable (2.98 ± 0.57 s for PicMut vs. 3.05 ± 0.23 s for PicWT).

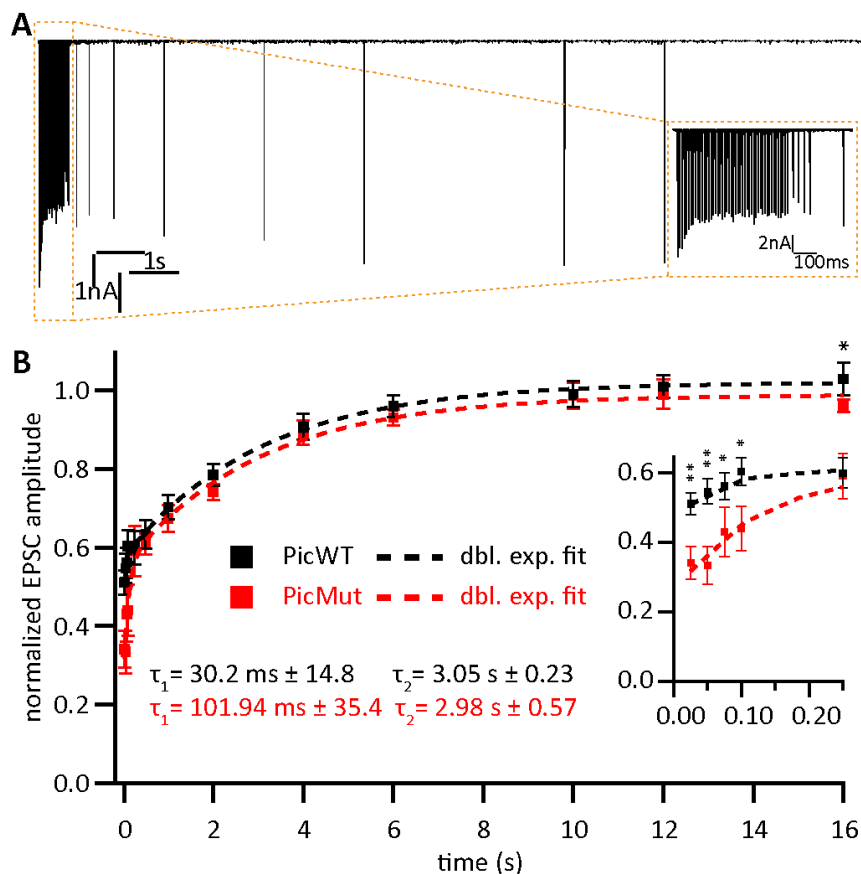


Figure 1b. 12: Recovery from short-term depression is slowed at Piccolo-deficient endbulb of Held synapses.

(A) Trace of a PicWT endbulb synapse to illustrate the recovery protocol. Following a conditioning 100Hz train of 50 stimuli, recovery from short-term depression was assessed by single test pulses presented after (in ms) 25, 50, 75, 100, 250, 500 (further in s) 1, 2, 4, 6, 10, 12 and 16. Inset shows the responses to the first 5 stimuli in detail. (B) Recovery plotted as mean (\pm S.E.M.) EPSC amplitude in response to test pulses normalized to the first EPSC amplitude of the conditioning train. Dashed lines are double exponential fits. The time constants (τ) are provided on the graph, amplitude ratios of the two recovery components (fast/slow) were 0.15 and 0.55 for PicWT and PicMut respectively. Inset shows the first 5 responses in detail. ** p-value < 0.01, * p-value < 0.05. Statistical significance between groups was determined by either unpaired Student's t-test (in case of normally distributed data with comparable variances between the groups) or Wilcoxon rank sum test (when data distribution did not satisfy the criteria). Normality of distribution was tested with Jarque-Bera test and variances were compared with F-test.

1b.5 In the absence of Piccolo, partial loss of Bassoon has no effect on spontaneous release, but influences evoked transmission, short-term depression and recovery from depression at the endbulb of Held

In addition to the mutation of Piccolo, the effect of disrupting (deleting exons 4 and 5, *Bsn* ^{Δ Ex4/5}) (Altrock et al., 2003b) one allele of Bassoon on vesicle replenishment rate was also studied. The mutant is henceforth referred to as PicBsn. In previous studies (Schulz et al., 2014), heterozygosity for *Bsn* ^{Δ Ex4/5} did not have any phenotype on synaptic transmission. However, in the absence of Piccolo, even partial loss of Bassoon seemed to aggravate the slowing of vesicle replenishment (141.2 ± 50.7 ms for the fast component of the double exponential fit in PicBsn synapses). The difference to PicMut, however, did not reach significance (Figure 1b. 13B).

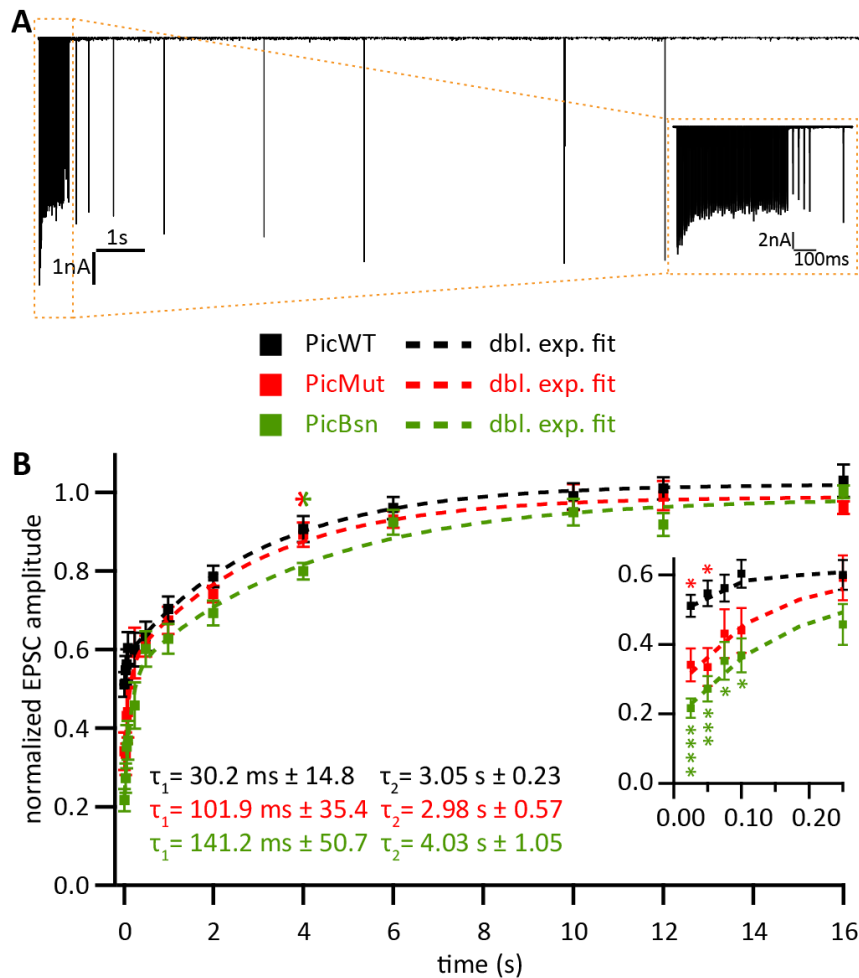


Figure 1b. 13: Recovery from short-term depression is slowed at PicBsn endbulb of Held synapses.

(A) Trace of a PicWT endbulb synapse to illustrate the recovery protocol. Following a conditioning 100Hz train of 50 stimuli, recovery from short-term depression was assessed by single test pulses presented after (in ms) 25, 50, 75, 100, 250, 500 (further in s) 1, 2, 4, 6, 10, 12 and 16. Inset shows the responses to the first 5 stimuli in detail. (B) Recovery plotted as mean (\pm S.E.M.) EPSC amplitude in response to test pulses normalized to the first EPSC amplitude of the conditioning train. Dashed lines are double exponential fits. The time constants (τ) are provided on the graph, amplitude ratios of the two recovery components (fast/slow) were 0.15, 0.55 and 0.67 for PicWT, PicMut and PicBsn respectively. Inset shows the first 5 responses in detail. **** p-value < 0.0001, *** p-value < 0.001, * p-value < 0.05. * - Significance between PicWT and PicMut; * - Significance between PicWT and PicBsn; * - Significance between PicMut and PicBsn. Parametric data were tested for significance by 1-way ANOVA with post-hoc correction with Tukey's multiple comparison test. Non-parametric data were tested for significance by Kruskal-Wallis test with post-hoc correction with Dunn's multiple comparison test.

Table 1b. 5: Quantification of recovery from short-term depression

Time (in s)	PicWT	PicMut	PicBsn
0.025	0.51 ± 0.03 (18)	0.34 ± 0.05 (15)	0.22 ± 0.03 (10)
0.050	0.55 ± 0.04 (16)	0.33 ± 0.05 (12)	0.27 ± 0.04 (10)
0.075	0.56 ± 0.04 (16)	0.43 ± 0.07 (14)	0.35 ± 0.05 (10)
0.100	0.60 ± 0.04 (15)	0.44 ± 0.06 (15)	0.37 ± 0.05 (10)
0.250	0.60 ± 0.04 (16)	0.59 ± 0.06 (14)	0.46 ± 0.06 (10)
0.500	0.63 ± 0.04 (13)	0.61 ± 0.03 (17)	0.60 ± 0.05 (10)
1.000	0.70 ± 0.03 (11)	0.67 ± 0.03 (20)	0.63 ± 0.04 (10)
2.000	0.79 ± 0.03 (12)	0.74 ± 0.02 (18)	0.69 ± 0.02 (10)
4.000	0.91 ± 0.03 (11)	0.89 ± 0.03 (20)	0.80 ± 0.03 (10)
6.000	0.96 ± 0.03 (13)	0.93 ± 0.02 (24)	0.92 ± 0.03 (10)
10.00	0.99 ± 0.03 (10)	0.99 ± 0.03 (12)	0.95 ± 0.03 (10)
12.00	1.01 ± 0.03 (13)	0.99 ± 0.04 (14)	0.92 ± 0.03 (10)
16.00	1.03 ± 0.04 (12)	0.96 ± 0.02 (14)	1.00 ± 0.02 (10)

Data presented as mean (grand average of the means of all BCs) ± S.E.M. of EPSC amplitude in response to test pulses normalized to the first EPSC amplitude of the conditioning train. Number of cells that were recorded from, in parentheses.

The aggravation of slowed recovery from vesicle depletion upon Bassoon disruption in addition to Piccolo mutation, provided the impetus to investigate synaptic transmission in PicBsn mice. For a comprehensive analysis all three modes of release (Kaeser and Regehr, 2014): spontaneous, asynchronous and evoked, were studied, just like for PicMut mice. All recordings were made in the presence of 1mM Kynurenic acid and 100µM Cyclothiazide to eliminate postsynaptic factors influencing the inference.

mEPSC, recorded as spontaneous events from postsynaptic BCs were comparable between PicWT and PicBsn. The analysis did not reveal any differences in the mEPSC amplitude, kinetics or frequency of events (p-value > 0.05 for all 3 quantities, Figure 1b. 14B-B''' Student's t-test, Figure 1b. 14B'''' Wilcoxon rank sum test).

Table 1b. 6: Miniature EPSC amplitude and kinetics unchanged in PicBsn

Parameter	PicWT	PicBsn	p-value
Amplitude (pA)	60.82 ± 2.29	60.82 ± 3.21	0.99
10-90 Rise time (ms)	0.119 ± 0.003	0.117 ± 0.004	0.68
FWHM (ms)	0.24 ± 0.01	0.26 ± 0.01	0.40
Decay time (ms)	0.24 ± 0.01	0.25 ± 0.01	0.61
Frequency (Hz)	4.04 ± 0.41	3.47 ± 0.72	0.37

Data presented as mean (grand average of the means of all BCs) \pm S.E.M. Statistical significance between groups was determined by either unpaired Student's t-test (in case of normally distributed data with comparable variances between the groups) or Wilcoxon rank sum test (when data distribution did not satisfy the criteria). Normality of distribution was tested with Jarque-Bera test and variances were compared with F-test. PicWT N = 23; n = 23, PicBsn N = 5; n = 13 (N, number of animals; n, number of BCs).

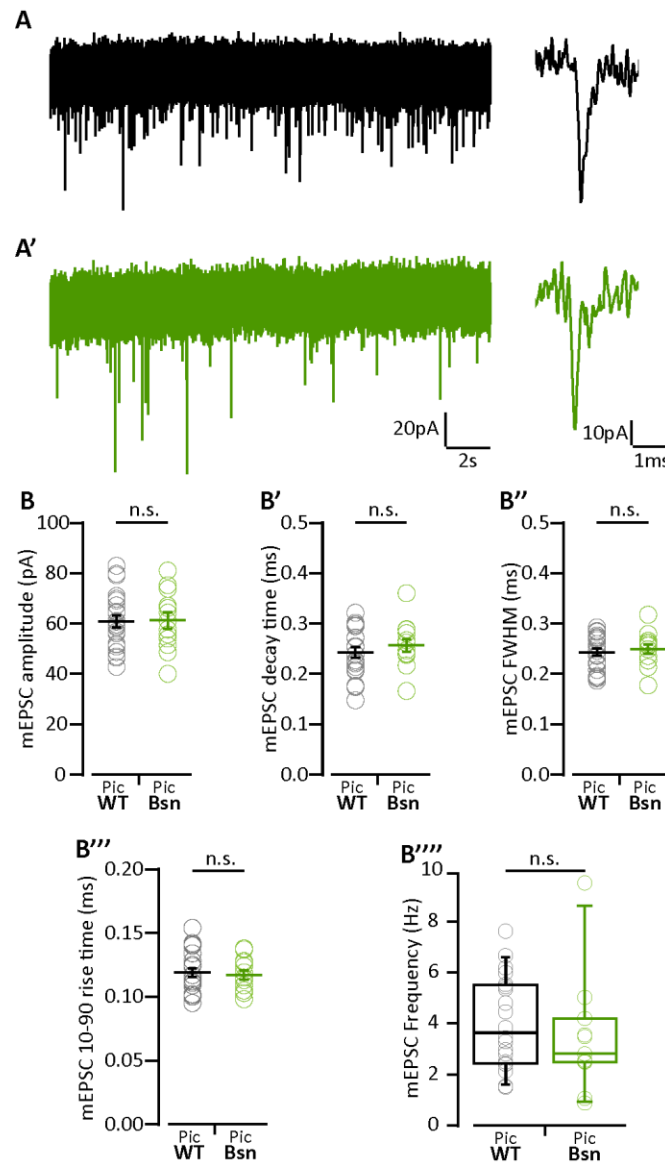


Figure 1b. 14: Miniature EPSC amplitude and kinetics preserved in PicBsn synapses

(A) Representative traces of mEPSC: Continuous recording (left) and exemplary individual mEPSCs (right) for PicWT (A) and PicBsn (A'). (B) Analysis of mEPSC: mEPSC amplitude (B), decay time (B'), full-width at half-maximum (FWHM; B'') rise time (B'''), and frequency (B''') remain unaltered. Each data point represents the mean estimate of a given BC. Normally distributed data presented as mean (grand average of the means of all BCs) \pm S.E.M. (B-B'''; n.s. – p-value > 0.05, Student's t-test). Non-normally distributed data presented as box and

whisker plot (grand median (of the means of all BCs), lower/upper quartiles, 10-90 percentiles; B''''; n.s. – p-value > 0.05, Wilcoxon rank sum test). PicWT N = 23; n = 23, PicBsn N = 5; n = 13 (N, number of animals; n, number of BCs).

Next, evoked transmission was analyzed. eEPSC elicited by single stimulations demonstrated a normal eEPSC amplitude for single AP stimulation, hence contrasting the reduction we found upon Piccolo mutation alone (Table 1b. 7, Figure 1b. 15A). The kinetics of rise and decay also remained unchanged (Table 1b. 7, Figure 1b. 15C-E). The only difference detected was that the synaptic delay was slightly shorter at PicBsn endbulbs (Table 1b. 7, Figure 1b. 15F).

Table 1b. 7: eEPSC amplitude and kinetics intact in PicBsn synapses but shorter synaptic delay

Parameter	PicWT	PicBsn	p-value
Amplitude (nA)	4.43 ± 0.37	4.10 ± 0.25	0.62
10-90 Rise time (ms)	0.19 ± 0.01	0.21 ± 0.01	0.12
FWHM (ms)	0.64 ± 0.03	0.66 ± 0.04	0.71
Decay time (ms)	0.56 ± 0.02	0.59 ± 0.03	0.53
Synaptic delay (ms)	0.89 ± 0.02	0.82 ± 0.01	0.013*

Data presented as mean (grand average of the means of all BCs) ± S.E.M. Statistical significance between groups was determined by unpaired Student's t-test. For ePSC amplitude PicWT N = 21; n = 35, PicBsn N = 6; n = 17. For kinetics and synaptic delay PicWT N = 19; n = 28, PicBsn N = 6; n = 17 (N, number of animals; n, number of BCs).

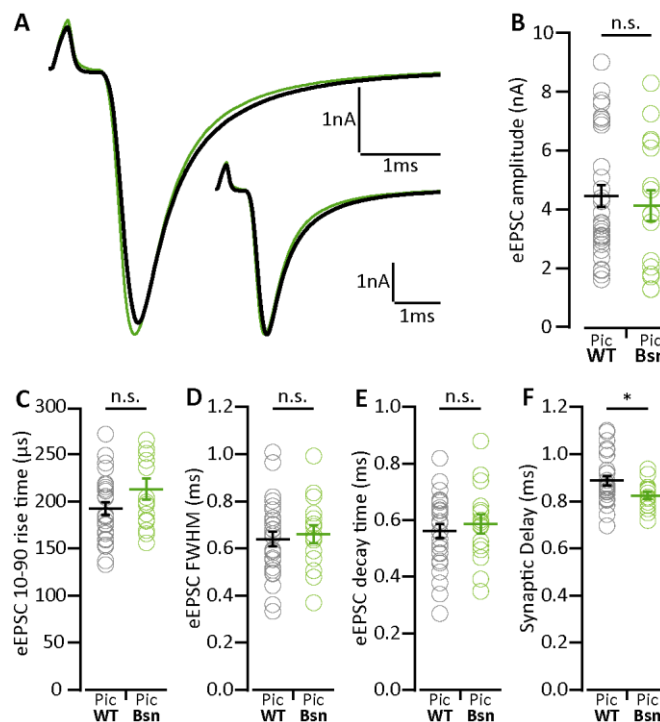


Figure 1b. 15: eEPSC amplitude and kinetics intact in PicBsn synapses but shorter synaptic delay

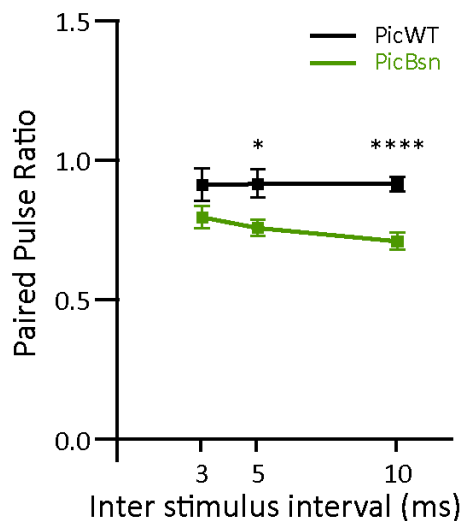
(A) Average traces of evoked EPSC (eEPSC) in PicWT (black) and PicBsn (green) showing reduced eEPSC amplitude in the mutant. Inset: Average PicBsn eEPSC trace scaled to the peak of the average wildtype trace demonstrating unaltered eEPSC kinetics in the mutant. Positive peak at onset of trace reflects the stimulation artifact. (B) Reduced eEPSC amplitude in PicBsn (N = 6; n = 17) as compared to PicWT (N = 21; n = 35). Each data point represents the mean estimate of a given BC, with thick bars representing grand average (of the means of all BCs) \pm S.E.M. (C-F) eEPSC kinetics: rise time (C), full-width at half-maximum (FWHM; D) and decay time (E) were not significantly altered in PicBsn (N= 6; n = 17) as compared to PicWT (N = 19; n = 28). Synaptic delay (F) was shorter at PicBsn endbulbs. Data presented as grand average (of the means of all BCs) \pm S.E.M. (n.s. – p-value > 0.05, * p-value < 0.05, Student's t-test). Data information: N, number of animals; n, number of BCs.

Although, the single eEPSCs were largely unaltered, investigating responses to pairs of stimuli revealed a lower paired pulse ratio (PPR) at the endbulbs of PicBsn mice at three (3, 5 and 10ms) inter stimulus intervals. PPR at 5 and 10ms were significantly lower, and at 3ms the difference was at the edge of statistical significance (p-value = 0.053; Wilcoxon rank sum test; Table 1b. 8, Figure 1b. 16).

Table 1b. 8: Reduced paired pulse ratio at endbulbs of PicBsn

Inter stimulus interval (ms)	PicWT	PicBsn	p-value
3	0.91 ± 0.06 (15)	0.79 ± 0.04 (13)	<u>0.053</u>
5	0.91 ± 0.05 (23)	0.75 ± 0.03 (14)	0.03 *
10	0.91 ± 0.02 (30)	0.70 ± 0.03 (16)	6.67x10⁻⁵ ****

Data presented as mean (grand average of the means of all BCs) ± S.E.M. Statistical significance between groups was determined by either unpaired Student's t-test (in case of normally distributed data with comparable variances between the groups) or Wilcoxon rank sum test (when data distribution did not satisfy the criteria). Normality of distribution was tested with Jarque-Bera test and variances were compared with F-test. Sample size (number of BCs recorded) given in parentheses.

**Figure 1b. 16: Reduced paired pulse ratio at endbulbs of PicBsn**

Data presented as mean (grand average of the means of all BCs) ± S.E.M. Statistical significance between groups was determined by either unpaired Student's t-test (in case of normally distributed data with comparable variances between the groups) or Wilcoxon rank sum test (when data distribution did not satisfy the criteria). Normality of distribution was tested with Jarque-Bera test and variances were compared with F-test. **** p-value < 0.0001, * p-value < 0.05. For sample size refer to Table 1b. 8

A lower PPR is indicative of a higher release probability which was not seen in PicMut mice (except for a mild difference at 10ms; Table 1b. 4). To further analyze the effects of Bassoon disruption in addition to the absence of Piccolo, responses to high frequency train stimulations were studied, to assess the RRP size, release probability and pool dynamics. The

evoked response was quantified using cumulative analysis as described previously in section 1b.4. Short-term depression at the endbulbs, as determined by τ (time constant of decay of the response to train stimulation) and $EPSC_{30-50}/EPSC_1$ (extent of depression), was slightly stronger at endbulbs of PicBsn mice than in PicWT, with maximum difference observed for 100Hz stimulation (Figure 1b. 17B).

Response to train stimulation decayed faster (smaller τ) in PicBsn endbulbs at 100Hz, but the effect diminished with increasing stimulation frequency (Table 1b. 9, Figure 1b. 17B-D). The steady state amplitude (the extent of depression, $EPSC_{30-50}/EPSC_1$) also tended to be lower in PicBsn endbulbs at all three frequencies, reaching statistical significance at 100 and 333 Hz. This contrasts with the phenotype observed with Piccolo mutation alone, where no discernible change in short-term depression was noted.

Though the additional Bassoon manipulation altered the short-term depression at the endbulb, release probability (P_r) estimates were still comparable to the wildtype.

Table 1b. 9: Comparison of pool size, vesicle replenishment, release probability and short-term depression at the endbulb of Held synapse in PicBsn and PicWT

Frequency	Parameter	PicWT	PicBsn	p-value
	q	60.82 pA	60.82 pA	0.99
100 Hz	RRP (# vesicles)	300.76 ± 31.28	264.43 ± 40.40	0.35
	Repl.(#vesicles/ms)	1.79 ± 0.14	1.49 ± 0.22	0.24
	P_r	0.26 ± 0.07	0.28 ± 0.02	0.37
	$EPSC_{30-50}/EPSC_1$	0.32 ± 0.03	0.23 ± 0.02	0.03 *
	τ (ms)	42.79 ± 3.31	31.24 ± 3.45	0.009 **
200 Hz	RRP (# vesicles)	393.05 ± 46.09	347.02 ± 54.09	0.58
	Repl.(#vesicles/ms)	2.11 ± 0.26	1.75 ± 0.30	0.38
	P_r	0.21 ± 0.02	0.23 ± 0.02	0.52
	$EPSC_{30-50}/EPSC_1$	0.20 ± 0.03	0.14 ± 0.01	0.13
	τ (ms)	25.32 ± 2.76	19.96 ± 1.94	0.12
333 Hz	RRP (# vesicles)	322.47 ± 37.88	389.48 ± 62.17	0.37
	Repl.(#vesicles/ms)	2.15 ± 0.22	1.79 ± 0.46	0.08
	P_r	0.24 ± 0.04	0.21 ± 0.01	0.89
	$EPSC_{30-50}/EPSC_1$	0.13 ± 0.02	0.07 ± 0.02	0.02 *
	τ (ms)	14.43 ± 1.95	13.28 ± 1.02	0.39

q: quantal size, taken from mEPSC amplitude; RRP: readily releasable pool; Repl.: replenishment rate of vesicles; P_r : release probability; $EPSC_{30-50}/EPSC_1$: average amplitude of EPSC 30 to 50 normalized to the amplitude of EPSC1; τ : time constant of a single exponential fit to the decay of evoked EPSC

amplitudes during train stimulation. Data presented as mean \pm S.E.M. Statistical significance between groups was determined by either unpaired Student's t-test (in case of normally distributed data with comparable variances between the groups) or Wilcoxon rank sum test (when data distribution did not satisfy the criteria). Normality of distribution was tested with Jarque-Bera test and variances were compared with F-test. Sample size for 100 Hz- PicWT N = 19; n = 28, PicBsn N = 6; n = 17, 200Hz- PicWT N = 13; n = 21, PicBsn N = 5; n = 15, and 333Hz- PicWT N = 9; n = 13, PicBsn N = 6; n = 14. N, number of animals; n, number of BCs.

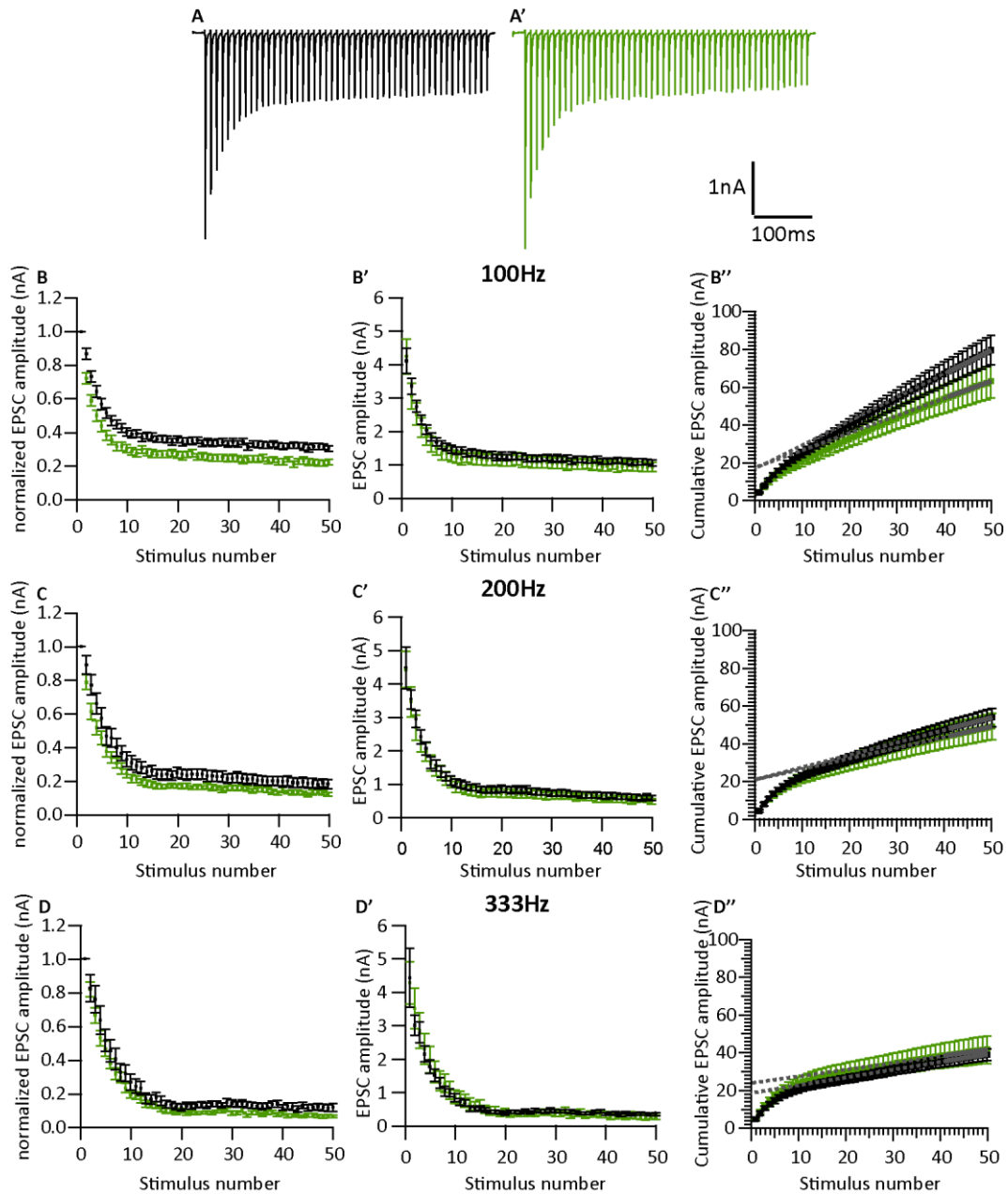


Figure 1b. 17: Analyzing vesicle pool dynamics during high-frequency stimulation at Piccolo-deficient endbulb of Held synapses with partial Bassoon deficiency

(A) Average traces of EPSCs evoked in response to 100Hz train stimulation, recorded from PicWT (A) and PicBsn (A') synapses, illustrating characteristic fast kinetics and short-term depression of bushy cell EPSCs. (B-D) Short-term depression (represented as normalized amplitude vs stimulus number)

slightly stronger in PicBsn (green) as compared PicWT (black), in response to high-frequency train stimulation at 100Hz (B), 200Hz (C) and 333Hz (D). (B'-D') Absolute eEPSC amplitude vs stimulus number in PicWT (black) and PicBsn (green) in response to high-frequency train stimulation at 100Hz (B'), 200Hz (C') and 333Hz (D'). (B''-D'') To estimate the readily releasable pool size, replenishment rate and release probability, EPSCs from trains were plotted cumulatively against stimulus number and the linear fit to the last ten steady-state amplitudes was back-extrapolated to the y-axis, for 100Hz (B''), 200Hz (C'') and 333Hz (D''). Data information: sample size for 100 Hz- PicWT N = 19; n = 28, PicBsn N = 6; n = 17, 200Hz- PicWT N = 13; n = 21, PicBsn N = 5; n = 15, and 333Hz- PicWT N = 9; n = 13, PicBsn N = 6; n = 14. N, number of animals; n, number of BCs.

Finally, the change in asynchronous release following the train stimulation was quantified as the rate of mEPSCs occurring in first 100ms after the end of 100Hz trains. Endbulb of Held synapses in the PicBsn mice tended to have more asynchronous activity as compared to wildtype synapses, but this did not yet reach statistical significance (Figure 1b. 18).

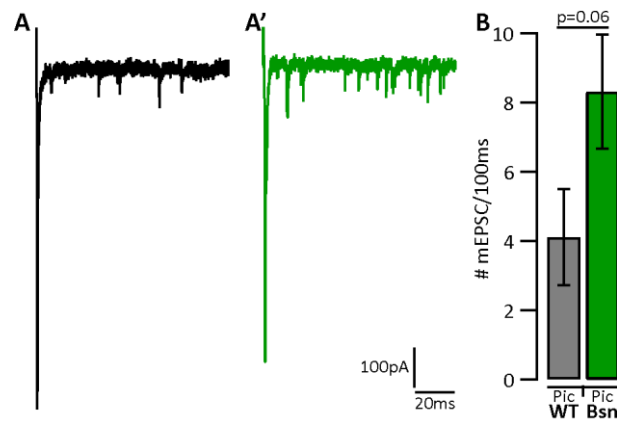


Figure 1b. 18: Endbulbs of Held in PicBsn aVCN tend to have more asynchronous release

(A) Example traces of asynchronous release events after 100Hz train stimulation in PicWT (A) and PicBsn (A'). Positive peaks at the beginning of each trace are the stimulus artifacts before the last EPSC of the train, which is followed by mEPSC corresponding to asynchronous release. (B) Asynchronous activity at the endbulb of Held synapse is quantified as number of mEPSC events per 100ms after the cessation of 100Hz train stimulation. PicBsn endbulbs (N=4; n=13) showed a trend towards higher asynchronous activity as compared to PicWT (N=7; n=9) (p-value = 0.06, Student's t-test). N, number of animals; n, number of BCs. Error bars represent S.E.M.

1c Discussion

The role of Piccolo in high frequency transmission was studied at the endbulb of Held synapses of the auditory pathway. Piccolo disruption elicited changes in the molecular composition of the AZ, some of which might partially compensate for Piccolo deficiency

(Bassoon) while the reduction of RIM1 might contribute to the observed deficit in vesicle replenishment. Through electrophysiology, evidence is provided for a role of Piccolo in maintaining the RRP size and efficiency of recovery from short-term depression.

1c.1 Changes in molecular composition of endbulb AZs upon Piccolo disruption

Deletion of exon 14 of *Pclo* along with insertion of a neomycin resistance cassette drastically reduced Piccolo expression as observed by semi-quantitative analysis by immunofluorescence. The reduction of Piccolo immunofluorescence on average amounted approximately to 90%, which is close to what was found by Western blotting of brain homogenate (95%; (Mukherjee et al., 2010)). Therefore, manipulation of Piccolo employed at the endbulb synapse was incomplete and, hence, the analysis likely underestimated the role of the protein. This calls for a refined genetic deletion that targets all splice variants. However, this drawback of the currently used *Pclo* manipulation also offered an advantage: the C-terminus, affected by the mutation, is absent from its shorter variant, Piccolino (Regus-Leidig et al., 2013, 2014), the predominant Piccolo isoform at the ribbon synapses of the IHCs. The data illustrate that the Piccolino expression remains intact at the IHCs of PicMut. ABR recordings corroborated the notion of intact IHC synapses and indicated overall normal cochlear function (Figure 1b. 2). This provided a unique opportunity to selectively study the effects of Piccolo disruption at the endbulb without any bias from the preceding synapse that was confounding the previous analysis of Bassoon function at the endbulb synapse (Schulz et al., 2014).

The gross morphology of the endbulb synapse was not affected by Piccolo disruption: the number of the auditory nerve fibers converging onto BCs and the number of AZs per endbulb remained unaltered. Since, Piccolo interacts directly or indirectly with most other CAZ proteins (Wang et al., 2009), how the molecular composition of AZ is affected upon its disruption was studied. Semi-quantitative expression analysis was employed by integrating immunofluorescence of excitatory and inhibitory AZs onto BCs. Since excitatory AZs were required to co-localize with Vglut1 that is thought to distinguish endbulb terminals from Vglut2-positive bouton endings (Heeringa et al., 2016), it is reasonable to consider the analysis of excitatory AZs to mostly report properties of endbulb AZs. Out of the 4 CAZ

proteins (Bassoon, RIM1, RIM2 and Munc13-1) investigated, expression levels of Bassoon and RIM1 were significantly altered at endbulb AZs. It is interesting to note, that the two proteins that were altered, share regions of homology with Piccolo (Wang et al., 1999). RIM and Piccolo share similarity in their Zn finger domain, PDZ domain and two C-terminal C₂ domains and Bassoon shares 10 highly conserved PBH domains (tom Dieck et al., 1998; Fenster et al., 2000; Wang et al., 1999). RIM1 level was reduced while the Bassoon level was increased. It can be speculated that the reduction in RIM1 level could be a consequence of it being not integrated properly at the synapse in the absence of its interaction with Piccolo, as Piccolo is thought to play an integral role in AZ assembly and scaffolding (Gundelfinger et al., 2016). Bassoon, on the other hand, thought to have partially overlapping functions with Piccolo (Waites et al., 2013), could be upregulated in PicMut as a compensatory mechanism. This is line with a previous report (Schulz et al., 2014), where Piccolo expression was upregulated in Bassoon deficient synapses, likely to compensate for the loss of some of Bassoon's function.

1c.2 Piccolo disruption mildly affects synaptic transmission at the endbulb of Held

So far a unifying picture of the role of Piccolo in synaptic transmission has been missing. While one study implicated Piccolo as a negative regulator of SV exocytosis (Leal-Ortiz et al., 2008), other ones claimed Piccolo plays no role in SV release (Mukherjee et al., 2010) or, together with Bassoon, contributes to maintenance of the structural integrity of the AZ (Waites et al., 2013). In the present study of the endbulb of Held synapse, an amplitude reduction of eEPSCs evoked by single action potentials was observed. Kinetics, on the other hand, were not changed either for eEPSCs or for mEPSCs. The unaltered mEPSC amplitude (quantal size) rules out post-synaptic changes in abundance or properties of AMPA receptors. In contrast, global disruption of Bassoon increased the quantal size (Schulz et al., 2014). This was suggested to reflect homeostatic upscaling of excitatory synaptic contacts in response to reduced SGN input to BCs due to impaired synaptic sound encoding in the cochlea. Excluding postsynaptic alterations and changes in vesicular glutamate content based on the unaltered mEPSCs, leaves two possibilities, either a reduction in release probability (P_r) or RRP size to explain the reduced eEPSC amplitude.

The cumulative analysis of eEPSC trains (Schneppenburger et al., 1999) indicated a reduced RRP size as the primary reason for the reduced eEPSC amplitude. P_r , on the other hand, seemed largely unaltered as per cumulative analysis and paired-pulse ratio (smaller only for 10ms). Vesicle replenishment was slower during high frequency stimulation and after cessation of the stimulus, where the fast phase of recovery was slowed by a factor of three. The impaired replenishment likely contributes to the reduced RRP, as the rate of vesicle supply to the RRP might not balance that of consumption by spontaneous release (Pangrsic et al., 2010) and/or the rate of unpriming (Smith et al., 1998). Piccolo's contribution to vesicle replenishment could be attributed to its interaction with actin regulatory protein like Daam1, required for F-actin assembly (Wagh et al., 2015), that may regulate conversion of reluctant SVs to the fast releasing RRP (Lee et al., 2012). Moreover, the reduction in RIM1 might contribute as RIMs play a crucial role in making vesicles fusion competent (Deng et al., 2011; Fernández-Busnadiego et al., 2013b; Gracheva et al., 2008; Han et al., 2011; Jung et al., 2015b; Kintscher et al., 2013; Wang et al., 1997) and hence in determining the RRP size (Han et al., 2015). With its extended reach into the cytosol, tens of nanometers beyond the dense projections of the CAZ (Limbach et al., 2011), Piccolo might escort SVs from further away in the presynaptic cytosol and deliver them to RIM to make them release ready. The reduction in RIM1 expression reported in this study could be in line with this synaptic interplay. Future electron microscopy analysis will be helpful to assess potential morphological correlates of the reduced RRP. Interestingly, a trend towards further slowing of the fast phase of recovery from short-term depression was observed upon disrupting one allele of Bassoon, in addition to the mutation of Piccolo. Nevertheless, finding reduced vesicle replenishment upon disruption of either Bassoon (Hallermann et al., 2010b; Schulz et al., 2014) or Piccolo suggests that neither protein is sufficient to maintain wildtype performance of SV replenishment, even despite a likely compensatory, up-regulation of the respective other gene.

This implies partially overlapping function, probably even at the same AZs as the majority of them contain both proteins (Dondzillo et al., 2010; Schulz et al., 2014), although Piccolo and Bassoon may promote replenishment through different molecular pathways. As discussed above, Piccolo might employ an interplay of F-actin assembly, interaction with other CAZ

proteins like RIM and its Ca²⁺ sensing domain. Bassoon on the other hand, might tether SVs via interactions with the SV associated protein Mover (Ahmed et al., 2013; Körber et al., 2015b) and could also assist in positioning of Ca²⁺ channels (Davydova et al., 2014) and SVs close to each other.

The conclusion of partially overlapping roles of Piccolo and Bassoon in vesicle replenishment has also been derived in a parallel study on the calyx of Held using virus-mediated knock-down of Piccolo (Partthier et al.). Future work will be required to dissect the precise molecular mechanisms by which Piccolo acts in vesicle replenishment. This should also target roles of Piccolo in SV endocytosis and low-affinity Ca²⁺ sensing. Piccolo binds actin associated proteins like Abp1 (Fenster et al., 2003), and GIT1 (Kim et al., 2003), both of which have been linked to SV endocytosis. As stated earlier, Piccolo plays a role in dynamic assembly of F-actin, which is needed for retrieval of SVs both by bulk (Nguyen et al., 2012) and ultrafast (Watanabe et al., 2013) endocytosis. The finding that only the fast component of recovery was affected would imply a rapid mechanism, such as ultrafast endocytosis or release-site clearance (Haucke et al., 2011), to be involved. The C₂A domain of Piccolo acts as a low- affinity Ca²⁺ sensor (Garcia et al., 2004; Gerber et al., 2001), which is ideal to sense Ca²⁺ build-up during high-frequency activity at the synapse. At the endbulb of Held, Ca²⁺ drives the fast component of recovery (Wang and Manis, 2008; Yang and Xu-Friedman, 2008) and Piccolo is an interesting candidate as the sensor driving this Ca²⁺ dependent rapid recovery.

1c.3 Segregation of the roles of Piccolo and Bassoon at the active zone

Disruption of either Piccolo or Bassoon leads to impaired vesicle replenishment (this study and (Schulz et al., 2014)). Therefore, Piccolo mutant mice with additional heterozygosity for a partial deletion of the Bassoon gene (PicBsn mice, Bsn: deletion of exons 4 and 5 (Altrock et al., 2003b)), were further probed for vesicle replenishment to elucidate potential overlapping functions of Bassoon and Piccolo. The phenotype observed was intermediate between the changes in neurotransmission seen in Piccolo- (reported in the study) and Bassoon-deficient endbulbs (Schulz et al., 2014), while Bassoon heterozygosity did not exert any synaptic deficits by itself (Schulz et al., 2014). However, at the endbulb of Held, Bassoon

heterozygotes in the absence of Piccolo demonstrate a reduced PPR indicative of an increased release probability, faster and greater extent of depression to train stimulation, and a tendency for higher asynchronous release upon cessation of high frequency stimulation.

One thing that seems surprising, is that the eESPC amplitude and RRP size, which were reduced in Piccolo deficient endbulbs, seem comparable to the PicWT values in PicBsn mice. In Bassoon KO, eEPSC amplitude was comparable to that of the wildtype because of homeostatic upscaling of excitatory synaptic contacts in response to reduced SGN input to BCs due to impaired synaptic sound encoding in the cochlea. However, this is not valid for PicBsn mice, as the cochlea does not suffer from Piccolo deficiency. Thus, one allele of Bassoon is sufficient to sustain neurotransmission at the cochlear ribbon synapses. This is reflected in the unaltered mEPSC amplitude, as opposed to an increase observed at endbulbs of Bassoon KO (Schulz et al., 2014). I speculate that normal eEPSC amplitude at PicBsn endbulbs, is likely due to their increased release probability.

However, the RRP estimation is contrary to expectation, as a reduced RRP was reported for both Bassoon (Schulz et al., 2014) and Piccolo deficient (this study) endbulbs individually. Here it should be noted that the RRP estimation for comparison between PicWT and PicBsn endbulbs might be compromised because of a lower steady-state amplitude (greater extent of decay) and a faster decay of depression in response to train stimulations in PicBsn endbulbs. The cumulative analysis (Schneggenburger et al., 1999) used to calculate RRP, reports the decrement of pool during stimulation and not the pool itself (Neher, 2015). Thus, because of greater depression in the PicBsn synapses as compared to PicWT endbulbs, there might be a larger estimate of RRP size than in the PicWT. Since, the release probability, decay kinetics and extent of depression were comparable in PicMut and PicWT endbulbs, even the subtle difference in RRP size might have been revealed. This error in RRP estimation could be overcome by either employing corrections for the change in release probability at the start and end of the response to train stimulation (Neher, 2015) or employing another analysis that does not calculate RRP by the decrease in response but the size of pool that exists before the stimulation, like the Elmqvist-Quastel estimation (Elmqvist and Quastel,

1965; Neher, 2015). Alternatively, more challenging approach of calculating RRP by presynaptic capacitance changes can be employed (Lin et al., 2011).

Taken together, partial lack of Bassoon in Piccolo deficient synapses seems to add changes in the release probability to the phenotype observed in PicMut mice. It is interesting to speculate that Piccolo and Bassoon indeed, maintain synaptic vesicle clustering at the synapse (Mukherjee et al., 2010), but while they both have collaborative role in vesicle replenishment, Bassoon might have a role in regulation of release as well. This hypothesis opens questions and a need for further investigations to probe the changes in interactions and compositions of the CAZ proteins, and the active zone ultrastructure in the absence of two of its largest proteins.

Chapter 2

RIM-BP2 as a regulator of neurotransmitter release at a central auditory synapse – the endbulb of Held

2a Introduction

Neurotransmitter release: Need for Speed

As the action potential invades the presynaptic compartment of the synapse, the VGCC are opened, resulting in a transient increase in local Ca^{2+} concentration at the presynaptic active zone. This Ca^{2+} reaches the calcium sensors (e.g. Synaptotagmin1/2/9 in CNS synapses) on the primed synaptic vesicles, setting in motion the machinery (SNAREs/SM proteins/other auxiliary proteins) for membrane fusion and eventual release of neurotransmitters from fused synaptic vesicles. The hallmark of this Ca^{2+} triggered release is its speed. Ca^{2+} triggers neurotransmitter release within a few hundred microseconds (e.g. Meinrenken et al., 2003). And the prerequisite for this speed is proximity of the source of Ca^{2+} to the vesicular release site. In fact, the distance of synaptic vesicles from VGCC determines the time course of their release (Chen et al., 2015), likely explaining the division of the pool of vesicles into fast and slow releasing sub-pools (Sakaba and Neher, 2001b).

Cytomatrix of the Active Zone: Coupling synaptic vesicles to VGCC

As discussed in the introduction (section 2) and chapter 1, the network of proteins at the active zone (AZ), the cytomatrix of the active zone (CAZ), plays an integral role in regulating neurotransmitter release. The CAZ proteins are involved in AZ formation (Maas et al., 2012; Shapira et al., 2003; Zhai et al., 2001) and maintenance (Waites et al., 2013), docking and priming of the pool of vesicles to be released (Augustin et al., 1999; Deng et al., 2011; Gracheva et al., 2008; Imig et al., 2014; Koushika et al., 2001; Schoch et al., 2002), and in clustering and positioning of the VGCC close to the synaptic vesicles (Frank et al., 2010; Han et al., 2011; Kaeser et al., 2011).

RIMs have been known to bind VGCC through their PDZ domain (Kaeser et al., 2011) and hence are essential for Ca^{2+} channels positioning at the AZ (Grabner et al., 2015; Han et al., 2011; Jung et al., 2015b; Kaeser et al., 2011; Kintscher et al., 2013). In addition to binding to the RIMs Ca^{2+} channels also bind to SH3 domain of RIM-BPs, which in turn are also interact with RIMs (Hibino et al., 2002). RIMs, as is well known, are essential for synaptic vesicle

docking and priming (Betz et al., 2001; Deng et al., 2011; Dulubova et al., 2005; Gracheva et al., 2008; Han et al., 2011; Koushika et al., 2001; Schoch et al., 2002; Wang et al., 1997). Basically, VGCC-RIM-RIM-BP can be envisaged as a tripartite complex linking the vesicles to the vicinity of Ca^{2+} channels, to be released (Figure 2a. 1).

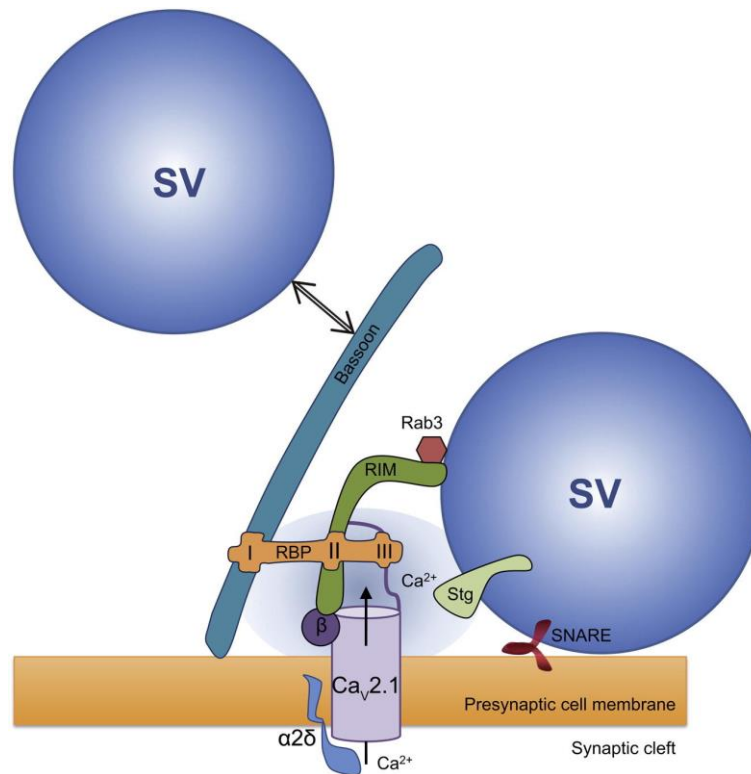


Figure 2a. 1: Illustration of interactions between RIM-BPs with Bassoon, RIM and VGCC

The interactions of RIM-BPs with other CAZ proteins (RIM and Bassoon) and the VGCC is proposed as the link coupling Ca^{2+} influx to synaptic vesicle release. Image taken from (Davydova et al., 2014).

More recently, Bassoon has joined this medley of proteins coupling synaptic vesicles to Ca^{2+} channels. Bassoon was reported to have a role in positioning and clustering of VGCC (Frank et al., 2010) but recently it was found to specifically regulate the positioning of P/Q- type Ca^{2+} channels at the AZ through its interactions with the SH3 domain of RIM-BP (Davydova et al., 2014). Since Bassoon has been implicated in recruitment of SVs to release sites (Frank et al., 2010; Hallermann et al., 2010b; Schulz et al., 2014), the triad of VGCC-Bassoon-RIM-BP is yet another bridge linking the SVs to Ca^{2+} channels (Figure 2a. 1). What stands out here is that the two proposed complexes regulating Ca^{2+} channels to SV proximity have RIM-BP at the central node.

Vertebrates express three RIM-BP genes: while RIM-BP1 and 2 are primarily found in the brain, RIM-BP3 is expressed outside of the brain (Mittelstaedt and Schoch, 2007). Studies from the drosophila neuromuscular junction (NMJ) AZ have shown that the absence of drosophila homolog of RIM-BP (DRBP) has severe structural and functional deficits (Liu et al., 2011; Müller et al., 2015). The studies conducted in mammalian synapses, however, did not report any dramatic effects of RIM-BP deletion at the synapse. The work from hippocampal synapses reported a subtle reduction in release probability in the absence of RIM-BP2 which led to increased facilitation at the synapse (Grauel et al., 2016). They also revealed an impaired VGCC clustering at the AZ, which in turn led to loosening of the coupling between Ca^{2+} channels and SV. They also found RIM-BP1 to exert no additional effect and RIM-BP2 to be the dominant isoform at hippocampal synapses.

A more elaborate study from the calyx of Held reported a very subtle phenotype (Acuna et al., 2015). They studied calyceal synapses deficient in both RIM-BP 1 and 2, and reported a reduced reliability of synaptic transmission and an increased distance between the Ca^{2+} channels and the SVs based on increased sensitivity to the 'slow' Ca^{2+} chelators EGTA. More recently, the same group proposed a functional redundancy between RIMs and RIM-BPs (Acuna et al., 2016) further undermining the role RIM-BP play in the orchestration of Ca^{2+} triggered neurotransmitter release.

In this study, constitutive RIM-BP2 knock-out mice have been used to elucidate its function at the hub of the release machinery. Again, the endbulb of Held synapse has been employed to study the physiological repercussions of RIM-BP2 deletion. As stated earlier (section 1a), given the high functional demands, these synapses are ideal to reveal any deficit in the synaptic machinery. Although, the studies in the calyx of Held (Acuna et al., 2015, 2016) did not reveal major implications of RIM-BP deficiency, it should be noted that they study was conducted in immature (P9-11) animals, hence potentially underestimating the impact. Here, at mature endbulbs of Held, RIM-BP2 deficiency seems to drastically change the characteristic short-term depression of the synapse to short-term facilitation, likely representing a reduction in release probability consistent with a deficit in coupling VGCC to vesicular release sites.

2b Results

2b.1 Knocking-out RIM-BP2 reduces the amplitude and alters the kinetics of evoked EPSCs at the endbulb of Held but leaves miniature EPSCs unaltered

To study the physiological implications of the loss of RIM-BP2 on synaptic transmission, the endbulb of Held was employed to study all three modes of release (Kaesler and Regehr, 2014): spontaneous, evoked and asynchronous. Starting with spontaneous, mEPSC were recorded as spontaneous events from postsynaptic bushy cells in the aVCN, as described in section 1b.3. The only difference is that in this study all recordings were made without Kynurenic acid or Cyclothiazide. The reason for this will be elaborated upon while discussing the short-term plasticity changes in the mutant in section 2c.1.

mEPSC were unaltered at the endbulb of Held in the absence of RIM-BP2. No difference was observed in the mEPSC amplitude (Table 2b. 1, Figure 2b. 1B'''), kinetics (Table 2b. 1, Figure 2b. 1B-B'') or frequency (Table 2b. 1, Figure 2b. 1B'''). This is agreement with the recent reports from hippocampal cultures and slices (Grauel et al., 2016) and the calyx of Held (Acuna et al., 2015).

Table 2b. 1: No change in mEPSC at the endbulb of Held in the absence of RIM-BP2

Parameter	WT	RIM-BP2 KO	p-value
Amplitude (pA)	130.54 ± 12.06	112.48 ± 4.03	0.22
10-90 Rise time (µs)	93.03 ± 2.80	93.72 ± 2.18	0.85
FWHM (µs)	181.02 ± 8.01	187.91 ± 4.19	0.46
Decay time (µs)	157.10 ± 9.64	167.50 ± 5.21	0.36
Frequency (Hz)	7.65 ± 1.28	8.01 ± 1.09	0.83

Data presented as mean (grand average of the means of all BCs) ± S.E.M. Statistical significance between groups was determined by either unpaired Student's t-test (in case of normally distributed data with comparable variances between the groups) or Wilcoxon rank sum test (when data distribution did not satisfy the criteria). Normality of distribution was tested with Jarque-Bera test and variances were compared with F-test. WT N = 4; n = 10, RIM-BP2 KO N = 7; n = 19 (N, number of animals; n, number of BCs).

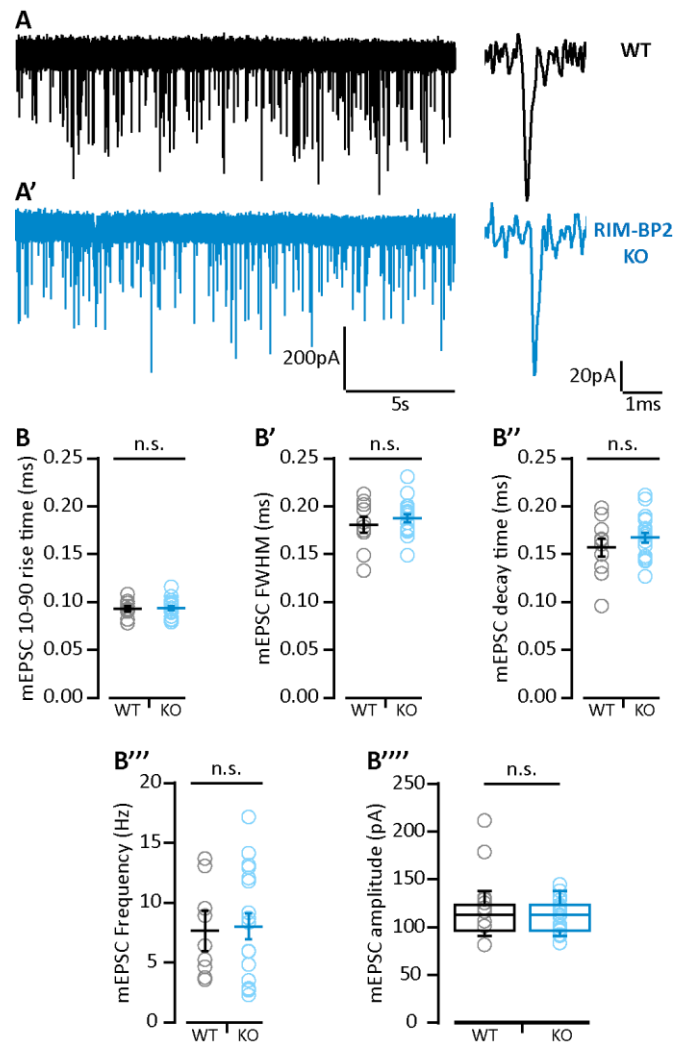


Figure 2b. 1: No change in mEPSC at the endbulb of Held in the absence of RIM-BP2

A) Representative traces of mEPSC: Continuous recording (left) and exemplary individual mEPSCs (right) for WT (A) and RIM-BP2 KO (A'). (B) Analysis of mEPSC: mEPSC amplitude (B), decay time (B'), full-width at half-maximum (FWHM; B'') rise time (B'''), and frequency (B''') remain unaltered. Each data point represents the mean estimate of a given BC. Normally distributed data presented as mean (grand average of the means of all BCs) \pm S.E.M. (B-B'''; n.s. – p-value > 0.05, Student's t-test). Non-normally distributed data presented as box and whisker plots (grand median (of the means of all BCs), lower/upper quartiles, 10-90 percentiles; B''''; n.s. – p-value > 0.05, Wilcoxon rank sum test). WT N = 4; n = 10, RIM-BP2 KO N = 7; n = 19 (N, number of animals; n, number of BCs).

For the analysis of evoked transmission, first the eEPSCs in response to single pulse stimulations were analyzed. This revealed reduced eEPSC amplitude in BCs of RIM-BP2 KO mice as compared to wildtype (Figure 2b. 2A, B), as was observed for hippocampal synapses (Grauel et al., 2016) and at the calyx of Held (Acuna et al., 2015). Additionally, eEPSC kinetics

were altered. Apart from rise time, half-width and decay times were both increased by 21% and 25% respectively (Figure 2b. 2A', D-E). Increased half-width was also observed at the calyx of Held (Acuna et al., 2015), but not the increase in decay time. RIM-BP2 even demonstrated a small but significant increase in synaptic delay at the endbulb of Held (Figure 2b. 2A,F), which was also reported for the calyx of Held (Acuna et al., 2015). For data analysis (Table 2b. 2, Figure 2b. 2) comprises of data points from RIM-BP2 KO littermate controls and C57/Bl6 wildtypes. The average traces (Figure 2b.2 A-A') for illustration of the phenotype depict only the dataset from RIM-BP2 KO and littermate WT.

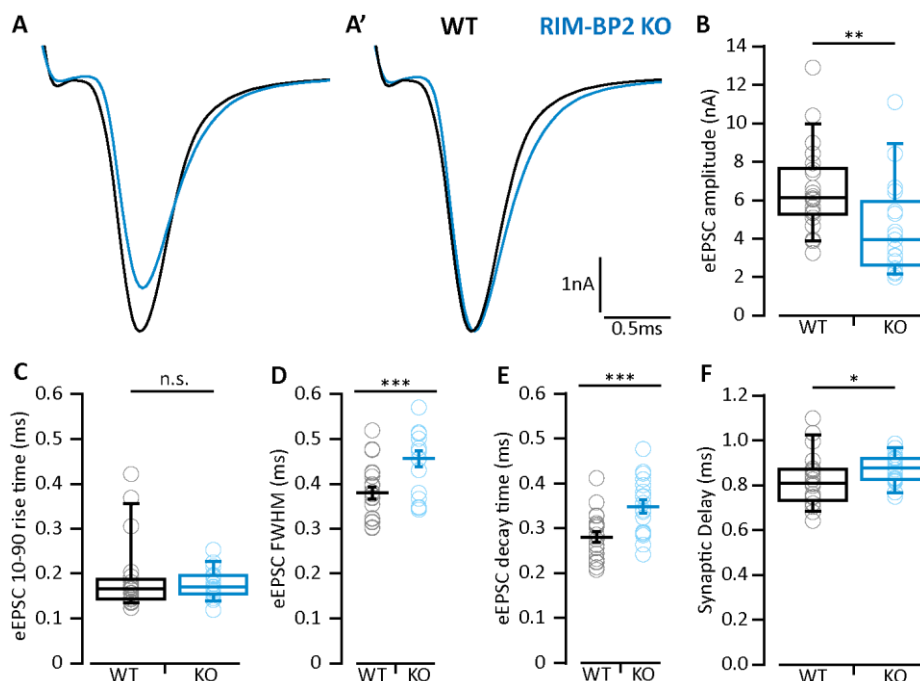


Figure 2b. 2: Reduced eEPSC amplitude and slower kinetics with increased synaptic delay at endbulbs of Held in RIM-BP2 KO mice

(A) Average traces of evoked EPSC (eEPSC) in littermate WT (black; N = 4; n = 6) and RIM-BP2 (blue; N = 6; n = 17) showing a reduced eEPSC amplitude in the mutant (A). Average RIM-BP2 eEPSC trace scaled to the peak of the average wildtype trace demonstrating altered eEPSC kinetics in the mutant. Positive peak at onset of trace reflects the stimulation artifact. (B) Reduced eEPSC amplitude in RIM-BP2 KO (N = 6; n = 17) as compared to WT (N = 17; n = 22). Each data point represents the mean estimate of a given BC, with thick bars representing grand average (of the means of all BCs) \pm S.E.M. (C-F) eEPSC kinetics: rise time (C) was unaltered; full-width at half-maximum (FWHM; D) and decay time (E) were significantly prolonged in RIM-BP2 KO (N = 7; n = 18) as compared to WT (N = 16; n = 21). Synaptic delay (F) was also increased at RIM-BP2 endbulbs. Each data point represents the mean estimate of a given BC. Normally distributed data presented as mean (grand average of the means of all BCs) \pm S.E.M. (C-D; *** – p-value < 0.001, Student's t-test). Non-normally distributed data presented as box and whisker plots (grand median (of the means of all BCs), lower/upper quartiles,

10-90 percentiles; B, C,F; n.s. – p-value > 0.05, ** – p-value < 0.01, * – p-value < 0.05 Wilcoxon rank sum test). N, number of animals; n, number of BCs.

Table 2b. 2: Reduced eEPSC amplitude and slower kinetics with increased synaptic delay at endbulbs of Held in RIM-BP2 KO mice

Parameter	WT	RIM-BP2 KO	p-value
Amplitude (nA)	6.57 ± 0.47	4.54 ± 0.75	0.004**
10-90 Rise time (ms)	0.19 ± 0.02	0.18 ± 0.01	0.49
FWHM (ms)	0.38 ± 0.01	0.46 ± 0.02	0.0005***
Decay time (ms)	0.28 ± 0.02	0.35 ± 0.02	0.0004***
Synaptic delay (ms)	0.82 ± 0.03	0.89 ± 0.02	0.013*

Data presented as mean (grand average of the means of all BCs) ± S.E.M. Statistical significance between groups was determined by either unpaired Student's t-test (in case of normally distributed data with comparable variances between the groups) or Wilcoxon rank sum test (when data distribution did not satisfy the criteria). Normality of distribution was tested with Jarque-Bera test and variances were compared with F-test. For sample size refer to Figure 2b.2.

2b.2 Absence of RIM-BP2 changes short-term depression characteristic for the endbulb of Held to short-term facilitation

To characterize the changes in short-term plasticity at the endbulb of Held in RIM-BP2 mice, responses to high frequency train stimulation were studied. BCs in the mouse aVCN normally demonstrate characteristic short-term depression in response to train stimulation (Chanda and Xu-Friedman, 2010). However, upon analysis, at RIM-BP2 KO endbulbs the PPR, calculated as the ratio of the amplitude of second EPSC in the train to that of the first EPSC of the train ($EPSC_2/EPSC_1$), was significantly increased by at least 35% at all three frequencies (Table 2b. 3, Figure 2b. 3). Other studies corroborate this increase in PPR in the absence of RIM-BP2 (Acuna et al., 2015; Grauel et al., 2016).

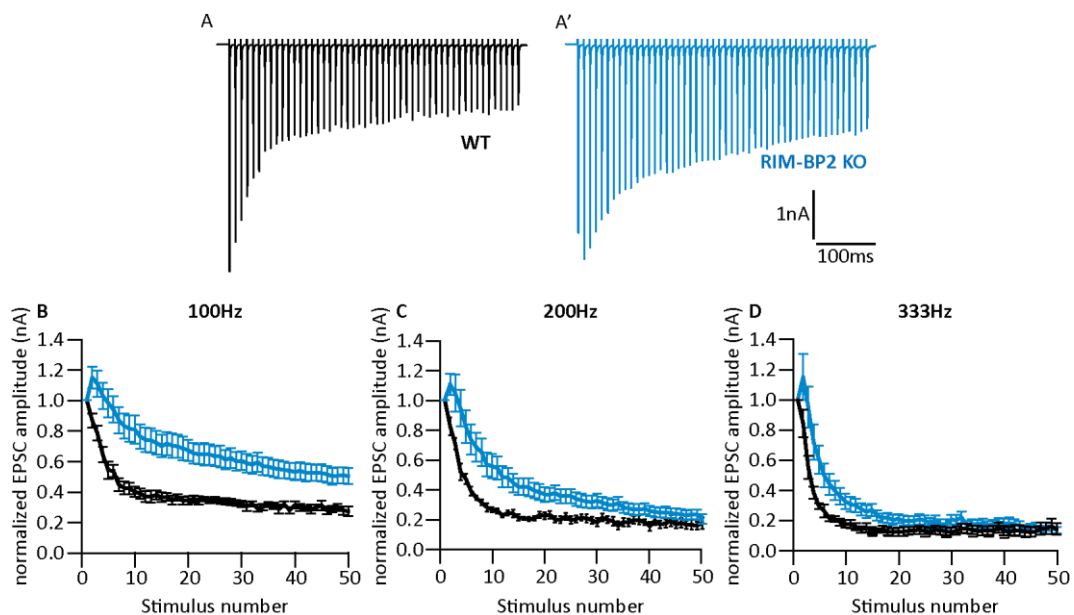
The bushy cell short-term depression was effectively replaced by an initial short-term facilitation due to the lack of RIM-BP2 at the synapse. Though, after the initial facilitation, the KO response decayed to a steady-state level comparable to that of the wildtype ($EPSC_{30-50}/EPSC_1$; Table 2b. 3, Figure 2b. 3).

Despite, the convergence of steady-state response in RIM-BP2 and WT, the decay of response in the mutant was significantly slower at all three frequencies (τ (ms); Table 2b. 3, Figure 2b. 3).

Table 2b. 3: Short-term depression replaced by facilitation at endbulbs of Held in RIM-BP2 KO mice

Frequency	Parameter	WT	RIM-BP2 KO	p-value
100Hz	PPR	0.84 ± 0.03	1.15 ± 0.01	1.85x10⁻⁵****
	EPSC ₃₀₋₅₀ /EPSC ₁	0.39 ± 0.03	0.54 ± 0.06	0.092
	τ (ms)	43.56 ± 5.01	126.20 ± 20.41	0.00012***
200Hz	PPR	0.81 ± 0.03	1.10 ± 0.07	0.0007***
	EPSC ₃₀₋₅₀ /EPSC ₁	0.27 ± 0.02	0.27 ± 0.04	0.92
	τ (ms)	20.66 ± 2.44	44.89 ± 7.02	0.0012**
333Hz	PPR	0.81 ± 0.04	1.15 ± 0.15	0.0056**
	EPSC ₃₀₋₅₀ /EPSC ₁	0.18 ± 0.02	0.17 ± 0.03	0.78
	τ (ms)	8.90 ± 0.89	15.38 ± 2.21	0.016*

Data presented as mean (grand average of the means of all BCs) ± S.E.M. Data information: WT comprises of data points from RIM-BP2 KO littermate controls and C57/B6 wildtypes. Sample size for 100 Hz:- WT N = 17; n = 22, RIM-BP2 N = 6; n = 17, 200Hz:- WT N = 17; n = 21, RIM-BP2 N = 7; n = 15, and 333Hz:- WT N = 12; n = 16, RIM-BP2 N = 5; n = 10. N, number of animals; n, number of BCs. Statistical significance between groups was determined by either unpaired Student's t-test (in case of normally distributed data with comparable variances between the groups) or Wilcoxon rank sum test (when data distribution did not satisfy the criteria). Normality of distribution was tested with Jarque-Bera test and variances were compared with F-test. **** p-value < 0.0001, *** p-value < 0.001, * p-value < 0.05.

**Figure 2b. 3: Short-term depression replaced by facilitation at endbulbs of Held in RIM-BP2 KO mice**

(A) Average traces of EPSCs evoked in response to 100Hz train stimulation, recorded from WT (A) illustrating characteristic fast kinetics and short-term depression of bushy cell EPSCs and RIM-BP2 KO (A') synapses, demonstrating the change in short-term depression to facilitation. (B-D) Short-term

plasticity (represented as normalized amplitude vs stimulus number) changes in RIM-BP2 (blue) as compared littermate WT (black), in response to high-frequency train stimulation at 100Hz (B), 200Hz (C) and 333Hz (D). Data represented as average trace \pm S.E.M. For illustration of the phenotype only the datasets from RIM-BP2 KO and littermate WT are shown (B-D). Data information: for 100Hz:- WT N = 4; n = 6, RIM-BP2 N = 6; n = 17, 200Hz:- WT N = 4; n = 6, RIM-BP2 N = 7; n = 15, and 333Hz:- WT N = 3; n = 5, RIM-BP2 N = 5; n = 10. N, number of animals; n, number of BCs.

2b.3 RIM-BP2 deficiency slows down the speed of recovery from short-term depression and leads to increased asynchronous release after stimulation at the endbulb of Held

Recovery after vesicle depletion was studied, by measuring eEPSC amplitudes elicited by single stimuli presented at varying time intervals after a conditioning 100Hz train of 50 pulses (Figure 2b. 4A). Recovery is displayed as eEPSC amplitudes normalized to the amplitude of the first eEPSC of the conditioning train (Figure 2b. 4B). A single exponential function was used to fit the time course of recovery. Normally, a double exponential function fits the time course of recovery from vesicle depletion at the endbulb of Held (Schulz et al., 2014; Yang and Xu-Friedman, 2008). However, in this case the time course of recovery in RIM-BP2 was fit better with a single exponential function. Hence, both the WT and KO time courses of recovery were described by single exponential fits to facilitate comparison. The endbulbs of RIM-BP2 KO mice show a slower recovery after vesicle depletion. However, this inference needs to be validated with further experiments due to the limited sample size. Other studies, in hippocampal synapses (Grauel et al., 2016) and the calyx of Held (Acuna et al., 2015), did not report a similar deficit in the recovery but a study from *Drosophila* neuromuscular junction reported a role of RIM binding protein (drbp) in vesicle resupply (Müller et al., 2015).

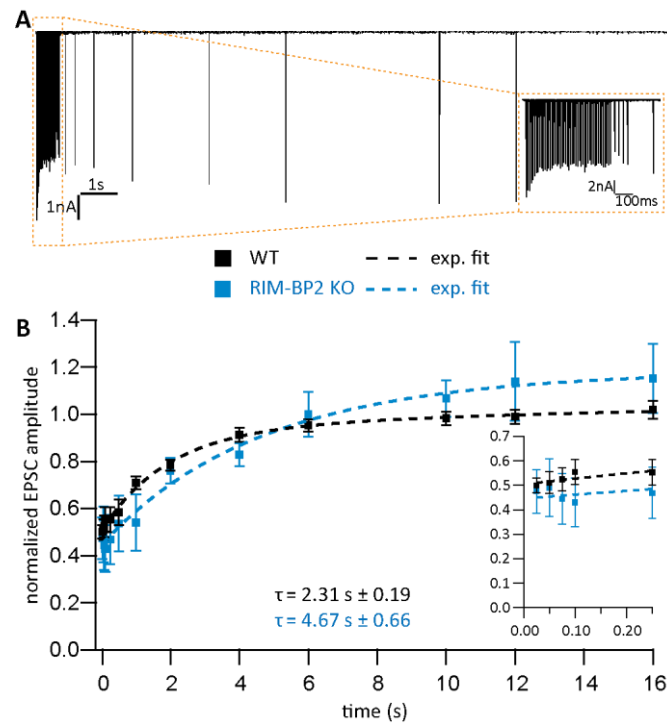


Figure 2b. 4: Slower recovery from short-term depression at endbulbs of Held lacking RIM-BP2

(A) Trace of a WT endbulb synapse to illustrate the recovery protocol. Following a conditioning 100Hz train of 50 stimuli, recovery from short-term depression was assessed by single test pulses presented after (in ms) 25, 50, 75, 100, 250, 500 (further in s) 1, 2, 4, 6, 10, 12 and 16. Inset shows the responses to the first 5 stimuli in detail. (B) Recovery plotted as mean (\pm S.E.M.) EPSC amplitude in response to test pulses normalized to the first EPSC amplitude of the conditioning train. Dashed lines are single exponential fits. The time constants (τ) are provided on the graph. WT comprises of data points from RIM-BP2 KO littermate controls and C57/B6 wildtypes. WT N = 19; n = 22, RIM-BP2 KO N = 3; n = 9.

Asynchronous release was analyzed as the rate of mEPSC events occurring in the first 100ms after the end of 100Hz train stimulation. As compared to wildtype, the endbulbs of RIM-BP2 KO mice show significantly higher asynchronous activity as compared to WT following the cessation of synchronous release in response to high frequency train stimulation (Figure 2b. 5).

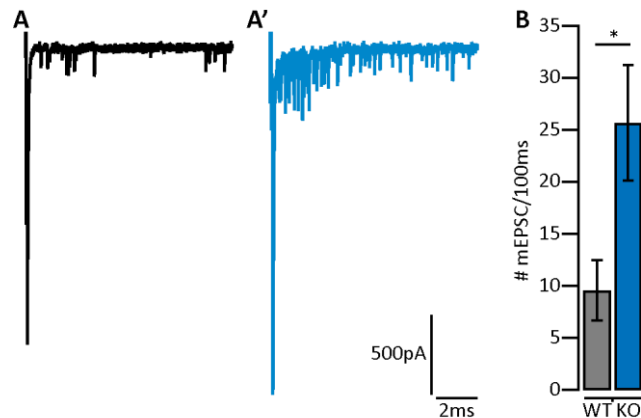


Figure 2b. 5: Increased asynchronous release at the endbulbs of Held in RIM-BP2 aVCN

(A) Example traces of asynchronous release events after 100Hz train stimulation in WT (A) and RIM-BP2 (A'). Positive peaks at the beginning of each trace are the stimulus artifacts before the last EPSC of the train, which is followed by mEPSC corresponding to asynchronous release. (B) Asynchronous activity at the endbulb of Held synapse is quantified as number of mEPSC events per 100ms after the cessation of 100Hz train stimulation. Asynchronous activity increased at the RIM-BP2 KO endbulbs (* – p-value < 0.05, Wilcoxon's rank sum test). Data information: WT (data points from RIM-BP2 KO littermate controls and C57/B6 wildtypes) WT N = 7; n = 10, RIM-BP2 N = 6; n = 18. Error bars represent S.E.M.

2c Discussion

Ca²⁺ evoked neurotransmitter release is remarkably fast (Borst and Sakmann, 1996) and is elicited within a few hundred microseconds after the action potential invades the presynaptic terminal (Meinrenken et al., 2003). This speed requires a tight coupling of voltage-gated Ca²⁺ influx and neurotransmitter release from SVs. To ensure this coupling VGCC are placed in close spatial proximity to the release-ready vesicles at the active zones (Eggermann et al., 2012). The data suggest that RIM-BP2 acts as a molecular linker contributing to this Ca²⁺ influx- exocytosis coupling.

2c.1 Loss of RIM-BP2 changes short-term plasticity at the endbulb of Held and impairs evoked release

The most striking observation at the endbulb of Held in the absence of RIM-BP2 was the increase in PPR and consequent change of short-term depression to initial facilitation. It should be noted that the recordings were made in the absence of Kynurenic acid or

Cyclothiazide, so the post-synaptic processes of receptor desensitization and saturation cannot be excluded. However, it can be reasoned that since the second EPSC facilitates, the release in the first EPSC did not saturate/desensitize the receptors in case of the RIM-BP2-deficient endbulbs. Rather, the synaptic phenotype might have even been underestimated, as a higher increase in PPR could result in the absence of receptor desensitization and saturation.

Since, the response to train stimulation failed to reach a steady-state plateau during the duration of the stimulus, cumulative analysis (Schneppenburger et al., 1999) could not be used to estimate release probability or RRP size (Neher, 2015). In this scenario, measuring exocytosis by calculating changes in presynaptic membrane capacitance (Sun and Wu, 2001) or by assessment of postsynaptic response to pool depleting presynaptic depolarization (Sakaba and Neher, 2001a), might provide better estimation of RRP and release probability.

Nevertheless, the increased PPR, and the slower kinetics and reduced extent of synaptic depression during train stimulation, point to a reduced release probability at the endbulb of Held in RIM-BP2 KO mice. The consequence of this reduced release probability is also seen in the reduced evoked EPSC amplitude. Even though one cannot eliminate the possibility of a reduced RRP that might contribute to a reduced EPSC amplitude, other studies (Acuna et al., 2015; Grauel et al., 2016) did not reveal any reduction in RRP at the calyx of Held synapse and hippocampal synapses respectively. Hence, it is safe to assume a reduced release probability as a major contributor to the reduced EPSC amplitude.

Beyond the lower amplitude, the single AP-evoked EPSC in the RIM-BP2 KO endbulbs also demonstrated an increased synaptic delay and slower kinetics (increased half-width and slower decay time). While, the synaptic delay is indicative of malfunction of the release apparatus, the slower kinetics could also be due to changes in postsynaptic receptors. However, unaltered kinetics of mEPSCs rule out postsynaptic contributions. Thus, both the synaptic delay and the slow kinetics seem to be presynaptic in origin.

Indeed, our preliminary results (data not shown) and Grauel et al., 2016 show that the KO phenotype was rescued by increasing extracellular Ca^{2+} concentration. This could imply that

the Ca^{2+} influx or the topography of presynaptic Ca^{2+} channels is impaired. Alternatively, the sensitivity of the release machinery to Ca^{2+} is reduced or the fusion competence of synaptic vesicles might be impaired at KO synapses. Given the interaction of RIM-BP2 with Ca^{2+} channels and with vesicular release sites via RIM, I favor the interpretation that the coupling of Ca^{2+} influx to exocytosis is compromised at RIM-BP2 deficient synapses. Acuna et al., 2015, through unchanged presynaptic Ca^{2+} currents claimed that the Ca^{2+} influx is unaffected at the calyx of Held. If the Ca^{2+} influx is unperturbed also at RIM-BP2 deficient endbulb synapses, the loss of sensitivity to Ca^{2+} might still be mediated through an increased coupling distance between the Ca^{2+} channels and the fusion machinery e.g. via changes in Ca^{2+} channel clustering at the synapse. Indeed Acuna et al., 2015 demonstrated a loosening of spatial coupling of Ca^{2+} channels to release sites based on higher sensitivity of release to slow Ca^{2+} buffer EGTA. However, this study was conducted at immature synapses (P10-12). Since there is a developmental change from loose spatial coupling of N- and P/Q type Ca^{2+} channels to release machinery in immature synapses, to a tightly coupled P/Q-type Ca^{2+} channels (Fedchyshyn and Wang, 2005), it might have underestimated the change in coupling distance brought about by the disruption of RIM-BPs. Indeed, the preliminary analysis of Ca^{2+} channel clusters at release sites of mature calyx of Held, by SEM analysis of SDS-PAGE replica (Nakamura et al., 2015), performed by our collaborators Harada and Shigemoto, revealed a change in Ca^{2+} channel clustering at the presynapse (Harada and Shigemoto, unpublished data).

The interpretation of the unchanged Ca^{2+} current at immature RIM-BP-deficient calyces of Held synapses (Acuna et al., 2015) needs caution. RIM-BPs and RIMs regulate the spatial arrangement of N- and P/Q-type Ca^{2+} channels (Hibino et al., 2002; Kaeser et al., 2011), while Bassoon and RIM-BPs specifically localize P/Q-type Ca^{2+} channels. N-type Ca^{2+} channels are present at immature synapses but not at mature ones which solely rely on P/Q-type channels (Scholz and Miller, 1995). Therefore, the loss of RIM-BPs alone may not affect Ca^{2+} influx at immature calyces, as RIMs also bind to the VGCC directly and can maintain Ca^{2+} channel clustering, and hence Ca^{2+} current at the synapse (Han et al., 2011; Kaeser et al., 2011). Consistent with this notion, only the elimination of both RIMs and RIM-BPs diminishes the presynaptic Ca^{2+} current (Acuna et al., 2016). Since Bassoon does not bind directly to

P/Q-type Ca^{2+} channels, predominant at mature synapse, but only through RIM-BPs (Davydova et al., 2014), the loss RIM-BPs may elicit a more drastic change in Ca^{2+} channel clustering and presynaptic Ca^{2+} influx in mature preparations. Hence, the change in presynaptic Ca^{2+} current should be revisited in mature synapses.

2c.2 Loss of RIM-BP2 increases asynchronous release which may slow down recovery from short-term depression

Asynchronous release more than doubled at RIM-BP2 KO endbulbs as compared to the wildtype. Although, the previous RIM-BP study (Acuna et al., 2015) did not report an increase in asynchronous component of release it showed a decrease in the ratio of fast to slow component of release during RRP depletion. This implies a reduction in the vesicles released from fast pool and a shift to the release from the slow pool. Since, the slow pool makes up the vesicles released asynchronously (Sakaba, 2006), it follows the observation that the RIM-BP2 deficient synapses show an increased asynchronous release at the cost of synchronous release.

This protracted release following high-frequency stimulation might be a contributing factor towards a slower recovery from short-term depression observed in the KO mice. The recovery at RIM-BP2 KO endbulbs was defined by a single exponential fit rather than the typical double exponential functions (Schulz et al., 2014; Yang and Xu-Friedman, 2008). This loss of the fast component, which corresponds to the recovery of slow pool (Sakaba and Neher, 2001a) and is calcium dependent (Yang and Xu-Friedman, 2008), may be a result of increased asynchronous release and loss of Ca^{2+} regulation in the absence of RIM-BP2. Other studies (Acuna et al., 2015; Grauel et al., 2016) did not report a recovery deficit, but there the recovery measurements were started from 100ms and 5s respectively, as opposed to 25ms, in this study at the endbulb of Held. However, further experiments are needed to confirm this hypothesis.

Chapter 3

Role of LRBA2 in cochlear hair cell function and hearing

3a Introduction

BEACH proteins and LRBA

Lipopolysaccharide-responsive beige like anchor protein or LRBA is one of nine members of the BEACH domain containing protein (BDCP) family Figure 3a. 1. The BEACH domain is a conserved ~300 amino acid domain (Jogl et al., 2002) that gets its name from the combination of ‘Beige and Chediak-Higashi’. It was the region within the lysosomal trafficking regulator (LYST) protein, found to be mutated in the Chediak-Higashi syndrome and beige was the name of the mouse model for it (Nagle et al., 1996). Other than the BEACH domain, BDCPs have pleckstrin homology (PH)- like domains, WD40 repeats and concanavalin A (ConA)- like lectin domains for bio-membrane and protein-protein interactions (Burgess et al., 2009; Jogl et al., 2002).

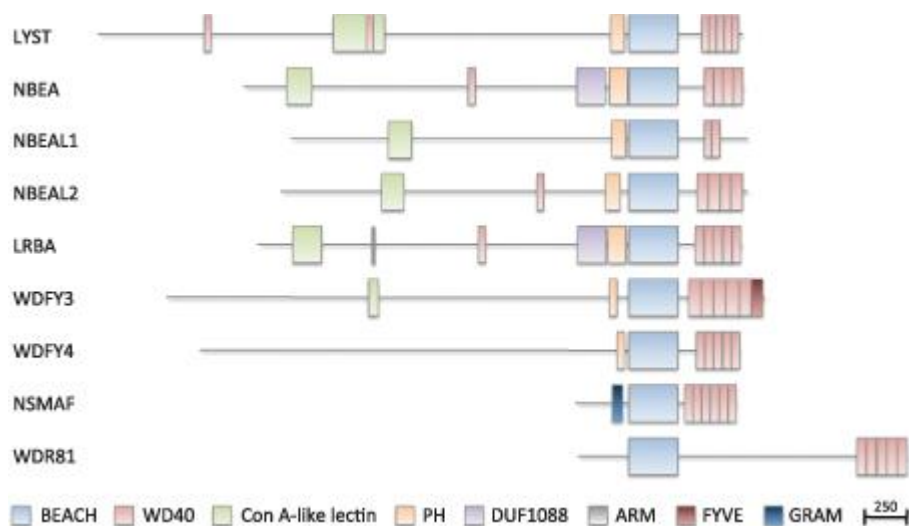


Figure 3a. 1: Domain structures of BEACH domain containing proteins (BDCPs)

Domain structures of all nine BEACH domain containing proteins (BDCPs) drawn to scale. Figure taken from Cullinane et al., 2013.

Even after nearly 20 years since their discovery, the role BDCPs in molecular and cellular functions remains unidentified. However, their importance in cellular mechanisms like vesicular transport, apoptosis, membrane dynamics and receptor-ligand signaling is reflected by the complex phenotypes manifested by BDCP mutations. Mutations in the BEACH domain of LYST cause Chediak–Higashi syndrome, characterized by enlarged lysosomes and related

organelles (Burkhardt et al., 1993; Nagle et al., 1996). Another BEACH protein, Neurobeachin (NBEA) was recently reported to be relevant for synaptic transmission by regulating the transport of neurotransmitter receptors to the synapse (Nair et al., 2013).

A physiological importance of LRBA has been revealed by studies reporting that its upregulation may facilitate cancer growth (Wang et al., 2004) and its deleterious mutations cause autoimmunity syndrome (Lo et al., 2015; Lopez-Herrera et al., 2012). Although, LRBA has elevated expression in immune cells, it is also expressed in many other tissues (Wang et al., 2001), where its function is even less understood.

Following the detection of possible hearing impairment in LRBA2-KO mice, during a phenotyping screen at the German Mouse Clinic (GMC), this study was undertaken to elucidate the role of LRBA in auditory function.

Sound encoding: Hair cells and Spiral ganglion neurons

Sound encoding proceeds in the organ of Corti that sits on the basilar membrane in the cochlea of the inner ear (Figure 3a. 2A). The organ of Corti hosts mechanosensory hair cells that reliably transduce the mechanical vibrations elicited by the incoming sound waves into graded receptor potentials and finally into a neural code that represents sound information with high temporal precision and frequency selectivity. This demanding task relies on the interplay of two types of hair cells: (i) outer hair cells (OHCs) that amplify the sound-induced oscillations of the basilar membrane and fine-tune frequency resolution and (ii) inner hair cells (IHCs) – which are the true sensory cells of the organ and transmit information to the spiral ganglion neurons (SGNs).

At their apical end, both types of hair cells have highly organized arrays of actin-rich microvilli (stereocilia), that form the characteristic hair bundle and harbor the components of the mechanotransduction machinery. Upon physical hair bundle deflection, the coordinated opening of mechanically-gated ion channels in the stereociliary tips mediates hair cell depolarization, which in turn leads to synchronized electromotile contraction of OHCs and presynaptic glutamate release from the 5-20 active zones in IHCs. Each IHC synapse carries a synaptic ribbon; a highly specialized structure which enables the turnover

of hundreds of vesicles per second with sub-millisecond temporal precision (Pangrsic et al., 2010). The postsynaptic SGNs then transmit the signal to higher auditory brain centers as action potential firing.

SGNs have been classified based on the extracellular recordings of firing from auditory nerve fibers (ANFs; central neurites of SGNs) (Figure 3a. 2B). This classification takes into consideration: (i) their spontaneous firing rate (SR; action potential firing in the absence of sound stimulus) (ii) sound intensity thresholds to pure tones presented at their characteristic frequency and (iii) the dynamic range of spiking in response to increasing sound intensity (rate-level function) (Liberman, 1978). One population of ANFs was characterized by low spontaneous rate of firing with high sound intensity thresholds and a broad dynamic range of spiking in response to increasing sound intensity. A second population of SGNs exhibited high spontaneous rate firing with low thresholds and a narrower dynamic range (Taberner and Liberman, 2005). Intriguingly, these SGN populations are also demarcated by their polarity of innervating IHC synapses. High spontaneous rate fibers primarily contact IHCs at the abneural side (pillar side) and low spontaneous rate fibers are preferentially located at the neural side (modiolar side) (Liberman, 1982). This heterogeneity in the firing pattern of SGNs has been subject to extensive research with both pre- and postsynaptic mechanisms contributing (e.g. Merchan-Perez and Liberman, 1996; Frank et al., 2009). The neural side seems to have larger presynaptic ribbons and more Ca²⁺ channels but operate on a more depolarized activation range (Ohn et al., 2016), that may contribute to the high threshold of firing of SGNs.

Here, studying LRBA2 deficiency in the context of auditory processing revealed impaired cochlear amplification of sound intensity and frequency tuning, with a loss of low spontaneous rate fibers.

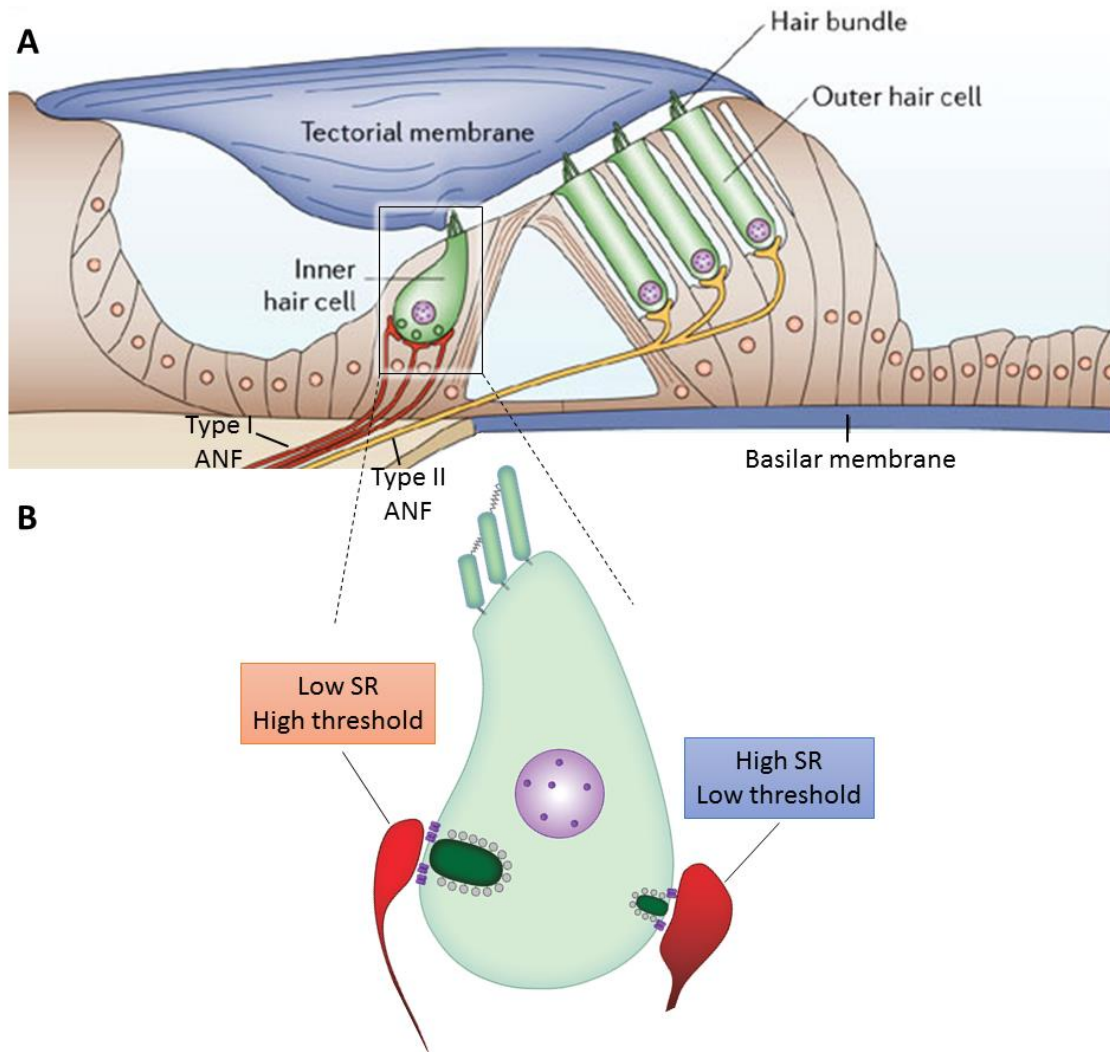


Figure 3a. 2: Organ of Corti and inner hair cell (IHC) with the classification of SGNs

(A) Illustration of organ of Corti sitting on the basilar membrane. The three rows of OHCs provide cochlear amplification of sound intensity and fine-tuning of sound resolution. Image adapted from Fettiplace and Hackney, 2006 (B) IHCs are the true sensory units of the organ which convert sound into graded receptor potential that then transmits the signal to SGNs through graded release of glutamate at the ribbon synapses. Figure depicts the distinction in the pre- and postsynaptic morphology contributing to heterogeneity in SGN response. Abneural (pillar side) with small ribbon (green bulb), less Ca^{2+} channels (purple blocks at the base of the ribbon) and large bouton (red) innervated by high SR low threshold fibers, while neural (modiolar side) with opposite gradient is innervated by low SR high threshold fibers.

3b Results

3b.1 Progressive hearing loss and compromised cochlear amplification in LRBA2 KO mice

A possible hearing impairment due to the loss of the BEACH protein, LRBA2 was first suggested upon finding reduced auditory startle responses during phenotypic screening of LRBA2 KO mice by the German Mouse Clinic (Figure 3b. 1).

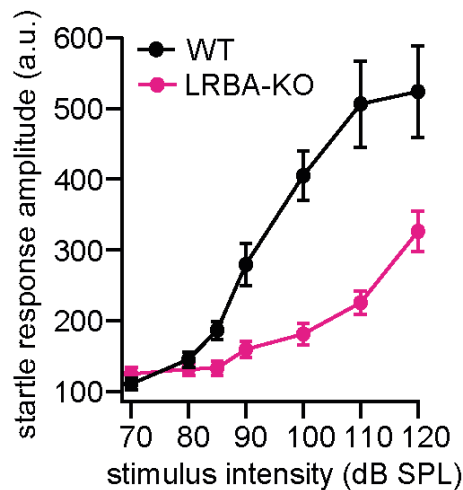


Figure 3b. 1: Reduced acoustic startle response amplitudes in LRBA2 KO compared to WT animals

Data represented as average trace \pm S.E.M. Animal number was 10 for both genotypes. Startle response was measured at the German mouse clinic (GMC).

Further assessment of hearing in LRBA2-KO mice was done by recording auditory brainstem responses (ABR). Immediately after hearing onset at P14-15, ABR thresholds to tone bursts and click stimulation were moderately elevated in LRBA2-KO mice. However, the hearing impairment progressively deteriorated with age (Figure 3b. 2A-B).

All ABR waves, reporting synchronous spiking in response to sound onset in SGNs (wave I) and neurons of the auditory brainstem (waves II-V) (Figure 3b. 2C), were markedly reduced in amplitude. In addition, ABR thresholds were elevated (Figure 3b. 2A) and ABR latencies were increased, indicating loss in acoustic sensitivity (Figure 3b. 2D).

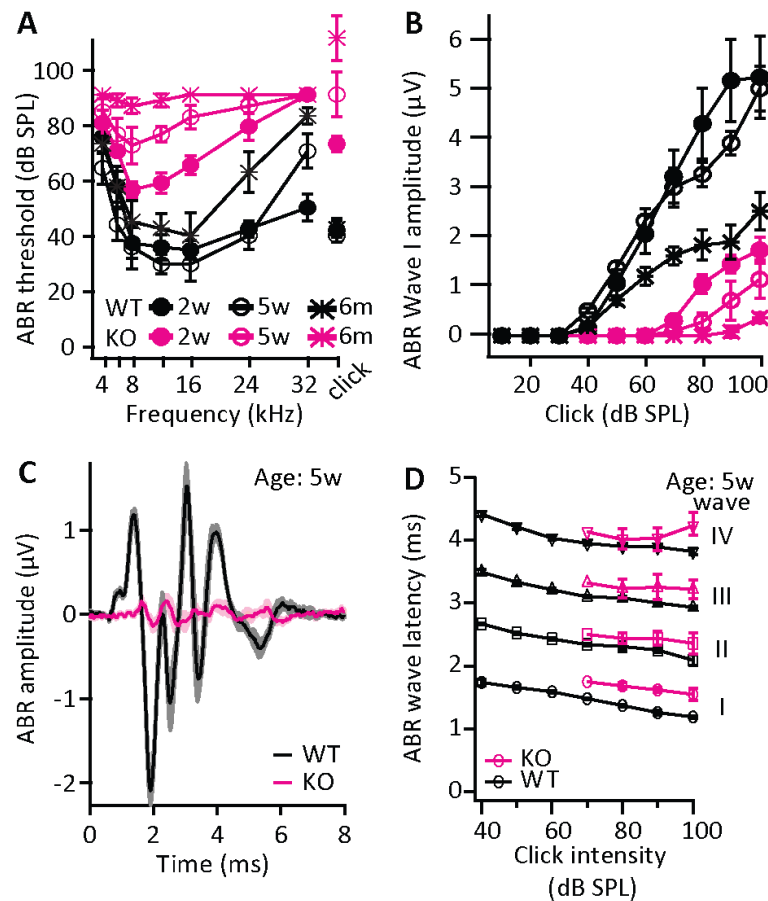


Figure 3b. 2: Progressive hearing loss in LRBA2 mutants.

(A) Auditory brainstem response (ABR) recordings from 2-3 weeks old (p14-19; filled circles, N=6 each), 4-5 weeks old (open circles, N=8 KO/9WT) and six months old (cross, N=5KO/4WT) LRBA2-KO mice (magenta) and WT littermates (black). Thresholds exceeding the maximum loudspeaker output (80dB for tone bursts, 120dB for clicks) were assigned values of 90/130dB for calculation of the average. (B) ABR wave I has dramatically decreased amplitudes with a shallower growth function in the mutants, progressively deteriorating with age (C) Grand averages \pm S.E.M. (shaded) of ABR to 80dB click stimuli show a strong reduction of ABR waves I-V in LRBA2-KO mice (magenta, N=9) compared to WT (black, N=8, age group 5 weeks). (D) ABR latencies in LRBA2 KO mice (N=8) are increased compared to WT (N=9; age group 5 weeks) when comparing for same stimulus intensities. N represents the number of animals. ABRs were measured by technical assistants Nadine Hermann and Stefan Thom.

Electrocochleography recordings corroborated the elevated thresholds and reported a reduction of the cochlear microphonic and summing potentials (Figure 3b. 3A-C), indicating an outer hair cell functional deficit. In addition to electrocochleography, outer hair cell function was also studied by distortion product otoacoustic emissions (DPOAE), which were greatly reduced in LRBA2 KO mice across all frequencies (Figure 3b. 3D). Electrocochleography and DPOAE together indicate that the loss in sound sensitivity is due

to impaired peripheral auditory function and involves a defect of cochlear amplification. However, the shallow growth of ABR wave I amplitude with intensity (Figure 3b.2B) after surpassing the hearing thresholds alludes to more than just OHC defect.

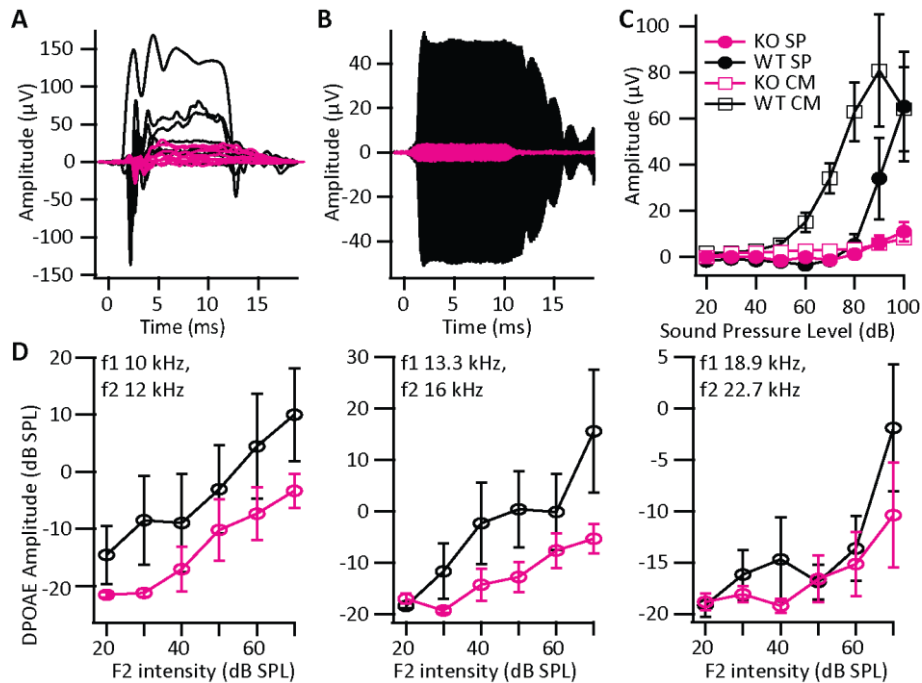


Figure 3b. 3: Reduced cochlear amplification and outer hair cell dysfunction

(A-C) Representative traces of (A) summing potentials and (B) cochlear microphonic potentials to 90dB 16kHz tone bursts. (C) Quantification of the amplitude of cochlear microphonic potentials (open squares) and summing potentials (closed circles) for 16kHz tone bursts at varying intensities (N=8 each, age 4-5 weeks). (D) Reduced amplitudes of distortion product otoacoustic emissions (DPOAE) in LRBA2 KO animals (magenta, N=9) compared to WT littermates (black, N=8) are suggestive of an amplifier defect (age 4-5 weeks). N represents the number of animals. Electrocochleography was performed by Dr. Nicola Strenzke. DPOAEs were measured by technical assistants Nadine Hermann and Stefan Thom.

3b.2 Hearing deficit in LRBA2 KO – *in vivo* analysis

The sound encoding deficit in the absence of LRBA2 was further characterized by investigating single units of auditory nerve fibers (central neurites of spiral ganglion neuron, SGN) *in vivo*. Both spontaneous and sound-evoked action potential firing of postsynaptic SGNs were recorded *in vivo*. The distribution of spontaneous SGN firing rates was clearly biased towards high SR (spontaneous rate) fibers in LRBA2-KO mice. (Figure 3b. 4A; median SR; WT: 6.6; LRBA2-KO: 30.20).

After characterizing spontaneous firing for each fiber, frequency tuning was assessed by determining sound thresholds for varying tone burst frequencies. While fibers from wild-type animals had normal, sharp tuning curves with low thresholds, LRBA2-KO fibers showed broadened tuning curves with poorly defined characteristic frequencies and highly elevated thresholds (Figure 3b.4B; median threshold; WT: 51dB; LRBA2-KO: 92dB).

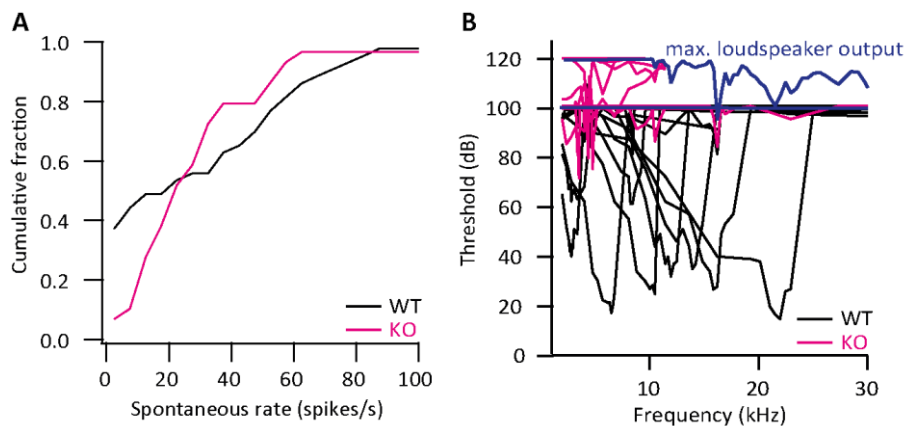


Figure 3b. 4: Reduced fraction of low-spontaneous-rate fibers and elevated sound thresholds and in LRBA2 KO animals.

(A) Distribution of spontaneous firing rates of SGN from WT and LRBA2 KO mice aged 5-6 weeks. Mutants (magenta, $n=54$) show a reduction in the fraction of low spontaneous rate fibers compared to WT (black, $n=49$). (B) Sound thresholds of LRBA2 KO (magenta) SGNs are highly elevated and lack the asymmetric V-shaped frequency tuning curve that is typical of WT SGNs (representative examples). The maximum stimulus intensity (blue line) was initially restricted to 100dB to avoid noise damage. Since mutant SGNs typically did not respond at that intensity, it was increased up to 120dB in later experiments with LRBA2 KO. n represents the number SGN units.

The rate level function (Figure 3b. 5) was obtained by quantifying the overall spike rate of the fiber units in response to increasing stimulus intensities presented at characteristic frequency of the unit (determined as well as it was possible given the poor frequency tuning). Of note is the significantly steeper rise in spike rates with stimulus level in LRBA2 KO than in the wildtype littermates (Figure 3b. 5B). Moreover, the dynamic range of LRBA2 KO SGNs tended to be reduced (Figure 3b. 5C). This is as expected for a defect in cochlear amplification.

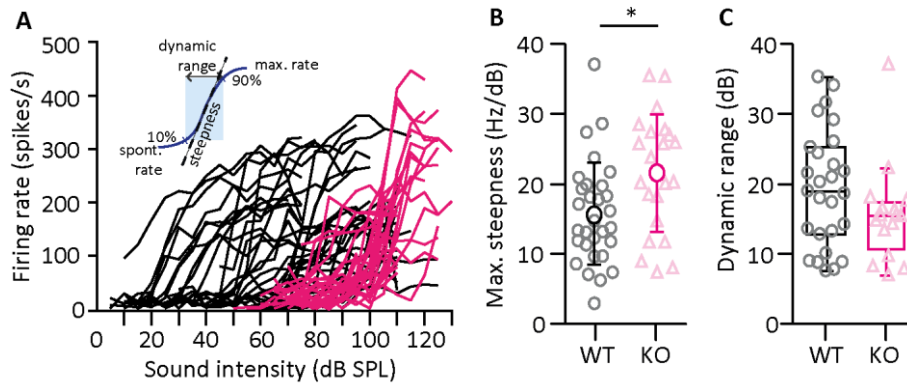


Figure 3b. 5: Rate level function: Spike rate in response to sound stimulus steeper in LRBA2 KO SGN units

(A-C) SGN firing rates in response to tone bursts of varying intensities (A): Mutants show elevated thresholds, a steeper increase in firing rate (B, WT n=30, KO n=22, $p=0.011$, Student's t test) and a trend for a reduced dynamic range (C, WT n=27, KO n=16, $p=0.126$, Mann-Whitney-U test). Each data point represents value from a single SGN unit. n represents the number SGN units.

The evoked spike rates and time courses of adaptation in response to tone bursts at high intensities – at which spike rates were saturated – were identical between LRBA2 KO and wildtype littermate controls (Figure 3b. 6A). Also, presynaptic vesicle pool depletion and recovery, as assessed in a paired pulse paradigm, were normal in LRBA2 KO mice (Figure 3b.6B).

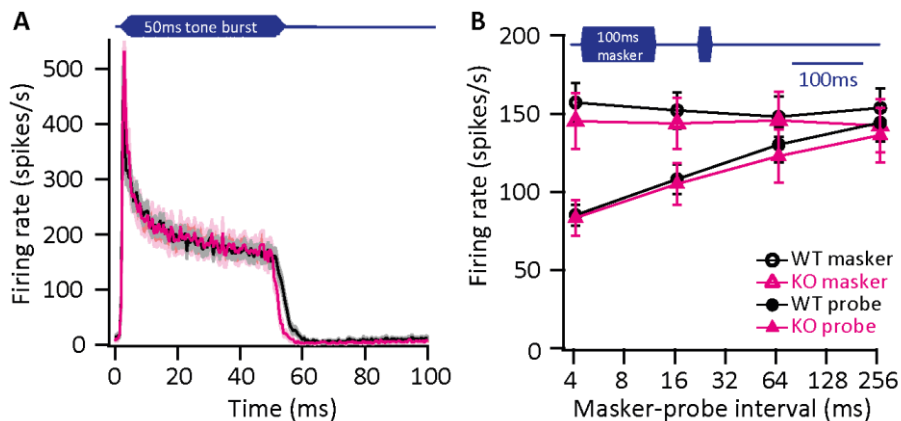


Figure 3b. 6: Evoked response to sound stimulus and recovery of response post stimulus is unchanged in LRBA2 KO SGN units

(A) In response to 50ms tone burst stimulation (characteristic/best frequency, 30dB above threshold in WT, at least 10dB above threshold in KO), response patterns, peak and steady-state firing rates as well as first spike latencies were comparable between both genotypes (WT n=37, KO n=22). (E) Top: illustration of the stimulus paradigm: 100ms masker tone and 15ms probe tone separated by a silent

interval of variable duration. Both stimuli were presented at characteristic/best frequency, 30dB above threshold in WT, at least 10dB above threshold in KO. Bottom: Forward masking effect and time course of recovery were not significantly different between WT (n=20) and KO (n=14) SGNs. n represents the number SGN units.

3c Discussion

The data indicate that the progressive hearing loss observed in LRBA2 KO mice is mainly owing to the deficit of active cochlear amplification in the mutants. The reduced cochlear microphonic and summing potentials in electrocochleography and the reduced DPAOE, confirm the defect in OHC function. However, the shallow amplitude growth functions of ABR wave I suggest an additional impairment of IHC synaptic transmission, since pure OHC dysfunction, would be marked by an increased steepness (Pauli-Magnus et al., 2007).

Direct measurements of the SGN spike responses (high threshold, poor frequency tuning, and steep spike rate growth with increasing intensity) were consistent with a primary defect of OHC function. However, the fraction of low-SR fibers was reduced in the mutants. Since, the number of IHC-SGN synapses in the mutants was unchanged (Figure 3c. 1; Vogl et al., unpublished), one might assume that the mutant IHC contacts as many low and high-SR fibers as the wildtype. The apparent loss of low-SR fibers could be a result of an experimental bias, such that a fraction of low-SR fibers, which typical have high sound thresholds (Liberman, 1978; Taberner and Liberman, 2005) were not identified by our search stimuli. Another possibility is that, the high intensities (at least 10-30dB higher than in the wildtype) employed for stimulation, noise-damaged low-SR fibers, which have been shown to be highly susceptible to noise-induced glutamate excitotoxicity (Furman et al., 2013).

The disruption of stereociliary hair bundles in both the OHCs and IHCs was the most prevalent morphological alteration observed in the LRBA2 KO mice (Figure 3c. 1; Vogl et al., unpublished). The degeneration of stereocilia was attributed to the loss of LRBA2 dependent subcellular targeting of hair bundle proteins, Radixin (RDX) and its interaction partner adaptor protein Nherf2. RDX is the predominant ezrin-radixin-moesin (ERM) in cochlear hair cells, likely involved in mechanical stabilization of the hair bundle by linking the central actin filament core to the cell membrane (Sauvanet et al., 2015).

This degeneration of stereocilia potentially led to a reduction in the number of available MET channels and impaired hair cell depolarization upon hair bundle deflection, which in turn impaired transduction and led to a concomitant reduction in IHC receptor potentials. This could be another contributing factor to the observed reduction in low-SR fibers whereby, the amount of depolarization may not suffice to reach the activation threshold of synaptic voltage-dependent calcium channels at low-SR synapses and hence, fails to initiate synaptic release (Frank et al., 2009; Ohn et al., 2016).

Thus, the combination of impaired OHC-mediated cochlear amplification and likely an additional IHC transduction deficit might have produced the observed auditory impairment.

For the purpose of the thesis, only self-contribution to the LRBA2 study has been discussed in the light of the findings of the entire study undertaken in Vogl et al, unpublished. The structural phenotype observed in the organ of Corti has been summarized in Figure 3c. 1.

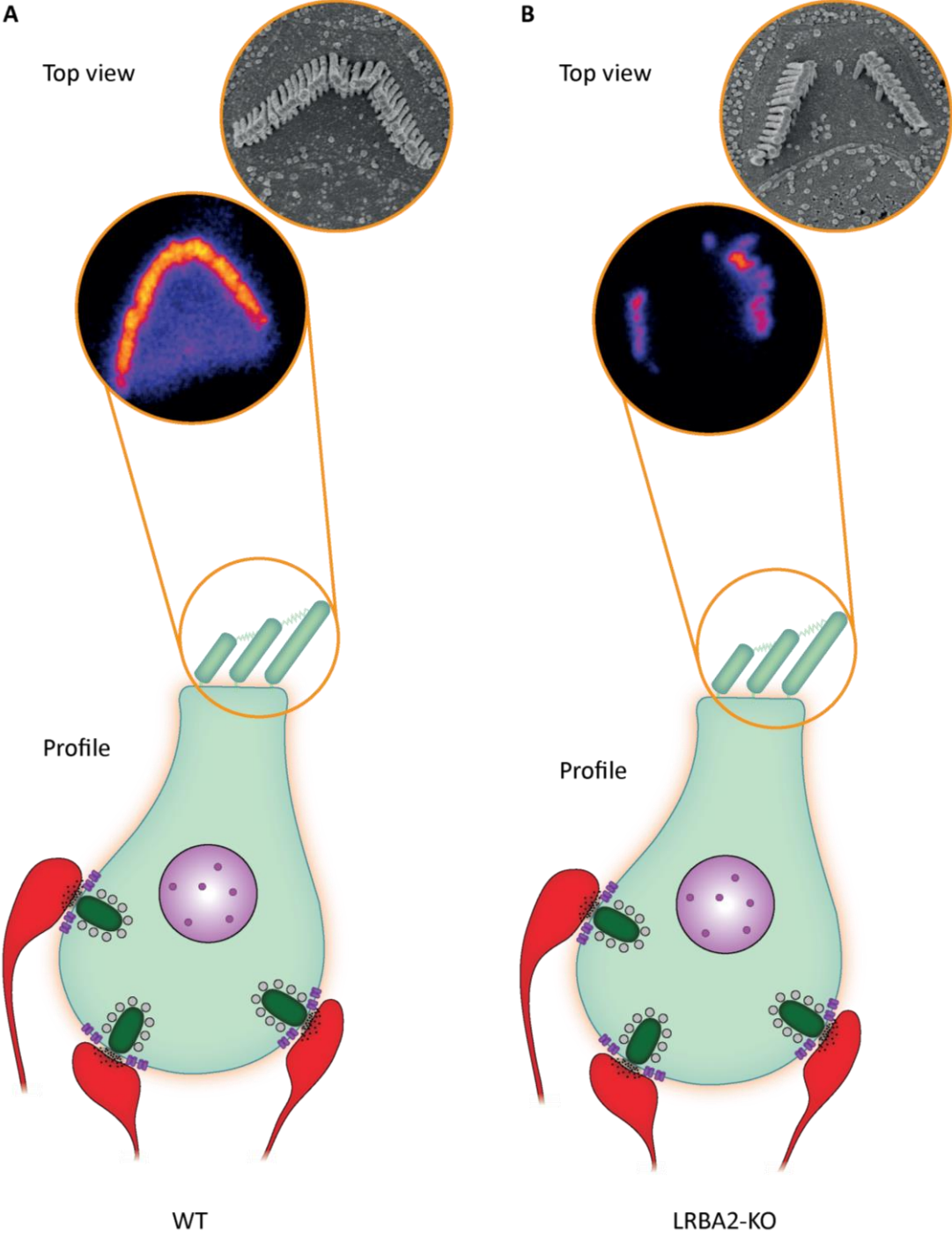


Figure 3c. 1: Hair bundles of LRBA2 KO hair cells develop a prominent central gap in their stereociliary array likely leading to impaired sound processing

(A) WT hair cell depicting typical V-shaped hair bundle morphology (top view) and ribbons synapses (green) contacting postsynaptic boutons (red) of SGNs (profile). (B) LRBA2 KO with unaltered synapse connections and gross hair cell morphology. However, the top view reveals hair bundle degeneration in LRBA2 KO hair cells, with a prominent central gap in their stereociliary array. Top panel: SEM (by Natja Haag) images illustrating hair bundles in p15 mice. Middle panel: Confocal projection of hair bundles of p15-16 mice labelled with a fluorophore-conjugated phalloidin (by Christian Vogl).

4 Outlook

Synaptic transmission is central to all the functions of the brain. Therefore, understanding and deciphering the principles and players in signal transfer across neurons is key to comprehend the basis of, for example sensory processing, motor function, learning and memory, as well as the disorders of the brain such as synaptopathies leading to sensory deficits and neuropsychiatric diseases, and the mode of action and effects of psychoactive drugs and neurotoxins. Since the CAZ proteins underlie synaptic transmission it is imperative to study their role to better understand the process itself. The studies presented here contribute to the elucidation of the role of key CAZ proteins: Piccolo, Bassoon and RIM-BP2, and of the BEACH protein LRBA2. Aside from the virtue of understanding of their physiological function the work also serves to decipher the implications of their malfunction. This is highly relevant as some of them have already been implicated in human disorders such as Piccolo in depression (Sullivan et al., 2008) and bipolar disorder (Choi et al., 2011), RIM-BPs in autism spectrum disorders (Bucan et al., 2009; Corominas et al., 2014; Pinto et al., 2010), and LRBA with cancer growth (Wang et al., 2004) and autoimmune syndromes (Lo et al., 2015; Lopez-Herrera et al., 2012).

4.1 CAZ: from individual proteins to the network

More than two decades of research has been dedicated into dissecting the function of each individual protein of the CAZ to build a comprehensive knowledge of the protein network. This study reveals the collaborative roles of Piccolo and Bassoon in maintaining synaptic vesicle replenishment following pool depletion, with Bassoon possibly having an additional role in regulating release probability at the synapse. This adds to the existing knowledge of the roles of the two proteins in maintaining synapse structure (Dick et al., 2003; tom Dieck et al., 2005; Khimich et al., 2005; Regus-Leidig et al., 2014), synaptic vesicle pool clusters (Mukherjee et al., 2010), maintaining protein turn-over and hence, synaptic integrity (Okerlund et al., 2017; Waites et al., 2013) and of Bassoon in fast reloading of synaptic vesicles (Hallermann et al., 2010b; Schulz et al., 2014).

Piccolo is the largest (550kDa; Fenster et al., 2000; Wang et al., 1999) among the CAZ family of proteins. Its N-terminus reaches into the cytoplasm for tens of nanometers, while its C-terminus extending across the dense projections of the AZ to possibly close to the docked SVs, spans the length of the active zone (Gundelfinger and Fejtova, 2012; Limbach et al., 2011). It is one of the precursors for synapse formation and interacts with the cytoskeletal proteins like actin, potentially regulating transport and endocytosis of SVs. Yet, its absence from the active zone elicited a rather subtle synaptic deficit. Though the RRP was reduced and the vesicle replenishment was hampered, the synapse was still able to respond to high frequency train stimulation (up to 333Hz was tested). Even the additional partial Bassoon loss, though aggravated the transmission deficit, did not cripple the synaptic machinery. However, it needs to be noted here, that the genetic disruption employed here, did not fully abolish the presence of Piccolo at the endbulb active zones.

In the light of multifold interactions of CAZ proteins and given the perturbation of one of them, it was important to examine the abundance and interactions of the remaining CAZ proteins. Undertaking a comprehensive quantitative analysis of changes in molecular composition of the CAZ proteins, this study revealed that RIM1 and Bassoon, two interactors of Piccolo, were altered. While the downregulation of RIM1 might have contributed to the reduced pool of SVs seen in PicMut mice, Bassoon upregulation might be a means to compensate for the loss of some Piccolo's functions. However, to get a holistic view of the network operations, interactions and compensation, and to decipher the molecular mechanisms and players behind them, it might be necessary to broaden the methodological approach. One way would be to employ mutations preventing interactions with other proteins, as was done in case of RIM (Kaeser et al., 2008, 2011) and Munc13 (Lipstein et al., 2013) to pin down the molecular mechanism by which the protein exerts its function. Another way to analyze changes in interactions and hence the architecture of the synapse would be to employ immunogold EM (e.g. Limbach et al., 2011) or super-resolution light microscopy of CAZ proteins (Frank et al., 2010, Grauel et al., 2016) -at synapses deficient in the protein of interest.

This conundrum of dissecting independent functions of individual proteins that are part of a functional network is also presented in the RIM-BP2 study. Although the role of RIM-BP2 in coupling presynaptic Ca^{2+} influx to vesicular exocytosis is discussed as the most likely hypothesis in this thesis, the exact mechanism by which it arbitrates this function remains to be investigated. Since RIM-BP is a part of two different tri-protein interactions (RIM-BP-VGCC-RIM (Hibino et al., 2002; Kaeser et al., 2011) and RIM-BP-VGCC-Bassoon (Davydova et al., 2014)), it will again be insightful to correlate physiological inferences to morphological and ultrastructural changes. A starting step would be the quantitative analysis of the changes in molecular composition of the CAZ protein at RIM-BP2 deficient synapse, as was done for Piccolo deficient synapses. Efforts are also underway to analyze the ultrastructural changes in Ca^{2+} channel clustering (by our collaborator Shigemoto) in the absence of RIM-BP2.

4.2 LRBA2: from systems function to molecular mechanism

LRBA2 was investigated because of the impaired hearing observed in LRBA2 KO mice. Through systems and synaptic physiology, and structural studies, the etiology of this hearing deficit was narrowed down to deficits in cochlear amplification by the OHCs and perhaps even an IHC transduction defect. The LRBA2 study is a fine example of how functional deficit (progressive hearing loss) was related to a morphological correlate (degeneration of hair bundles of cochlear hair cells). A next step in a functional-morphological-molecular analysis would be pinning down the molecular mechanism that relies on LRBA2. Vogl et al. (unpublished), implicated two proteins (RDX and Nherf2) as effectors of LRBA2, whose faulty targeting at the hair bundles, might be the causative molecular mechanism imposed by the absence of LRBA2. This hypothesis is based on reduced expression of RDX in LRBA2 KO mice (Vogl et al., unpublished) and strikingly similar functional and morphological phenotype observed in RDX KO mice (Kitajiri et al., 2004). Hence, it might be useful to check for LRBA2-RDX interactions by co-immunoprecipitation and pull-down assays and if the phenotype can be rescued by expression of this interaction node.

5 References

- Abbott, L.F., and Regehr, W.G. (2004). Synaptic computation. *Nature* *431*, 796–803.
- Acuna, C., Liu, X., Gonzalez, A., and Südhof, T.C. (2015). RIM-BPs Mediate Tight Coupling of Action Potentials to Ca²⁺-Triggered Neurotransmitter Release. *Neuron* *87*, 1234–1247.
- Acuna, C., Liu, X., and Südhof, T.C. (2016). How to Make an Active Zone: Unexpected Universal Functional Redundancy between RIMs and RIM-BPs. *Neuron* *91*, 792–807.
- Ahmed, S., Wittenmayer, N., Kremer, T., Hoeber, J., Kiran Akula, A., Urlaub, H., Islinger, M., Kirsch, J., Dean, C., and Dresbach, T. (2013). Mover is a homomeric phospho-protein present on synaptic vesicles. *PLoS One* *8*, e63474.
- Alabi, A.A., and Tsien, R.W. (2012). Synaptic Vesicle Pools and Dynamics. *Cold Spring Harb. Perspect. Biol.* *4*, a013680.
- Alabi, A.A., and Tsien, R.W. (2013). Perspectives on kiss-and-run: role in exocytosis, endocytosis, and neurotransmission. *Annu. Rev. Physiol.* *75*, 393–422.
- Altrock, W.D., tom Dieck, S., Sokolov, M., Meyer, A.C., Sigler, A., Brakebusch, C., Fässler, R., Richter, K., Boeckers, T.M., Potschka, H., et al. (2003a). Functional inactivation of a fraction of excitatory synapses in mice deficient for the active zone protein bassoon. *Neuron* *37*, 787–800.
- Altrock, W.D., tom Dieck, S., Sokolov, M., Meyer, A.C., Sigler, A., Brakebusch, C., Fässler, R., Richter, K., Boeckers, T.M., Potschka, H., et al. (2003b). Functional inactivation of a fraction of excitatory synapses in mice deficient for the active zone protein bassoon. *Neuron* *37*, 787–800.
- Augustin, I., Rosenmund, C., Südhof, T.C., and Brose, N. (1999). Munc13-1 is essential for fusion competence of glutamatergic synaptic vesicles. *Nature* *400*, 457–461.
- Basu, J., Shen, N., Dulubova, I., Lu, J., Guan, R., Guryev, O., Grishin, N.V., Rosenmund, C., and Rizo, J. (2005). A minimal domain responsible for Munc13 activity. *Nat. Struct. Mol. Biol.* *12*, 1017–1018.
- Betz, A., Thakur, P., Junge, H.J., Ashery, U., Rhee, J.S., Scheuss, V., Rosenmund, C., Rettig, J., and Brose, N. (2001). Functional interaction of the active zone proteins Munc13-1 and RIM1 in synaptic vesicle priming. *Neuron* *30*, 183–196.
- Borst, J.G.G., and Sakmann, B. (1996). Calcium influx and transmitter release in a fast CNS synapse. *Nature* *383*, 431–434.
- Brownell, W.E. (1990). Outer Hair Cell Electromotility and Otoacoustic Emissions. *Ear Hear.* *11*, 82–92.

References

- Bucan, M., Abrahams, B.S., Wang, K., Glessner, J.T., Herman, E.I., Sonnenblick, L.I., Retuerto, A.I.A., Imielinski, M., Hadley, D., Bradfield, J.P., et al. (2009). Genome-Wide Analyses of Exonic Copy Number Variants in a Family-Based Study Point to Novel Autism Susceptibility Genes. *PLOS Genet.* 5, e1000536.
- Buran, B.N., Strenzke, N., Neef, A., Gundelfinger, E.D., Moser, T., and Liberman, M.C. (2010). Onset coding is degraded in auditory nerve fibers from mutant mice lacking synaptic ribbons. *J. Neurosci. Off. J. Soc. Neurosci.* 30, 7587–7597.
- Burgess, A., Mornon, J.-P., de Saint-Basile, G., and Callebaut, I. (2009). A concanavalin A-like lectin domain in the CHS1/LYST protein, shared by members of the BEACH family. *Bioinforma. Oxf. Engl.* 25, 1219–1222.
- Burkhardt, J.K., Wiebel, F.A., Hester, S., and Argon, Y. (1993). The giant organelles in beige and Chediak-Higashi fibroblasts are derived from late endosomes and mature lysosomes. *J. Exp. Med.* 178, 1845–1856.
- Cant, N.B. (1981). The fine structure of two types of stellate cells in the anterior division of the anteroventral cochlear nucleus of the cat. *Neuroscience* 6, 2643–2655.
- Cant, N.B., and Morest, D.K. (1979). The bushy cells in the anteroventral cochlear nucleus of the cat. A study with the electron microscope. *Neuroscience* 4, 1925–1945.
- Cao, X.-J., and Oertel, D. (2010). Auditory Nerve Fibers Excite Targets Through Synapses That Vary in Convergence, Strength, and Short-Term Plasticity. *J. Neurophysiol.* 104, 2308–2320.
- del Castillo, J., and Katz, B. (1954). Quantal components of the end-plate potential. *J. Physiol.* 124, 560–573.
- Chance, F.S., Nelson, S.B., and Abbott, L.F. (1998). Synaptic depression and the temporal response characteristics of V1 cells. *J. Neurosci. Off. J. Soc. Neurosci.* 18, 4785–4799.
- Chanda, S., and Xu-Friedman, M.A. (2010). A Low-Affinity Antagonist Reveals Saturation and Desensitization in Mature Synapses in the Auditory Brain Stem. *J. Neurophysiol.* 103, 1915–1926.
- Chen, Z., Das, B., Nakamura, Y., DiGregorio, D.A., and Young, S.M. (2015). Ca²⁺ Channel to Synaptic Vesicle Distance Accounts for the Readily Releasable Pool Kinetics at a Functionally Mature Auditory Synapse. *J. Neurosci.* 35, 2083–2100.
- Choi, K.H., Higgs, B.W., Wendland, J.R., Song, J., McMahon, F.J., and Webster, M.J. (2011). Gene Expression and Genetic Variation Data Implicate PCLO in Bipolar Disorder. *Biol. Psychiatry* 69, 353–359.
- Chung, S., Li, X., and Nelson, S.B. (2002). Short-term depression at thalamocortical synapses contributes to rapid adaptation of cortical sensory responses in vivo. *Neuron* 34, 437–446.

- Clayton, E.L., and Cousin, M.A. (2009). The Molecular Physiology of Activity-Dependent Bulk Endocytosis of Synaptic Vesicles. *J. Neurochem.* *111*, 901–914.
- Connors, B.W., and Long, M.A. (2004). Electrical synapses in the mammalian brain. *Annu. Rev. Neurosci.* *27*, 393–418.
- Cook, D.L., Schwindt, P.C., Grande, L.A., and Spain, W.J. (2003). Synaptic depression in the localization of sound. *Nature* *421*, 66–70.
- Corominas, R., Yang, X., Lin, G.N., Kang, S., Shen, Y., Ghamsari, L., Broly, M., Rodriguez, M., Tam, S., Trigg, S.A., et al. (2014). Protein interaction network of alternatively spliced isoforms from brain links genetic risk factors for autism. *Nat. Commun.* *5*, 3650.
- Cullinane, A.R., Schäffer, A.A., and Huizing, M. (2013). The BEACH Is Hot: A LYST of Emerging Roles for BEACH-Domain Containing Proteins in Human Disease. *Traffic* *14*, 749–766.
- Davydova, D., Marini, C., King, C., Klueva, J., Bischof, F., Romorini, S., Montenegro-Venegas, C., Heine, M., Schneider, R., Schröder, M.S., et al. (2014). Bassoon Specifically Controls Presynaptic P/Q-type Ca²⁺ Channels via RIM-Binding Protein. *Neuron* *82*, 181–194.
- Deng, P.-Y., and Klyachko, V.A. (2011). The diverse functions of short-term plasticity components in synaptic computations. *Commun. Integr. Biol.* *4*, 543–548.
- Deng, L., Kaeser, P.S., Xu, W., and Südhof, T.C. (2011). RIM Proteins Activate Vesicle Priming by Reversing Autoinhibitory Homodimerization of Munc13. *Neuron* *69*, 317–331.
- Denker, A., and Rizzoli, S.O. (2010). Synaptic Vesicle Pools: An Update. *Front. Synaptic Neurosci.* *2*.
- Denker, A., Kröhnert, K., Bückers, J., Neher, E., and Rizzoli, S.O. (2011). The reserve pool of synaptic vesicles acts as a buffer for proteins involved in synaptic vesicle recycling. *Proc. Natl. Acad. Sci. U. S. A.* *108*, 17183–17188.
- Dick, O., tom Dieck, S., Altmann, W.D., Ammermüller, J., Weiler, R., Garner, C.C., Gundelfinger, E.D., and Brandstätter, J.H. (2003). The presynaptic active zone protein bassoon is essential for photoreceptor ribbon synapse formation in the retina. *Neuron* *37*, 775–786.
- tom Dieck, S., Sanmartí-Vila, L., Langnaese, K., Richter, K., Kindler, S., Soyke, A., Wex, H., Smalla, K.H., Kämpf, U., Fränzer, J.T., et al. (1998). Bassoon, a novel zinc-finger CAG/glutamine-repeat protein selectively localized at the active zone of presynaptic nerve terminals. *J. Cell Biol.* *142*, 499–509.
- tom Dieck, S., Altmann, W.D., Kessels, M.M., Qualmann, B., Regus, H., Brauner, D., Fejtová, A., Bracko, O., Gundelfinger, E.D., and Brandstätter, J.H. (2005). Molecular dissection of the photoreceptor ribbon synapse: physical interaction of Bassoon and RIBEYE is essential for the assembly of the ribbon complex. *J. Cell Biol.* *168*, 825–836.

References

- Dondzillo, A., Sätzler, K., Horstmann, H., Altmann, W.D., Gundelfinger, E.D., and Kuner, T. (2010). Targeted three-dimensional immunohistochemistry reveals localization of presynaptic proteins Bassoon and Piccolo in the rat calyx of Held before and after the onset of hearing. *J. Comp. Neurol.* *518*, 1008–1029.
- Dulubova, I., Lou, X., Lu, J., Huryeva, I., Alam, A., Schneggenburger, R., Südhof, T.C., and Rizo, J. (2005). A Munc13/RIM/Rab3 tripartite complex: from priming to plasticity? *EMBO J.* *24*, 2839–2850.
- Eggermann, E., Bucurenciu, I., Goswami, S.P., and Jonas, P. (2012). Nanodomain coupling between Ca²⁺ channels and sensors of exocytosis at fast mammalian synapses. *Nat. Rev. Neurosci.* *13*, 7–21.
- Elmqvist, D., and Quastel, D.M. (1965). A quantitative study of end-plate potentials in isolated human muscle. *J. Physiol.* *178*, 505–529.
- Elmslie, K.S., and Yoshikami, D. (1985). Effects of kynurenate on root potentials evoked by synaptic activity and amino acids in the frog spinal cord. *Brain Res.* *330*, 265–272.
- Farsi, Z., Preobraschenski, J., Bogaart, G. van den, Riedel, D., Jahn, R., and Woehler, A. (2016). Single-vesicle imaging reveals different transport mechanisms between glutamatergic and GABAergic vesicles. *Science* *351*, 981–984.
- Fatt, P., and Katz, B. (1950). Some Observations on Biological Noise. *Nature* *166*, 597–598.
- Fatt, P., and Katz, B. (1952). Spontaneous subthreshold activity at motor nerve endings. *J. Physiol.* *117*, 109–128.
- Fedchyshyn, M.J., and Wang, L.-Y. (2005). Developmental Transformation of the Release Modality at the Calyx of Held Synapse. *J. Neurosci.* *25*, 4131–4140.
- Fekete, D.M., Rouiller, E.M., Liberman, M.C., and Ryugo, D.K. (1984). The central projections of intracellularly labeled auditory nerve fibers in cats. *J. Comp. Neurol.* *229*, 432–450.
- Fenster, S.D., Chung, W.J., Zhai, R., Cases-Langhoff, C., Voss, B., Garner, A.M., Kaempfer, U., Kindler, S., Gundelfinger, E.D., and Garner, C.C. (2000). Piccolo, a Presynaptic Zinc Finger Protein Structurally Related to Bassoon. *Neuron* *25*, 203–214.
- Fenster, S.D., Kessels, M.M., Qualmann, B., Chung, W.J., Nash, J., Gundelfinger, E.D., and Garner, C.C. (2003). Interactions between Piccolo and the actin/dynamin-binding protein Abp1 link vesicle endocytosis to presynaptic active zones. *J. Biol. Chem.* *278*, 20268–20277.
- Fernández-Busnadiego, R., Asano, S., Oprisoreanu, A.-M., Sakata, E., Doengi, M., Kochovski, Z., Zürner, M., Stein, V., Schoch, S., Baumeister, W., et al. (2013a). Cryo-electron tomography reveals a critical role of RIM1 α in synaptic vesicle tethering. *J Cell Biol* *201*, 725–740.

- Fernández-Busnadiego, R., Asano, S., Oprisoreanu, A.-M., Sakata, E., Doengi, M., Kochovski, Z., Zürner, M., Stein, V., Schoch, S., Baumeister, W., et al. (2013b). Cryo-electron tomography reveals a critical role of RIM1 α in synaptic vesicle tethering. *J. Cell Biol.* *201*, 725–740.
- Fettiplace, R., and Hackney, C.M. (2006). The sensory and motor roles of auditory hair cells. *Nat. Rev. Neurosci.* *7*, 19–29.
- Fitzpatrick, D.C., Batra, R., Stanford, T.R., and Kuwada, S. (1997). A neuronal population code for sound localization. *Nature* *388*, 871–874.
- Fortune, E.S., and Rose, G.J. (2001). Short-term synaptic plasticity as a temporal filter. *Trends Neurosci.* *24*, 381–385.
- Frank, T., Khimich, D., Neef, A., and Moser, T. (2009). Mechanisms contributing to synaptic Ca²⁺ signals and their heterogeneity in hair cells. *Proc. Natl. Acad. Sci. U. S. A.* *106*, 4483–4488.
- Frank, T., Rutherford, M.A., Strenzke, N., Neef, A., Pangršič, T., Khimich, D., Fejtova, A., Gundelfinger, E.D., Liberman, M.C., Harke, B., et al. (2010). Bassoon and the Synaptic Ribbon Organize Ca²⁺ Channels and Vesicles to Add Release Sites and Promote Refilling. *Neuron* *68*, 724–738.
- Fredj, N.B., and Burrone, J. (2009). A resting pool of vesicles is responsible for spontaneous vesicle fusion at the synapse. *Nat. Neurosci.* *12*, 751–758.
- Fujimoto, K., Shibasaki, T., Yokoi, N., Kashima, Y., Matsumoto, M., Sasaki, T., Tajima, N., Iwanaga, T., and Seino, S. (2002). Piccolo, a Ca²⁺ Sensor in Pancreatic β -Cells INVOLVEMENT OF cAMP-GEFII-Rim2-PICCOLO COMPLEX IN cAMP-DEPENDENT EXOCYTOSIS. *J. Biol. Chem.* *277*, 50497–50502.
- Furman, A.C., Kujawa, S.G., and Liberman, M.C. (2013). Noise-induced cochlear neuropathy is selective for fibers with low spontaneous rates. *J. Neurophysiol.* *110*, 577–586.
- Furukawa, T., and Matsuura, S. (1978). Adaptive rundown of excitatory post-synaptic potentials at synapses between hair cells and eight nerve fibres in the goldfish. *J. Physiol.* *276*, 193–209.
- Garcia, J., Gerber, S.H., Sugita, S., Südhof, T.C., and Rizo, J. (2004). A conformational switch in the Piccolo C2A domain regulated by alternative splicing. *Nat. Struct. Mol. Biol.* *11*, 45–53.
- Gebhart, M., Juhasz-Vedres, G., Zuccotti, A., Brandt, N., Engel, J., Trockenbacher, A., Kaur, G., Obermair, G.J., Knipper, M., Koschak, A., et al. (2010). Modulation of Cav1.3 Ca²⁺ channel gating by Rab3 interacting molecule. *Mol. Cell. Neurosci.* *44*, 246–259.
- Gerber, S.H., Garcia, J., Rizo, J., and Südhof, T.C. (2001). An unusual C2-domain in the active-zone protein piccolo: implications for Ca²⁺ regulation of neurotransmitter release. *EMBO J.* *20*, 1605–1619.

References

- Gerber, S.H., Rah, J.-C., Min, S.-W., Liu, X., de Wit, H., Dulubova, I., Meyer, A.C., Rizo, J., Arancillo, M., Hammer, R.E., et al. (2008). Conformational switch of syntaxin-1 controls synaptic vesicle fusion. *Science* *321*, 1507–1510.
- von Gersdorff, H., and Borst, J.G.G. (2002). Short-term plasticity at the calyx of held. *Nat. Rev. Neurosci.* *3*, 53–64.
- von Gersdorff, H., and Matthews, G. (1994). Dynamics of synaptic vesicle fusion and membrane retrieval in synaptic terminals. *Nature* *367*, 735–739.
- Glowatzki, E., and Fuchs, P.A. (2002). Transmitter release at the hair cell ribbon synapse. *Nat. Neurosci.* *5*, 147–154.
- Gómez-Nieto, R., and Rubio, M.E. (2009). A bushy cell network in the rat ventral cochlear nucleus. *J. Comp. Neurol.* *516*, 241–263.
- Goutman, J.D., and Glowatzki, E. (2007). Time course and calcium dependence of transmitter release at a single ribbon synapse. *Proc. Natl. Acad. Sci. U. S. A.* *104*, 16341–16346.
- Grabner, C.P., Gandini, M.A., Rehak, R., Le, Y., Zamponi, G.W., and Schmitz, F. (2015). RIM1/2-Mediated Facilitation of Cav1.4 Channel Opening Is Required for Ca²⁺-Stimulated Release in Mouse Rod Photoreceptors. *J. Neurosci.* *35*, 13133–13147.
- Gracheva, E.O., Hadwiger, G., Nonet, M.L., and Richmond, J.E. (2008). Direct interactions between *C. elegans* RAB-3 and Rim provide a mechanism to target vesicles to the presynaptic density. *Neurosci. Lett.* *444*, 137–142.
- Grael, M.K., Maglione, M., Reddy-Alla, S., Willmes, C.G., Brockmann, M.M., Trimbuch, T., Rosenmund, T., Pangalos, M., Vardar, G., Stumpf, A., et al. (2016). RIM-binding protein 2 regulates release probability by fine-tuning calcium channel localization at murine hippocampal synapses. *Proc. Natl. Acad. Sci.* *113*, 11615–11620.
- Groemer, T.W., and Klingauf, J. (2007). Synaptic vesicles recycling spontaneously and during activity belong to the same vesicle pool. *Nat. Neurosci.* *10*, 145–147.
- Grothe, B., Pecka, M., and McAlpine, D. (2010). Mechanisms of Sound Localization in Mammals. *Physiol. Rev.* *90*, 983–1012.
- Gundelfinger, E.D., and Fejtova, A. (2012). Molecular organization and plasticity of the cytomatrix at the active zone. *Synaptic Struct. Funct.* *22*, 423–430.
- Gundelfinger, E.D., Reissner, C., and Garner, C.C. (2016). Role of Bassoon and Piccolo in Assembly and Molecular Organization of the Active Zone. *Front. Synaptic Neurosci.* *7*.
- Hallermann, S., Fejtova, A., Schmidt, H., Weyhersmüller, A., Silver, R.A., Gundelfinger, E.D., and Eilers, J. (2010a). Bassoon Speeds Vesicle Reloading at a Central Excitatory Synapse. *Neuron* *68*, 710–723.

- Hallermann, S., Fejtova, A., Schmidt, H., Weyhersmüller, A., Silver, R.A., Gundelfinger, E.D., and Eilers, J. (2010b). Bassoon Speeds Vesicle Reloading at a Central Excitatory Synapse. *Neuron* 68, 710–723.
- Han, Y., Kaeser, P.S., Südhof, T.C., and Schneggenburger, R. (2011). RIM Determines Ca²⁺ Channel Density and Vesicle Docking at the Presynaptic Active Zone. *Neuron* 69, 304–316.
- Han, Y., Babai, N., Kaeser, P., Südhof, T.C., and Schneggenburger, R. (2015). RIM1 and RIM2 redundantly determine Ca²⁺ channel density and readily releasable pool size at a large hindbrain synapse. *J. Neurophysiol.* 113, 255–263.
- Harata, N., Pyle, J.L., Aravanis, A.M., Mozhayeva, M., Kavalali, E.T., and Tsien, R.W. (2001). Limited numbers of recycling vesicles in small CNS nerve terminals: implications for neural signaling and vesicular cycling. *Trends Neurosci.* 24, 637–643.
- Haucke, V., Neher, E., and Sigrist, S.J. (2011). Protein scaffolds in the coupling of synaptic exocytosis and endocytosis. *Nat. Rev. Neurosci.* 12, 127–138.
- He, L., Wu, X.-S., Mohan, R., and Wu, L.-G. (2006). Two modes of fusion pore opening revealed by cell-attached recordings at a synapse. *Nature* 444, 102–105.
- Heeringa, A.N., Stefanescu, R.A., Raphael, Y., and Shore, S.E. (2016). Altered vesicular glutamate transporter distributions in the mouse cochlear nucleus following cochlear insult. *Neuroscience* 315, 114–124.
- Held, H. (1893). Die zentrale Gehörleitung. *Arch Anat Physiol Anat Abt* 17, 201–248.
- Hibino, H., Pironkova, R., Onwumere, O., Vologodskaja, M., Hudspeth, A.J., and Lesage, F. (2002). RIM Binding Proteins (RBPs) Couple Rab3-Interacting Molecules (RIMs) to Voltage-Gated Ca²⁺ Channels. *Neuron* 34, 411–423.
- Hormuzdi, S.G., Filippov, M.A., Mitropoulou, G., Monyer, H., and Bruzzone, R. (2004). Electrical synapses: a dynamic signaling system that shapes the activity of neuronal networks. *Biochim. Biophys. Acta BBA - Biomembr.* 1662, 113–137.
- Hosoi, N., Holt, M., and Sakaba, T. (2009). Calcium Dependence of Exo- and Endocytotic Coupling at a Glutamatergic Synapse. *Neuron* 63, 216–229.
- Howard, M.A., and Rubel, E.W. (2010). Dynamic Spike Thresholds during Synaptic Integration Preserve and Enhance Temporal Response Properties in the Avian Cochlear Nucleus. *J. Neurosci.* 30, 12063–12074.
- Hua, Y., Sinha, R., Martineau, M., Kahms, M., and Klingauf, J. (2010). A common origin of synaptic vesicles undergoing evoked and spontaneous fusion. *Nat. Neurosci.* 13, 1451–1453.
- Hua, Y., Sinha, R., Thiel, C.S., Schmidt, R., Hüve, J., Martens, H., Hell, S.W., Egner, A., and Klingauf, J. (2011). A readily retrievable pool of synaptic vesicles. *Nat. Neurosci.* 14, 833–839.

References

- Imig, C., Min, S.-W., Krinner, S., Arancillo, M., Rosenmund, C., Südhof, T.C., Rhee, J., Brose, N., and Cooper, B.H. (2014). The Morphological and Molecular Nature of Synaptic Vesicle Priming at Presynaptic Active Zones. *Neuron* *84*, 416–431.
- Isaacson, J.S., and Walmsley, B. (1995). Receptors underlying excitatory synaptic transmission in slices of the rat anteroventral cochlear nucleus. *J. Neurophysiol.* *73*, 964–973.
- Ivanova, D., Dirks, A., Montenegro-Venegas, C., Schöne, C., Altmann, W.D., Marini, C., Frischknecht, R., Schanze, D., Zenker, M., Gundelfinger, E.D., et al. (2015). Synaptic activity controls localization and function of CtBP1 via binding to Bassoon and Piccolo. *EMBO J.* *34*, 1056–1077.
- Ivanova, D., Dirks, A., and Fejtova, A. (2016). Bassoon and piccolo regulate ubiquitination and link presynaptic molecular dynamics with activity-regulated gene expression. *J. Physiol.* *594*, 5441–5448.
- Jagger, D.J., and Forge, A. (2015). Connexins and gap junctions in the inner ear – it’s not just about K⁺ recycling. *Cell Tissue Res.* *360*, 633–644.
- Jing, Z., Rutherford, M.A., Takago, H., Frank, T., Fejtova, A., Khimich, D., Moser, T., and Strenzke, N. (2013). Disruption of the Presynaptic Cytomatrix Protein Bassoon Degrades Ribbon Anchorage, Multiquantal Release, and Sound Encoding at the Hair Cell Afferent Synapse. *J. Neurosci.* *33*, 4456–4467.
- Jogl, G., Shen, Y., Gebauer, D., Li, J., Wiegmann, K., Kashkar, H., Krönke, M., and Tong, L. (2002). Crystal structure of the BEACH domain reveals an unusual fold and extensive association with a novel PH domain. *EMBO J.* *21*, 4785–4795.
- Joris, P.X., Smith, P.H., and Yin, T.C. (1994). Enhancement of neural synchronization in the anteroventral cochlear nucleus. II. Responses in the tuning curve tail. *J. Neurophysiol.* *71*, 1037–1051.
- Jung, S., Maritzen, T., Wichmann, C., Jing, Z., Neef, A., Revelo, N.H., Al-Moyed, H., Meese, S., Wojcik, S.M., Panou, I., et al. (2015a). Disruption of adaptor protein 2 μ (AP-2 μ) in cochlear hair cells impairs vesicle reloading of synaptic release sites and hearing. *EMBO J.* *34*, 2686–2702.
- Jung, S., Oshima-Takago, T., Chakrabarti, R., Wong, A.B., Jing, Z., Yamanbaeva, G., Picher, M.M., Wojcik, S.M., Göttfert, F., Predoehl, F., et al. (2015b). Rab3-interacting molecules 2 α and 2 β promote the abundance of voltage-gated CaV1.3 Ca²⁺ channels at hair cell active zones. *Proc. Natl. Acad. Sci.* *112*, E3141–E3149.
- Kaesler, P.S., and Regehr, W.G. (2014). Molecular mechanisms for synchronous, asynchronous, and spontaneous neurotransmitter release. *Annu. Rev. Physiol.* *76*, 333–363.

- Kaesler, P.S., Kwon, H.-B., Blundell, J., Chevaleyre, V., Morishita, W., Malenka, R.C., Powell, C.M., Castillo, P.E., and Südhof, T.C. (2008). RIM1 α phosphorylation at serine-413 by protein kinase A is not required for presynaptic long-term plasticity or learning. *Proc. Natl. Acad. Sci. U. S. A.* *105*, 14680–14685.
- Kaesler, P.S., Deng, L., Wang, Y., Dulubova, I., Liu, X., Rizo, J., and Südhof, T.C. (2011). RIM Proteins Tether Ca²⁺ Channels to Presynaptic Active Zones via a Direct PDZ-Domain Interaction. *Cell* *144*, 282–295.
- Kaesler, P.S., Deng, L., Fan, M., and Südhof, T.C. (2012). RIM genes differentially contribute to organizing presynaptic release sites. *Proc. Natl. Acad. Sci. U. S. A.* *109*, 11830–11835.
- Kessels, M.M., Engqvist-Goldstein, Å.E.Y., Drubin, D.G., and Qualmann, B. (2001). Mammalian Abp1, a Signal-Responsive F-Actin-Binding Protein, Links the Actin Cytoskeleton to Endocytosis via the Gtpase Dynamin. *J. Cell Biol.* *153*, 351–366.
- Khimich, D., Nouvian, R., Pujol, R., tom Dieck, S., Egner, A., Gundelfinger, E.D., and Moser, T. (2005). Hair cell synaptic ribbons are essential for synchronous auditory signalling. *Nature* *434*, 889–894.
- Kim, S., Ko, J., Shin, H., Lee, J.-R., Lim, C., Han, J.-H., Altroock, W.D., Garner, C.C., Gundelfinger, E.D., Premont, R.T., et al. (2003). The GIT Family of Proteins Forms Multimers and Associates with the Presynaptic Cytomatrix Protein Piccolo. *J. Biol. Chem.* *278*, 6291–6300.
- Kintscher, M., Wozny, C., Johanning, F.W., Schmitz, D., and Breustedt, J. (2013). Role of RIM1 α in short- and long-term synaptic plasticity at cerebellar parallel fibres. *Nat. Commun.* *4*, 2392.
- Kitajiri, S., Fukumoto, K., Hata, M., Sasaki, H., Katsuno, T., Nakagawa, T., Ito, J., Tsukita, S., and Tsukita, S. (2004). Radixin deficiency causes deafness associated with progressive degeneration of cochlear stereocilia. *J. Cell Biol.* *166*, 559–570.
- Kiyonaka, S., Wakamori, M., Miki, T., Uriu, Y., Nonaka, M., Bito, H., Beedle, A.M., Mori, E., Hara, Y., De Waard, M., et al. (2007). RIM1 confers sustained activity and neurotransmitter vesicle anchoring to presynaptic Ca²⁺ channels. *Nat. Neurosci.* *10*, 691–701.
- Klyachko, V.A., and Stevens, C.F. (2006). Excitatory and feed-forward inhibitory hippocampal synapses work synergistically as an adaptive filter of natural spike trains. *PLoS Biol.* *4*, e207.
- Kononenko, N.L., Puchkov, D., Classen, G.A., Walter, A.M., Pechstein, A., Sawade, L., Kaempfer, N., Trimbuch, T., Lorenz, D., Rosenmund, C., et al. (2014). Clathrin/AP-2 Mediate Synaptic Vesicle Reformation from Endosome-like Vacuoles but Are Not Essential for Membrane Retrieval at Central Synapses. *Neuron* *82*, 981–988.
- Kopp-Scheinflug, C., and Tempel, B.L. (2015). Decreased temporal precision of neuronal signaling as a candidate mechanism of auditory processing disorder. *Hear. Res.* *330, Part B*, 213–220.

References

- Körber, C., Horstmann, H., Venkataramani, V., Herrmannsdörfer, F., Kremer, T., Kaiser, M., Schwenger, D.B., Ahmed, S., Dean, C., Dresbach, T., et al. (2015a). Modulation of Presynaptic Release Probability by the Vertebrate-Specific Protein Mover. *Neuron* 87, 521–533.
- Körber, C., Horstmann, H., Venkataramani, V., Herrmannsdörfer, F., Kremer, T., Kaiser, M., Schwenger, D.B., Ahmed, S., Dean, C., Dresbach, T., et al. (2015b). Modulation of Presynaptic Release Probability by the Vertebrate-Specific Protein Mover. *Neuron* 87, 521–533.
- Koushika, S.P., Richmond, J.E., Hadwiger, G., Weimer, R.M., Jorgensen, E.M., and Nonet, M.L. (2001). A post-docking role for active zone protein Rim. *Nat. Neurosci.* 4, 997–1005.
- Kremer, T., Kempf, C., Wittenmayer, N., Nawrotzki, R., Kuner, T., Kirsch, J., and Dresbach, T. (2007). Mover is a novel vertebrate-specific presynaptic protein with differential distribution at subsets of CNS synapses. *FEBS Lett.* 581, 4727–4733.
- Kuba, H., Koyano, K., and Ohmori, H. (2002). Synaptic depression improves coincidence detection in the nucleus laminaris in brainstem slices of the chick embryo. *Eur. J. Neurosci.* 15, 984–990.
- Kuenzel, T., Borst, J.G.G., and Heijden, M. van der (2011). Factors Controlling the Input–Output Relationship of Spherical Bushy Cells in the Gerbil Cochlear Nucleus. *J. Neurosci.* 31, 4260–4273.
- Lakso, M., Pichel, J.G., Gorman, J.R., Sauer, B., Okamoto, Y., Lee, E., Alt, F.W., and Westphal, H. (1996). Efficient in vivo manipulation of mouse genomic sequences at the zygote stage. *Proc. Natl. Acad. Sci. U. S. A.* 93, 5860–5865.
- Leal-Ortiz, S., Waites, C.L., Terry-Lorenzo, R., Zamorano, P., Gundelfinger, E.D., and Garner, C.C. (2008). Piccolo modulation of Synapsin1a dynamics regulates synaptic vesicle exocytosis. *J. Cell Biol.* 181, 831–846.
- Lee, J.S., Ho, W.-K., and Lee, S.-H. (2012). Actin-dependent rapid recruitment of reluctant synaptic vesicles into a fast-releasing vesicle pool. *Proc. Natl. Acad. Sci.* 109, E765–E774.
- Lieberman, M.C. (1978). Auditory-nerve response from cats raised in a low-noise chamber. *J. Acoust. Soc. Am.* 63, 442–455.
- Lieberman, M.C. (1982). Single-neuron labeling in the cat auditory nerve. *Science* 216, 1239–1241.
- Lieberman, M.C., Gao, J., He, D.Z.Z., Wu, X., Jia, S., and Zuo, J. (2002). Prestin is required for electromotility of the outer hair cell and for the cochlear amplifier. *Nature* 419, 300–304.
- Limbach, C., Laue, M.M., Wang, X., Hu, B., Thiede, N., Hultqvist, G., and Kilimann, M.W. (2011). Molecular in situ topology of Aczonin/Piccolo and associated proteins at the mammalian neurotransmitter release site. *Proc. Natl. Acad. Sci.* 108, E392–E401.

- Lin, K.-H., Oleskevich, S., and Taschenberger, H. (2011). Presynaptic Ca²⁺ influx and vesicle exocytosis at the mouse endbulb of Held: a comparison of two auditory nerve terminals. *J. Physiol.* *589*, 4301–4320.
- Lipstein, N., Sakaba, T., Cooper, B.H., Lin, K.-H., Strenzke, N., Ashery, U., Rhee, J.-S., Taschenberger, H., Neher, E., and Brose, N. (2013). Dynamic control of synaptic vesicle replenishment and short-term plasticity by Ca²⁺-calmodulin-Munc13-1 signaling. *Neuron* *79*, 82–96.
- Liu, K.S.Y., Siebert, M., Mertel, S., Knoche, E., Wegener, S., Wichmann, C., Matkovic, T., Muhammad, K., Depner, H., Mettke, C., et al. (2011). RIM-Binding Protein, a Central Part of the Active Zone, Is Essential for Neurotransmitter Release. *Science* *334*, 1565–1569.
- Lo, B., Zhang, K., Lu, W., Zheng, L., Zhang, Q., Kanellopoulou, C., Zhang, Y., Liu, Z., Fritz, J.M., Marsh, R., et al. (2015). AUTOIMMUNE DISEASE. Patients with LRBA deficiency show CTLA4 loss and immune dysregulation responsive to abatacept therapy. *Science* *349*, 436–440.
- Lohmann, C., and Friauf, E. (1996). Distribution of the calcium-binding proteins parvalbumin and calretinin in the auditory brainstem of adult and developing rats. *J. Comp. Neurol.* *367*, 90–109.
- Lopez-Herrera, G., Tampella, G., Pan-Hammarström, Q., Herholz, P., Trujillo-Vargas, C.M., Phadwal, K., Simon, A.K., Moutschen, M., Etzioni, A., Mory, A., et al. (2012). Deleterious mutations in LRBA are associated with a syndrome of immune deficiency and autoimmunity. *Am. J. Hum. Genet.* *90*, 986–1001.
- Lu, J., Machius, M., Dulubova, I., Dai, H., Südhof, T.C., Tomchick, D.R., and Rizo, J. (2006). Structural Basis for a Munc13–1 Homodimer to Munc13–1/RIM Heterodimer Switch. *PLoS Biol.* *4*.
- Lu, Y., Harris, J.A., and Rubel, E.W. (2007). Development of Spontaneous Miniature EPSCs in Mouse AVCN Neurons During a Critical Period of Afferent-Dependent Neuron Survival. *J. Neurophysiol.* *97*, 635–646.
- Ma, C., Li, W., Xu, Y., and Rizo, J. (2011). Munc13 mediates the transition from the closed syntaxin-Munc18 complex to the SNARE complex. *Nat. Struct. Mol. Biol.* *18*, 542–549.
- Maas, C., Torres, V.I., Altroch, W.D., Leal-Ortiz, S., Wagh, D., Terry-Lorenzo, R.T., Fejtova, A., Gundelfinger, E.D., Ziv, N.E., and Garner, C.C. (2012). Formation of Golgi-Derived Active Zone Precursor Vesicles. *J. Neurosci.* *32*, 11095–11108.
- MacLeod, K.M. (2011). Short-term synaptic plasticity and intensity coding. *Hear. Res.* *279*, 13–21.
- Meinrenken, C.J., Borst, J.G.G., and Sakmann, B. (2003). Local routes revisited: the space and time dependence of the Ca²⁺ signal for phasic transmitter release at the rat calyx of Held. *J. Physiol.* *547*, 665–689.

References

- Melcher, J.R., and Kiang, N.Y. (1996). Generators of the brainstem auditory evoked potential in cat. III: Identified cell populations. *Hear. Res.* *93*, 52–71.
- Melcher, J.R., Knudson, I.M., Fullerton, B.C., Guinan, J.J., Norris, B.E., and Kiang, N.Y. (1996a). Generators of the brainstem auditory evoked potential in cat. I. An experimental approach to their identification. *Hear. Res.* *93*, 1–27.
- Melcher, J.R., Guinan, J.J., Knudson, I.M., and Kiang, N.Y. (1996b). Generators of the brainstem auditory evoked potential in cat. II. Correlating lesion sites with waveform changes. *Hear. Res.* *93*, 28–51.
- Merchan-Perez, A., and Liberman, M.C. (1996). Ultrastructural differences among afferent synapses on cochlear hair cells: correlations with spontaneous discharge rate. *J. Comp. Neurol.* *371*, 208–221.
- Meyer, A.C., Frank, T., Khimich, D., Hoch, G., Riedel, D., Chapochnikov, N.M., Yarin, Y.M., Harke, B., Hell, S.W., Egner, A., et al. (2009). Tuning of synapse number, structure and function in the cochlea. *Nat. Neurosci.* *12*, 444–453.
- Midorikawa, M., Okamoto, Y., and Sakaba, T. (2014). Developmental changes in Ca²⁺ channel subtypes regulating endocytosis at the calyx of Held. *J. Physiol.* *592*, 3495–3510.
- Mittelstaedt, T., and Schoch, S. (2007). Structure and evolution of RIM-BP genes: Identification of a novel family member. *Gene* *403*, 70–79.
- Montesinos, M.S., Dong, W., Goff, K., Das, B., Guerrero-Given, D., Schmalzigaug, R., Premont, R.T., Satterfield, R., Kamasawa, N., and Young Jr., S.M. (2015). Presynaptic Deletion of GIT Proteins Results in Increased Synaptic Strength at a Mammalian Central Synapse. *Neuron* *88*, 918–925.
- Moser, T., and Beutner, D. (2000). Kinetics of exocytosis and endocytosis at the cochlear inner hair cell afferent synapse of the mouse. *Proc. Natl. Acad. Sci.* *97*, 883–888.
- Moser, T., Neef, A., and Khimich, D. (2006). Mechanisms underlying the temporal precision of sound coding at the inner hair cell ribbon synapse. *J. Physiol.* *576*, 55–62.
- Mukherjee, K., Yang, X., Gerber, S.H., Kwon, H.-B., Ho, A., Castillo, P.E., Liu, X., and Südhof, T.C. (2010). Piccolo and bassoon maintain synaptic vesicle clustering without directly participating in vesicle exocytosis. *Proc. Natl. Acad. Sci.* *107*, 6504–6509.
- Müller, M., Genç, Ö., and Davis, G.W. (2015). RIM-Binding Protein Links Synaptic Homeostasis to the Stabilization and Replenishment of High Release Probability Vesicles. *Neuron* *85*, 1056–1069.
- Nagle, D.L., Karim, M.A., Woolf, E.A., Holmgren, L., Bork, P., Misumi, D.J., McGrail, S.H., Dussault, B.J., Perou, C.M., Boissy, R.E., et al. (1996). Identification and mutation analysis of the complete gene for Chediak-Higashi syndrome. *Nat. Genet.* *14*, 307–311.

- Nair, R., Lauks, J., Jung, S., Cooke, N.E., Wit, H. de, Brose, N., Kilimann, M.W., Verhage, M., and Rhee, J. (2013). Neurobeachin regulates neurotransmitter receptor trafficking to synapses. *J Cell Biol* 200, 61–80.
- Nakamura, Y., Harada, H., Kamasawa, N., Matsui, K., Rothman, J.S., Shigemoto, R., Silver, R.A., DiGregorio, D.A., and Takahashi, T. (2015). Nanoscale distribution of presynaptic Ca²⁺ channels and its impact on vesicular release during development. *Neuron* 85, 145–158.
- Neher, E. (2010). What is Rate-Limiting during Sustained Synaptic Activity: Vesicle Supply or the Availability of Release Sites. *Front. Synaptic Neurosci.* 2.
- Neher, E. (2015). Merits and Limitations of Vesicle Pool Models in View of Heterogeneous Populations of Synaptic Vesicles. *Neuron* 87, 1131–1142.
- Neher, E. (2017). Some Subtle Lessons from the Calyx of Held Synapse. *Biophys. J.* 112, 215–223.
- Nelson, N., and Lill, H. (1994). Porters and neurotransmitter transporters. *J. Exp. Biol.* 196, 213–228.
- Nguyen, T.H., Maucort, G., Sullivan, R.K.P., Schenning, M., Lavidis, N.A., McCluskey, A., Robinson, P.J., and Meunier, F.A. (2012). Actin- and Dynamin-Dependent Maturation of Bulk Endocytosis Restores Neurotransmission following Synaptic Depletion. *PLOS ONE* 7, e36913.
- Nicol, M.J., and Walmsley, B. (2002). Ultrastructural basis of synaptic transmission between endbulbs of Held and bushy cells in the rat cochlear nucleus. *J. Physiol.* 539, 713–723.
- Nouvian, R., Beutner, D., Parsons, T.D., and Moser, T. (2006). Structure and Function of the Hair Cell Ribbon Synapse. *J. Membr. Biol.* 209, 153–165.
- Oesch, N.W., and Diamond, J.S. (2011). Ribbon synapses compute temporal contrast and encode luminance in retinal rod bipolar cells. *Nat. Neurosci.* 14, 1555–1561.
- Ohn, T.-L., Rutherford, M.A., Jing, Z., Jung, S., Duque-Afonso, C.J., Hoch, G., Picher, M.M., Scharinger, A., Strenzke, N., and Moser, T. (2016). Hair cells use active zones with different voltage dependence of Ca²⁺ influx to decompose sounds into complementary neural codes. *Proc. Natl. Acad. Sci. U. S. A.* 113, E4716–E4725.
- Ohtsuka, T., Takao-Rikitsu, E., Inoue, E., Inoue, M., Takeuchi, M., Matsubara, K., Deguchi-Tawarada, M., Satoh, K., Morimoto, K., Nakanishi, H., et al. (2002). Cast: a novel protein of the cytomatrix at the active zone of synapses that forms a ternary complex with RIM1 and munc13-1. *J. Cell Biol.* 158, 577–590.
- Okada, Y., Yamazaki, H., Sekine-Aizawa, Y., and Hirokawa, N. (1995). The neuron-specific kinesin superfamily protein KIF1A is a unique monomeric motor for anterograde axonal transport of synaptic vesicle precursors. *Cell* 81, 769–780.

References

- Okerlund, N.D., Schneider, K., Leal-Ortiz, S., Montenegro-Venegas, C., Kim, S.A., Garner, L.C., Gundelfinger, E.D., Reimer, R.J., and Garner, C.C. (2017). Bassoon Controls Presynaptic Autophagy through Atg5. *Neuron* *93*, 897–913.e7.
- Pangrsic, T., Lasarow, L., Reuter, K., Takago, H., Schwander, M., Riedel, D., Frank, T., Tarantino, L.M., Bailey, J.S., Strenzke, N., et al. (2010). Hearing requires otoferlin-dependent efficient replenishment of synaptic vesicles in hair cells. *Nat. Neurosci.* *13*, 869–876.
- Pauli-Magnus, D., Hoch, G., Strenzke, N., Anderson, S., Jentsch, T.J., and Moser, T. (2007). Detection and differentiation of sensorineural hearing loss in mice using auditory steady-state responses and transient auditory brainstem responses. *Neuroscience* *149*, 673–684.
- Paxinos, G., and Franklin, K. (2001). *Mouse Brain Atlas*.
- Pereda, A.E. (2014). Electrical synapses and their functional interactions with chemical synapses. *Nat. Rev. Neurosci.* *15*, 250–263.
- Pinto, D., Pagnamenta, A.T., Klei, L., Anney, R., Merico, D., Regan, R., Conroy, J., Magalhaes, T.R., Correia, C., Abrahams, B.S., et al. (2010). Functional impact of global rare copy number variation in autism spectrum disorders. *Nature* *466*, 368–372.
- Podufall, J., Tian, R., Knoche, E., Puchkov, D., Walter, A.M., Rosa, S., Quentin, C., Vukoja, A., Jung, N., Lampe, A., et al. (2014). A Presynaptic Role for the Cytomatrix Protein GIT in Synaptic Vesicle Recycling. *Cell Rep.* *7*, 1417–1425.
- Raino, J., Khvotchev, M., Liu, P., Darios, F., Li, Y.C., Ramirez, D.M.O., Adachi, M., Lemieux, P., Toth, K., Davletov, B., et al. (2012). VAMP4 directs synaptic vesicles to a pool that selectively maintains asynchronous neurotransmission. *Nat. Neurosci.* *15*, 738–745.
- Regus-Leidig, H., Ott, C., Löhner, M., Atorf, J., Fuchs, M., Sedmak, T., Kremers, J., Fejtová, A., Gundelfinger, E.D., and Brandstätter, J.H. (2013). Identification and Immunocytochemical Characterization of Piccolino, a Novel Piccolo Splice Variant Selectively Expressed at Sensory Ribbon Synapses of the Eye and Ear. *PLOS ONE* *8*, e70373.
- Regus-Leidig, H., Fuchs, M., Löhner, M., Leist, S.R., Leal-Ortiz, S., Chiodo, V.A., Hauswirth, W.W., Garner, C.C., and Brandstätter, J.H. (2014). In vivo knockdown of Piccolino disrupts presynaptic ribbon morphology in mouse photoreceptor synapses. *Front. Cell. Neurosci.* *8*.
- Richmond, J.E., Weimer, R.M., and Jorgensen, E.M. (2001). An open form of syntaxin bypasses the requirement for UNC-13 in vesicle priming. *Nature* *412*, 338–341.
- Rizzoli, S.O., and Betz, W.J. (2005). Synaptic vesicle pools. *Nat. Rev. Neurosci.* *6*, 57–69.
- Rouiller, E.M., Cronin-Schreiber, R., Fekete, D.M., and Ryugo, D.K. (1986). The central projections of intracellularly labeled auditory nerve fibers in cats: an analysis of terminal morphology. *J. Comp. Neurol.* *249*, 261–278.

- Rutherford, M.A., Chapochnikov, N.M., and Moser, T. (2012). Spike Encoding of Neurotransmitter Release Timing by Spiral Ganglion Neurons of the Cochlea. *J. Neurosci.* *32*, 4773–4789.
- Sakaba, T. (2006). Roles of the Fast-Releasing and the Slowly Releasing Vesicles in Synaptic Transmission at the Calyx of Held. *J. Neurosci.* *26*, 5863–5871.
- Sakaba, T., and Neher, E. (2001a). Calmodulin Mediates Rapid Recruitment of Fast-Releasing Synaptic Vesicles at a Calyx-Type Synapse. *Neuron* *32*, 1119–1131.
- Sakaba, T., and Neher, E. (2001b). Quantitative Relationship between Transmitter Release and Calcium Current at the Calyx of Held Synapse. *J. Neurosci.* *21*, 462–476.
- Sakaba, T., and Neher, E. (2003). Involvement of Actin Polymerization in Vesicle Recruitment at the Calyx of Held Synapse. *J. Neurosci.* *23*, 837–846.
- Sara, Y., Virmani, T., Deák, F., Liu, X., and Kavalali, E.T. (2005). An Isolated Pool of Vesicles Recycles at Rest and Drives Spontaneous Neurotransmission. *Neuron* *45*, 563–573.
- Sauvanet, C., Wayt, J., Pelaseyed, T., and Bretscher, A. (2015). Structure, regulation, and functional diversity of microvilli on the apical domain of epithelial cells. *Annu. Rev. Cell Dev. Biol.* *31*, 593–621.
- Schikorski, T., and Stevens, C.F. (2001). Morphological correlates of functionally defined synaptic vesicle populations. *Nat. Neurosci.* *4*, 391–395.
- Schneggenburger, R., Meyer, A.C., and Neher, E. (1999). Released Fraction and Total Size of a Pool of Immediately Available Transmitter Quanta at a Calyx Synapse. *Neuron* *23*, 399–409.
- Schneggenburger, R., Sakaba, T., and Neher, E. (2002). Vesicle pools and short-term synaptic depression: lessons from a large synapse. *Trends Neurosci.* *25*, 206–212.
- Schneider, C.A., Rasband, W.S., and Eliceiri, K.W. (2012). NIH Image to ImageJ: 25 years of image analysis. *Nat. Methods* *9*, 671–675.
- Schoch, S., and Gundelfinger, E.D. (2006). Molecular organization of the presynaptic active zone. *Cell Tissue Res.* *326*, 379–391.
- Schoch, S., Castillo, P.E., Jo, T., Mukherjee, K., Geppert, M., Wang, Y., Schmitz, F., Malenka, R.C., and Sudhof, T.C. (2002). RIM1[alpha] forms a protein scaffold for regulating neurotransmitter release at the active zone. *Nature* *415*, 321–326.
- Scholz, K.P., and Miller, R.J. (1995). Developmental changes in presynaptic calcium channels coupled to glutamate release in cultured rat hippocampal neurons. *J. Neurosci.* *15*, 4612–4617.

References

- Schulz, A.M., Jing, Z., Caro, J.M.S., Wetzell, F., Dresbach, T., Strenzke, N., Wichmann, C., and Moser, T. (2014). Bassoon-disruption slows vesicle replenishment and induces homeostatic plasticity at a CNS synapse. *EMBO J.* *33*, 512–527.
- Shapira, M., Zhai, R.G., Dresbach, T., Bresler, T., Torres, V.I., Gundelfinger, E.D., Ziv, N.E., and Garner, C.C. (2003). Unitary Assembly of Presynaptic Active Zones from Piccolo-Bassoon Transport Vesicles. *Neuron* *38*, 237–252.
- Shibasaki, T., Sunaga, Y., Fujimoto, K., Kashima, Y., and Seino, S. (2004). Interaction of ATP Sensor, cAMP Sensor, Ca²⁺ Sensor, and Voltage-dependent Ca²⁺ Channel in Insulin Granule Exocytosis. *J. Biol. Chem.* *279*, 7956–7961.
- Siddiqui, T.J., and Craig, A.M. (2011). Synaptic organizing complexes. *Curr. Opin. Neurobiol.* *21*, 132–143.
- Smith, C., Moser, T., Xu, T., and Neher, E. (1998). Cytosolic Ca²⁺ acts by two separate pathways to modulate the supply of release-competent vesicles in chromaffin cells. *Neuron* *20*, 1243–1253.
- Soykan, T., Kaempf, N., Sakaba, T., Vollweiter, D., Goerdeler, F., Puchkov, D., Kononenko, N.L., and Haucke, V. (2017). Synaptic Vesicle Endocytosis Occurs on Multiple Timescales and Is Mediated by Formin-Dependent Actin Assembly. *Neuron* *93*, 854–866.e4.
- Spassova, M.A., Avissar, M., Furman, A.C., Crumling, M.A., Saunders, J.C., and Parsons, T.D. (2004). Evidence that rapid vesicle replenishment of the synaptic ribbon mediates recovery from short-term adaptation at the hair cell afferent synapse. *J. Assoc. Res. Otolaryngol. JARO* *5*, 376–390.
- Stevens, D.R., Wu, Z.-X., Matti, U., Junge, H.J., Schirra, C., Becherer, U., Wojcik, S.M., Brose, N., and Rettig, J. (2005). Identification of the minimal protein domain required for priming activity of Munc13-1. *Curr. Biol. CB* *15*, 2243–2248.
- Südhof, T.C. (2012). The Presynaptic Active Zone. *Neuron* *75*, 11–25.
- Südhof, T.C. (2013). Neurotransmitter Release: The Last Millisecond in the Life of a Synaptic Vesicle. *Neuron* *80*, 675–690.
- Südhof, T.C., and Rizo, J. (2011). Synaptic Vesicle Exocytosis. *Cold Spring Harb. Perspect. Biol.* *3*, a005637.
- Sullivan, P.F., de Geus, E.J.C., Willemsen, G., James, M.R., Smit, J.H., Zandbelt, T., Arolt, V., Baune, B.T., Blackwood, D., Cichon, S., et al. (2008). Genome-wide association for major depressive disorder: a possible role for the presynaptic protein piccolo. *Mol. Psychiatry* *14*, 359–375.

- Sun, J.-Y., and Wu, L.-G. (2001). Fast Kinetics of Exocytosis Revealed by Simultaneous Measurements of Presynaptic Capacitance and Postsynaptic Currents at a Central Synapse. *Neuron* 30, 171–182.
- Taberner, A.M., and Liberman, M.C. (2005). Response Properties of Single Auditory Nerve Fibers in the Mouse. *J. Neurophysiol.* 93, 557–569.
- Takamori, S., Holt, M., Stenius, K., Lemke, E.A., Grønborg, M., Riedel, D., Urlaub, H., Schenck, S., Brügger, B., Ringler, P., et al. (2006). Molecular Anatomy of a Trafficking Organelle. *Cell* 127, 831–846.
- Takao-Rikitsu, E., Mochida, S., Inoue, E., Deguchi-Tawarada, M., Inoue, M., Ohtsuka, T., and Takai, Y. (2004). Physical and functional interaction of the active zone proteins, CAST, RIM1, and Bassoon, in neurotransmitter release. *J. Cell Biol.* 164, 301–311.
- Tang, A.-H., Chen, H., Li, T.P., Metzbower, S.R., MacGillavry, H.D., and Blanpied, T.A. (2016). A trans-synaptic nanocolumn aligns neurotransmitter release to receptors. *Nature* 536, 210–214.
- Taschenberger, H., Woehler, A., and Neher, E. (2016). Superpriming of synaptic vesicles as a common basis for intersynapse variability and modulation of synaptic strength. *Proc. Natl. Acad. Sci. U. S. A.* 113, E4548-4557.
- Trussell, L.O. (1999). Synaptic mechanisms for coding timing in auditory neurons. *Annu. Rev. Physiol.* 61, 477–496.
- Vogl, C., Butola, T., Haag, N., Leitner, M., Moutschen, M., Lefebvre, P.P., Speckmann, C., Garrett, L., Becker, L., Fuchs, H., et al. The BEACH protein LRBA is Required for Hair Bundle Maintenance in Cochlear Hair Cells and for Hearing. *Rev.*
- Wagh, D., Terry-Lorenzo, R., Waites, C.L., Leal-Ortiz, S.A., Maas, C., Reimer, R.J., and Garner, C.C. (2015). Piccolo Directs Activity Dependent F-Actin Assembly from Presynaptic Active Zones via Daam1. *PLOS ONE* 10, e0120093.
- Wahl, S., Katiyar, R., and Schmitz, F. (2013). A local, periaxonal endocytic machinery at photoreceptor synapses in close vicinity to synaptic ribbons. *J. Neurosci. Off. J. Soc. Neurosci.* 33, 10278–10300.
- Waites, C.L., Craig, A.M., and Garner, C.C. (2005). Mechanisms of vertebrate synaptogenesis. *Annu. Rev. Neurosci.* 28, 251–274.
- Waites, C.L., Leal-Ortiz, S.A., Andlauer, T.F.M., Sigrist, S.J., and Garner, C.C. (2011). Piccolo Regulates the Dynamic Assembly of Presynaptic F-Actin. *J. Neurosci.* 31, 14250–14263.
- Waites, C.L., Leal-Ortiz, S.A., Okerlund, N., Dalke, H., Fejtova, A., Altmann, W.D., Gundelfinger, E.D., and Garner, C.C. (2013). Bassoon and Piccolo maintain synapse integrity by regulating protein ubiquitination and degradation. *EMBO J.* 32, 954–969.

References

- Wang, L.-Y., and Kaczmarek, L.K. (1998). High-frequency firing helps replenish the readily releasable pool of synaptic vesicles. *Nature* *394*, 384–388.
- Wang, Y., and Manis, P.B. (2008). Short-Term Synaptic Depression and Recovery at the Mature Mammalian Endbulb of Held Synapse in Mice. *J. Neurophysiol.* *100*, 1255–1264.
- Wang, B., Hu, B., and Yang, S. (2015). Cell junction proteins within the cochlea: A review of recent research. *J. Otol.* *10*, 131–135.
- Wang, J.W., Howson, J., Haller, E., and Kerr, W.G. (2001). Identification of a novel lipopolysaccharide-inducible gene with key features of both A kinase anchor proteins and chs1/beige proteins. *J. Immunol. Baltim. Md 1950* *166*, 4586–4595.
- Wang, J.-W., Gamsby, J.J., Highfill, S.L., Mora, L.B., Bloom, G.C., Yeatman, T.J., Pan, T., Ramne, A.L., Chodosh, L.A., Cress, W.D., et al. (2004). Deregulated expression of LRBA facilitates cancer cell growth. *Oncogene* *23*, 4089–4097.
- Wang, X., Kibschull, M., Laue, M.M., Lichte, B., Petrasch-Parwez, E., and Kilimann, M.W. (1999). Aczonin, a 550-Kd Putative Scaffolding Protein of Presynaptic Active Zones, Shares Homology Regions with Rim and Bassoon and Binds Profilin. *J. Cell Biol.* *147*, 151–162.
- Wang, X., Hu, B., Zieba, A., Neumann, N.G., Kasper-Sonnenberg, M., Honsbein, A., Hultqvist, G., Conze, T., Witt, W., Limbach, C., et al. (2009). A Protein Interaction Node at the Neurotransmitter Release Site: Domains of Aczonin/Piccolo, Bassoon, CAST, and Rim Converge on the N-Terminal Domain of Munc13-1. *J. Neurosci.* *29*, 12584–12596.
- Wang, Y., Okamoto, M., Schmitz, F., Hofmann, K., and Südhof, T.C. (1997). Rim is a putative Rab3 effector in regulating synaptic-vesicle fusion. *Nature* *388*, 593–598.
- Wang, Y., O'Donohue, H., and Manis, P. (2011). Short-term plasticity and auditory processing in the ventral cochlear nucleus of normal and hearing-impaired animals. *Hear. Res.* *279*, 131–139.
- Watanabe, S., Rost, B.R., Camacho-Pérez, M., Davis, M.W., Söhl-Kielczynski, B., Rosenmund, C., and Jorgensen, E.M. (2013). Ultrafast endocytosis at mouse hippocampal synapses. *Nature* *504*, 242–247.
- Watanabe, S., Trimbuch, T., Camacho-Pérez, M., Rost, B.R., Brokowski, B., Söhl-Kielczynski, B., Felies, A., Davis, M.W., Rosenmund, C., and Jorgensen, E.M. (2014). Clathrin regenerates synaptic vesicles from endosomes. *Nature* *515*, 228–233.
- Wichmann, C. (2015). Molecularly and structurally distinct synapses mediate reliable encoding and processing of auditory information. *Hear. Res.* *330, Part B*, 178–190.
- Wilhelm, B.G., Groemer, T.W., and Rizzoli, S.O. (2010). The same synaptic vesicles drive active and spontaneous release. *Nat. Neurosci.* *13*, 1454–1456.

- Wu, S.H., and Oertel, D. (1984). Intracellular injection with horseradish peroxidase of physiologically characterized stellate and bushy cells in slices of mouse anteroventral cochlear nucleus. *J. Neurosci.* *4*, 1577–1588.
- Wu, L.-G., Ryan, T.A., and Lagnado, L. (2007). Modes of Vesicle Retrieval at Ribbon Synapses, Calyx-Type Synapses, and Small Central Synapses. *J. Neurosci.* *27*, 11793–11802.
- Wu, Y., O'Toole, E.T., Girard, M., Ritter, B., Messa, M., Liu, X., McPherson, P.S., Ferguson, S.M., and Camilli, P.D. (2014). A dynamin 1-, dynamin 3- and clathrin-independent pathway of synaptic vesicle recycling mediated by bulk endocytosis. *eLife* *3*, e01621.
- Xue, L., Zhang, Z., McNeil, B.D., Luo, F., Wu, X.-S., Sheng, J., Shin, W., and Wu, L.-G. (2012). Voltage-dependent calcium channels at the plasma membrane, but not vesicular channels, couple exocytosis to endocytosis. *Cell Rep.* *1*, 632–638.
- Yamada, K.A., and Tang, C.M. (1993). Benzothiadiazides inhibit rapid glutamate receptor desensitization and enhance glutamatergic synaptic currents. *J. Neurosci.* *13*, 3904–3915.
- Yamashita, T., Eguchi, K., Saitoh, N., von Gersdorff, H., and Takahashi, T. (2010). Developmental shift to a mechanism of synaptic vesicle endocytosis requiring nanodomain Ca²⁺. *Nat. Neurosci.* *13*, 838–844.
- Yang, H., and Xu-Friedman, M.A. (2008). Relative Roles of Different Mechanisms of Depression at the Mouse Endbulb of Held. *J. Neurophysiol.* *99*, 2510–2521.
- Yin, T.C., and Chan, J.C. (1990). Interaural time sensitivity in medial superior olive of cat. *J. Neurophysiol.* *64*, 465–488.
- Yu, W.-M., and Goodrich, L.V. (2014). Morphological and physiological development of auditory synapses. *Hear. Res.* *311*, 3–16.
- Zhai, R.G., Vardinon-Friedman, H., Cases-Langhoff, C., Becker, B., Gundelfinger, E.D., Ziv, N.E., and Garner, C.C. (2001). Assembling the Presynaptic Active Zone: A Characterization of an Active Zone Precursor Vesicle. *Neuron* *29*, 131–143.
- Zheng, J., Shen, W., He, D.Z.Z., Long, K.B., Madison, L.D., and Dallos, P. (2000). Prestin is the motor protein of cochlear outer hair cells. *Nature* *405*, 149–155.

Acknowledgements

I would like to thank the following people:

Prof. Tobias Moser for his constant support and encouragement. His enthusiasm while discussing science or accompanying at the setup during an experiment is infectious and a tremendous motivating force.

Prof. Tobias Moser, Prof. Erwin Neher and Prof. Thomas Dresbach for their time, ideas, and advice as my thesis advisory committee members. It was an honor and a tremendous boost to be discussing my scientific progress with such experienced and erudite scientists.

Dr. Alejandro Mendoza Schulz and Dr. Yang Yang for teaching slice physiology with extreme patience and initiating my scientific journey.

Dr. Nicola Strenzke for teaching me *in vivo* recording of extracellular field potentials from spiral ganglion neurons, and Dr. Christian Vogl for his motivating encouragement and really taking the LRBA project forward.

Christiane Senger-Freitag and Sandra Gerke for their technical support with genotyping and innumerable organizational chores in the lab.

Nadine Hermann and Stefan Thom for measuring the ABRs for the projects.

Gerhard Hoch for his sophisticated MATLAB programs for image analysis, and for troubleshooting MATLAB glitches to make my life in the lab a lot easier.

Dr. Chao-Hua Huang and Dr. Maria Magdalena Picher for their insightful discussions, analytical reasoning, great feedback and critique, their company and shared enthusiasm for music during long experiments, and much more than can be mentioned here. They made my time in the lab and in Göttingen fun and memorable.

All the members of the InnerEarLab for sharing the past four years and providing an encouraging and stimulating work environment.

Prof. Michael Hörner and Sandra Drube from the Neuroscience coordination office for their unfailing and tremendous support and guidance. Without them it would not have been possible to get through the grueling course of the PhD in a land away from home with long complicated forms in German.

I furthermore acknowledge the financial support provided by the Göttingen Graduate School of Neurosciences, biophysics and Molecular Biosciences (GGNB) Excellence fellowship (DFG Grant GSC 226/1).

I am very grateful to my friends who have been there all throughout and especially during this last stretch of doctorate work, while writing the thesis. I thank Olga Babaev for the long walks and conversations during the writing period, that kept me sane. Dr. Agata Witkowska and Lukasz Jablonski for feeding me when I was too absent-minded to care. Georg Hafner and Julio Santos Viotti for constant motivation and data discussion. Prithi Singh for his prowess in English and help with proof-reading.

In the end, I would like to thank my family and friends for their support, encouragement and understanding throughout, in all aspects.

List of abbreviations

ABR	Auditory brainstem response	ELV	Endosome like vacuoles
aCSF	Artificial cerebrospinal fluid	EPSC	Excitatory postsynaptic current
AMPA	α -amino-3-hydroxy-5-methyl-4-isoxazolepropionic acid receptor	ERM	ezrin-radixin-moesin
aVCN	Anterior ventral cochlear nucleus	ES cells	Embryonic stem cells
AZ	Active zone	FITC	Fluorescein isothiocyanate
BC	Bushy cell	FN	Fibronectin
BDCP	BEACH domain containing protein	FWHM	Full width at half maximum
BEACH	Beige and Chediak-Higashi	GBC	Globular bushy cell
CAZ	Cytomatrix of the active zone	GSDB	Goat serum dilution buffer
CB	Cerebellum	IHC	Inner hair cells
CC	Coiled-coiled domain	ILD	interaural level difference
CME	Clathrin mediated endocytosis	ITD	interaural time difference
CNS	Central nervous system	Kyn	Kynurenic acid
ConA	ConcanavalinA	LRBA	Lipopolysaccharide-responsive beige like anchor protein
CTZ	Cyclothiazide	LSO	lateral superior olive
DC	Dorsal cochlear nucleus	mEPSC	miniature excitatory postsynaptic current
DIC	Differential interference contrast	MET	Mechano-electrical transduction
DPOAE	Distortion product otoacoustic emissions	MNTB	Medial nucleus of trapezoid body
DRBP	Drosophila RIM binding protein	MSO	Medial superior olive
eEPSC	Evoked excitatory postsynaptic current	N	Number of vesicular release site
EGTA	ethylene glycol-bis(β -aminoethyl ether)-N,N,N',N'-tetraacetic acid	NA	Numerical aperture

List of abbreviations

NBEA	Neurobeachin	SH3	SRC homology
NMJ	Neuromuscular junction	SM	Sec1/Munc18
NSF	N-ethylmaleimide sensitive factor	SNARE	Soluble NSF attachment receptor
OHC	Outer hair cell	SPL	Sound pressure level
PBH	Piccolo Bassoon homology domain	SR	Spontaneous rate
PBS	Phosphate buffer saline	Stx	Syntaxin
PCR	Polymerase chain reaction	SV	Synaptic vesicle
PE	Peak equivalent	Syb	Synaptobrevin
PFA	Paraformaldehyde	Syt	Synaptotagmin
PH	Pleckstrin homology domain	τ	Tau (time constant of decay)
PPR	Paired pulse ratio	Vgat	Vesicular GABA transporter
Pr	Release probability	VGCC	Voltage gated calcium channel
PTV	Piccolo-Bassoon transport vesicles	Vglut1	Vesicular Glutamate transporter
q	quantum size	ZF	Zinc finger domain
RDX	Radixin		
RRP	Rapidly releasable pool		
S.E.M.	Standard error of mean		
SBC	Spherical bushy cell		
SC	Stellate cell		
SEM	Scanning electron microscopy		
SGN	Spiral ganglion neuron		

List of figures

Figure I. 1: Structure of a chemical synapse	4
Figure I. 2: Synaptic vesicle cycle	6
Figure I. 3: Schematic of SNARE/SM protein cycle illustrating the vesicle fusion machinery ...	9
Figure I. 4: Cytomatrix of the active zone	12
Figure I. 5: The auditory pathway	20
Figure M. 1: LRBA2 KO generation	22
Figure M. 2: Colour code used in the thesis for different genotypes	23
Figure M. 3: Illustration of the sagittal slice preparation of the aVCN	24
Figure M. 4: Illustration of the sagittal slice preparation of the aVCN	27
Figure 1b. 1: Selective expression of Piccolo (Aczonin) in central synapses	37
Figure 1b. 2: Auditory brainstem response (ABR) indicates preserved cochlear function but alteration in signal propagation at the cochlear nucleus in PicMut	38
Figure 1b. 3: Number of endbulbs and endbulb AZ per bushy cell in aVCN	40
Figure 1b. 4: Unchanged immunofluorescence intensity of Vglut1 and Gephyrin in PicMut aVCN	41
Figure 1b. 5: Molecular composition altered at aVCN synapses in PicMut.....	42
Figure 1b. 6: Morphological distinction between bushy cells and stellate cells of the aVCN .	44
Figure 1b. 7: Miniature EPSC amplitude and kinetics preserved in PicMut synapses	45

Figure 1b. 8: Paired pulse ratio (PPR) recorded with and without 1mM Kynurenic acid (Kyn) and 100 μ M Cyclothiazide (CTZ) demonstrating receptor desensitization and (or) saturation in PicMut	47
Figure 1b. 9: Reduced evoked EPSC amplitude in PicMut	48
Figure 1b. 10: Analyzing vesicle pool dynamics during high-frequency stimulation at Piccolo-deficient endbulb of Held synapses	51
Figure 1b. 11: Unchanged asynchronous release at endbulb synapse in PicMut aVCN.....	52
Figure 1b. 12: Recovery from short-term depression is slowed at Piccolo-deficient endbulb of Held synapses.....	53
Figure 1b. 13: Recovery from short-term depression is slowed at PicBsn endbulb of Held synapses.....	55
Figure 1b. 14: Miniature EPSC amplitude and kinetics preserved in PicBsn synapses	57
Figure 1b. 15: eEPSC amplitude and kinetics intact in PicBsn synapses but shorter synaptic delay	59
Figure 1b. 16: Reduced paired pulse ratio at endbulbs of PicBsn	60
Figure 1b. 17: Analyzing vesicle pool dynamics during high-frequency stimulation at Piccolo-deficient endbulb of Held synapses with partial Bassoon deficiency.....	62
Figure 1b. 18: Endbulbs of Held in PicBsn aVCN tend to have more asynchronous release...	63
Figure 2a. 1: Illustration of interactions between RIM-BPs with Bassoon, RIM and VGCC.....	73
Figure 2b. 1: No change in mEPSC at the endbulb of Held in the absence of RIM-BP2	76
Figure 2b. 2: Reduced eEPSC amplitude and slower kinetics with increased synaptic delay at endbulbs of Held in RIM-BP2 KO mice	77

List of figures

Figure 2b. 3: Short-term depression replaced by facilitation at endbulbs of Held in RIM-BP2 KO mice	79
Figure 2b. 4: Slower recovery from short-term depression at endbulbs of Held lacking RIM-BP2.....	81
Figure 2b. 5: Increased asynchronous release at the endbulbs of Held in RIM-BP2 aVCN	82
Figure 3a. 1: Domain structures of BEACH domain containing proteins (BDCPs)	88
Figure 3a. 2: Organ of Corti and inner hair cell (IHC) with the classification of SGNs	91
Figure 3b. 1: Reduced acoustic startle response amplitudes in LRBA2 KO compared to WT animals	92
Figure 3b. 2: Progressive hearing loss in LRBA2 mutants.	93
Figure 3b. 3: Reduced cochlear amplification and outer hair cell dysfunction	94
Figure 3b. 4: Reduced fraction of low-spontaneous-rate fibers and elevated sound thresholds and in LRBA2-KO animals.	95
Figure 3b. 5: Rate level function: Spike rate in response to sound stimulus steeper in LRBA2 KO SGN units	96
Figure 3b. 6: Evoked response to sound stimulus and recovery of response post stimulus unchanged in LRBA2 KO SGN units	96
Figure 3c. 1: Hair bundles of LRBA-KO hair cells develop a prominent central gap in their stereociliary array likely leading to impaired sound processing.....	99

List of tables

Table 1b. 1: Miniature EPSC (mEPSC) amplitude and kinetics unchanged in PicMut..... 45

Table 1b. 2: Quantification of PPR recorded with and without 1mM Kynurenic acid (Kyn) and 100µM Cyclothiazide (CTZ)..... 47

Table 1b. 3: Reduced evoked EPSC amplitude in PicMut 49

Table 1b. 4: Comparison of pool size, vesicle replenishment, release probability and short-term depression at the endbulb of Held synapse in PicWT and PicMut 50

Table 1b. 5: Quantification of recovery from short-term depression 56

Table 1b. 6: Miniature EPSC amplitude and kinetics unchanged in PicBsn 56

Table 1b. 7: eEPSC amplitude and kinetics intact in PicBsn synapses but shorter synaptic delay 58

Table 1b. 8: Reduced paired pulse ratio at endbulbs of PicBsn..... 60

Table 1b. 9: Comparison of pool size, vesicle replenishment, release probability and short-term depression at the endbulb of Held synapse in PicBsn and PicWT 61

Table 2b. 1: No change in mEPSC at the endbulb of Held in the absence of RIM-BP2..... 784

Table 2b. 2: Reduced eEPSC amplitude and slower kinetics with increased synaptic delay at endbulbs of Held in RIM-BP2 KO mice 78

Table 2b. 3: Short-term depression replaced by facilitation at endbulbs of Held in RIM-BP2 KO mice 79

Declaration

Herewith I declare, that I prepared the doctoral thesis 'Molecular physiology of signal transmission along the auditory pathway' on my own and with no other sources and aids than quoted.

Tanvi Butola

Göttingen, March 31, 2017

Curriculum Vitae

Tanvi Butola

Personal information

Hanssenstraße 18
37073, Göttingen
Germany

Date of Birth: 27 November 1989
+49 176 613 407 24
tani.butola@gmail.com
Nationality: Indian

Education & Research

2013- Present **Doctoral student – Synaptic Nanophysiology at Max Planck Institute for Biophysical chemistry, Göttingen, Germany**

Project 1: Role of cytomatrix of active zone protein, Piccolo, in high frequency transmission at a central auditory synapse.

Project 2: RIM binding protein 2 (RBP2) as a regulator of synaptic release.

Project 3: Mechanism of progressive hearing loss due to the absence of LPS-responsive beige-like anchor protein, LRBA2.

2011-2013 **International Max Planck Research School – Neuroscience Program, Göttingen, Germany**

Master thesis: Electrophysiological characterization of Piccolo deficient synapses in the cochlear nucleus.

2007-2011 **University Institute of Engineering and Technology, Panjab University Chandigarh, India**

Bachelor of Engineering (B.E.) in Biotechnology.

Bachelor research carried out at Centre for Cellular and Molecular Biology (CCMB), Hyderabad, India.

Bachelor thesis: Mild stroke induced changes in striatum of rodents with special reference to neurogenesis.

Awards & Fellowships

2013-2016 GGNB Excellence Fellowship, Georg-August University, Göttingen

2011-2012	Excellence Foundation Stipend, Max Planck Society
2011	University Gold Medal, Panjab University, Chandigarh, India
2010	DAAD (German Academic Exchange Service) Summer School Scholarship 2010 (DAAD Hochschulsommerkursstipendium, 2010)
2009	University Merit Scholarship, Panjab University, Chandigarh, India
2008	University Topper's Scholarship, Panjab University, Chandigarh, India
2008, 2007	University Sports Scholarship, Panjab University, Chandigarh, India

Conferences & Symposia

Poster presentations:

Dec 2016	4th GGNB Science Day, Göttingen, Germany Role of Piccolo in high frequency transmission at a central auditory synapse: T. Butola and T. Moser
Nov 2016	46th Annual Meeting of the Society of Neuroscience, San Diego, USA Role of Piccolo in high frequency transmission at a central auditory synapse: T. Butola and T. Moser
Sep 2014	DFG thematic conference on ultrafast and temporally precise information processing, Bad Münster, Germany Role of LRBA (LPS responsive, beige like anchor protein) in auditory function: T. Butola, Christian Vogl, Tzu-lun Wang, Michael Leitner, Natja Haag, Britta Qualmann, Michael Kessels, Dominik Oliver, Manfred Kilimann, Tobias Moser and Nicola Strenzke
Sep 2014	Gordon Research Conference for Synaptic Transmission, New Hampshire, USA Role of Piccolo in high frequency transmission at central auditory synapses: T. Butola and T. Moser
May 2013	5th Biennial Neuroscience Conference Neurizons, Göttingen, Germany Electrophysiological Characterization of Piccolo deficient synapses in the cochlear nucleus: T. Butola and T. Moser
Mar 2010	Chandigarh Science Congress (CHASCON), Chandigarh, India Detection and Bioremediation of Cadmium, and its utilization to generate power by Ni-Cd batteries: T. Butola
Feb 2009	International Symposium on recent developments in molecular technologies, Chandigarh, India

siRNA - vehicle for drug delivery: T. Butola and A. Arora

Talks:

- Mar 2017 **12th Göttingen Meeting of the German Neuroscience Society, Göttingen, Germany**
Role of Piccolo in high frequency transmission at a central auditory synapse
- Sep 2015 **Core to Core symposium on Synaptic Transmission, Paris, France**
Role of Piccolo in high frequency transmission at a central auditory synapse
- Mar 2015 **11th Göttingen Meeting of the German Neuroscience Society, Göttingen, Germany**
Role of Piccolo in high frequency transmission at a central auditory synapse
- Sep 2013 **Ribbon Synapse Symposium, Göttingen, Germany**
Role of Piccolo in high frequency transmission at a central auditory synapse
- Sep 2013 **HUJI-GAU cooperation meeting, Jerusalem, Israel**
Role of Piccolo in high frequency transmission at a central auditory synapse
- Feb 2011 **Chandigarh National Congress (CHASCON), Chandigarh, India**
Mild stroke induced changes in striatum of rodents with special reference to neurogenesis